COPY 1 of 1 COPIES

REPORT NO. SH-64-1

BAND-PASS SHOCK ABSORBER STUDIES

April 1964

Prepared Under BuWeps Contract No. NOw 60-0373-C
by the
Analytical Mechanics Department
Bendix Products Aerospace Division
The Bendix Corporation
South Bend, Indiana 46620

TABLE OF CONTENTS

TABLE OF CONTENTS (Continued)

LIST OF ILLUSTRATIONS

LIST OF ILLUSTRATIONS (Continued)

LIST OF ILLUSTRATIONS (Continued)

LIST OF ILLUSTRATIONS (Continued)

FOREWORD

This report was prepared by the Bendix Products Aerospace Division of The Bendix Corporation, South Bend, Indiana, under BuWeps Contract No. NOw 60-0373-c.

Contractor Project Engineer for this program was Mr. R. M. Palmer, of the Analytical Mechanics Engineering Department. The theoretical analysis phase of the program was under the direction of Mr. R. J. Black of the Analytical Mechanics Engineering Department. Mr. T. H. Moraczewski conducted the linearized study of the band-pass unit and assisted in setting up the simplified model. All computer work was directed by Mr. J. J. Fredlake, Supervisor of the Analog Computer Section. Mr. D. C. Irwin, of the Energy Absorber Test Laboratory, supervised all experimental work including data reduction.

The data, equipment, and suggestions rendered by other organizations, in particular The McDonnell Aircraft Corporation, North American Aviation Corporation, the B. F. Goodrich Company, and the U. S. Rubber Company, were greatly appreciated and hereby acknowledged.

ABSTRACT

The principal objective of this program was to study the application of the band-pass principle to aircraft landing gear shock struts. The program included both theoretical and experimental evaluation. The first portion of the theoretical studies was devoted to the design and evaluation of a band-pass unit for the McDonnell F4H-1 MLG shock strut. The second part of the theoretical studies was the design and evaluation of a unit for the North American A3J-1 MLG shock strut.

The experimental program consisted of the fabrication of a band-pass unit and modification of the A3J-1 shock strut to utilize it and the test program conducted in the drop test tower over the 120 inch dynamometer.

The principal result or conclusion coming from the program is that loads arising from arresting cable impact, into the unsprung mass (tire, wheel, axle, and inner cylinder of shock strut) are not alleviated to any appreciable degree through use of the band-pass principle. The incremental increases in loads through the landing gear attach points into the aircraft structure, however, may be reduced up to 50%.

This report covers all phases of study as outlined above.

PUBLICATION REVIEW

The publication of this report does not constitute approval by the Bureau of Naval Weapons of the findings or conclusions contained herein. It is published only for the exchange and stimulation of ideas.

SIGNATURE: R. F. Gregoritz

R. F. Gregoritz
By Direction
Bureau of Naval Weapons
Representative/Mishawaka, Ind.

SECTION I

INTRODUCTION

The principle of "band-pass", as taken from electrical analogy, was first applied to shock absorbers by Mr. Emanuel Schnitzer while working for NACA. A paper was presented explaining this principle - NACA Technical Note 3803 dated October, 1956, and the principle was further studied by experimental test as reported in NACA Technical Note 4387, dated September, 1958.

The basic concept of "band-pass" as applied to a landing gear system is to provide a shock-absorbing system capable of satisfactory performance under normal landing impact operation, and at the same time provide satisfactory performance at higher frequency impact such as bump contacts. The basic mechanism to achieve this aim, termed "band-pass," consists of a preloaded poppet valve backed up by a control chamber. An inlet and outlet bleed system on this chamber causes the pressure within the chamber to vary according to the rate of fluid transfer from the main dynamic chamber to the upper chamber of the strut. A high rate of fluid transfer causes the pressure to drop considerably below the fluid pressure within the dynamic chamber, thus opening the valve. A low rate of fluid transfer causes the pressure within the control chamber to be only slightly less than that of the dynamic chamber, allowing the preload of the valve to maintain it in a closed position. In summary, the principle of the mechanism is to increase the fluid metering orifice size for high rates of fluid transfer (bump loading) while maintaining the conventional metered orifice for normal rates of fluid transfer such as encountered in landing impact.

There are many possible design approaches for "band-pass." However, prior to the present program only one was experimentally tested in a shock strut. As stated by Mr. Schnitzer in his report, the intent of his test program was to verify the principles, and not to optimize any one design. The results obtained indicated that "bandpass" reduced the loads transferred to the support structure and wheel assembly from "bump-type" impact loads. The test gear was compared directly with the same gear incorporating a conventional fixed-orifice design. It must be pointed out however, that this test gear was a very simple design and not characteristic of present-day high performance fighter aircraft. This indicated the need for further engineering and analytical effort to substantiate the practicality of the "band-pass" principle in present and future landing gear designs. Further tests were required to determine if there were any inherent disadvantages to the system before consideration could be given to including it on any production hardware.

As a result of Schnitzer's work, a "band-pass" modified shock strut appeared attractive for numerous applications. Failures of wheel flanges caused by bottoming of the tire when landing over the cable on carrier operation could possibly be reduced and weight reduction realized with the band-pass modified shock strut. With faster telescoping velocities, such as encountered with bumps, "band-pass" might enable the strut to absorb higher peak loads and reduce the wheel flange loadings. The spin-up loads of the gear might be reduced by the "band-pass" action and could result in possible structural weight reduction. The magnitude of this load reduction would have to be determined from a test program since there are so many physical variables that could alter the performance.

"Band-pass" modified shock struts could possibly permit operation from dispersed sites that have been heretofore impractical. This would include more liberal operational use in choppy water and rougher terrain in the Arctic. All gains in performance and versatility are dependent on the degree of load reduction and basic design limitations. Another possibility of improvement would be controlled gear extension after carrier catapulting. A history of failures have been experienced from this type of operation and the corrective change results in weight addition.

If proper performance could be realized with "band-pass," the net result might be weight reduction and solutions of the problems mentioned above. The above improvements were all conjectures that the "band-pass" design might be completely successful. Only by a thorough engineering study and development would a definite conclusion be available.

The Bendix Products Aerospace Division therefore embarked upon a program of study, both theoretical and experimental, to evaluate the "band-pass" modified shock strut. This report will discuss the program and the results obtained.

SECTION II

TECHNICAL DISCUSSION - McDONNELL F4H-1 MLG THEORETICAL STUDIES

INTRODUCTION

The purpose of the analytical study of the band-pass mechanism as applied to landing gear shock strut operation is threefold. The first purpose of the study is to provide a means for the rapid evaluation of any particular band-pass shock strut configuration. The analytical simulation of the band-pass mechanism incorporated into a complete landing gear system allows one to study the dynamic loads and other performance criteria for a variety of landing and taxiing conditions.

Closely linked to this first purpose is the second purpose of the analytical study, the improvement in any given design of the band-pass shock strut mechanism by parameter adjustment. Through use of the analytical simulation, it is possible to adjust any one of the system's parameters so as to improve the performance for the whole spectrum of landing conditions.

The third purpose of the analytical study is to provide general design criteria by making use of performance data obtained for a wide range of system parameter variations. As noted in the original proposal, concise generalized design criteria may not be possible to develop due to the large number of variables involved in the system, but the minimum results of this study were to be the development of techniques for the rapid analytical investigation of any given system. Both of these objectives have been achieved. This will be discussed later in the report.

Discussion of Band-Pass Mechanism

Since the problem to be attacked was new in several respects, the mathematical model used in the analysis was fairly extensive. Fortunately, portions of the problem were studied previously and use was made of results obtained in these studies in the analysis of the present mechanism and the formulation of a suitable mathematical model.

The landing gear system was idealized to a three-mass lumped-mass system. The three masses are:

1. The mass of the weight supported by a single gear (the main mass)
2. The mass of the unsprung parts (the unsprung mass)

3. The effective fore and aft lumped-mass at the axle.

Each of these masses has a degree of freedom associated with it. The vertical motion of the main mass will be designated as Z_1, the vertical motion of the unsprung mass will be designated as Z_2, and the fore and aft motion of the effective mass at the axle will be designated as x. There is also the degree of freedom ω, which is the angular velocity of the tire.

In addition to the assumption of a lumped-mass system, further assumptions include: the assumption that the inclination of the strut may be ignored for caster angles up to ten degrees, the assumption that the bearing friction force is independent of the relative velocity between the bearings and their sliding surfaces, the assumption that the fore and aft stiffness of the strut is independent of the stroke, the assumption that the dynamic effect of the moving-bearing normal force is insignificant, the assumption that the polytropic constant of the air compression process is constant and unity, the assumption that the orifice discharge coefficient of all orifices within the system is constant, the assumption that the fluid flow is turbulent at all times, and the assumption that the highest modes of motion of the strut fore and aft motion do not exist. The idealization afforded by the above assumptions has been found to be adequate in experimental and theoretical studies of the landing impact problem.

Two types of band-pass mechanisms were considered initially. The first is the complex multi-function system which was built and used in the experimental studies described in Reference 2. The second is a simplified system which performs only the function of a rate sensitive orifice size.

Schematics of Type I and Type II Band-Pass Mechanisms along with the mathematical models and derivation of the equations of motion are shown in Appendix A.

Section II Program

The work accomplished falls under the following categories:

1. Incorporation of changes in the mathematical model as specified in the contract; namely, modifications of the model to take into account the pitch angle of the landing gear and airplane

2. Changes in the mathematical model found necessary for simulation of the cable impact phenomena; namely, modification of the tire model to one having regions of differing elasticity and modification of the bump contour to simulate the tire mode shape.

3. Computer investigation of the F4H-1 main landing gear system with a band-pass unit for normal landing and bump impact conditions

4. Analysis of computer results

5. Investigation of possible modifications in the F4H-1 main gear to make it adaptable to a band-pass unit.

DISCUSSION

Gear Pitch Angle

Based on previous experience the pitch angle of the landing gear was assumed to be constant even though fore and aft bending of the strut takes place during the landing roll. This was found previously to be the better of two equally complex mathematical models (equal number of degrees of freedom) approximating the actions of the gear. The two models are shown in Figure 2-1 along with the pertinent implications of each model.

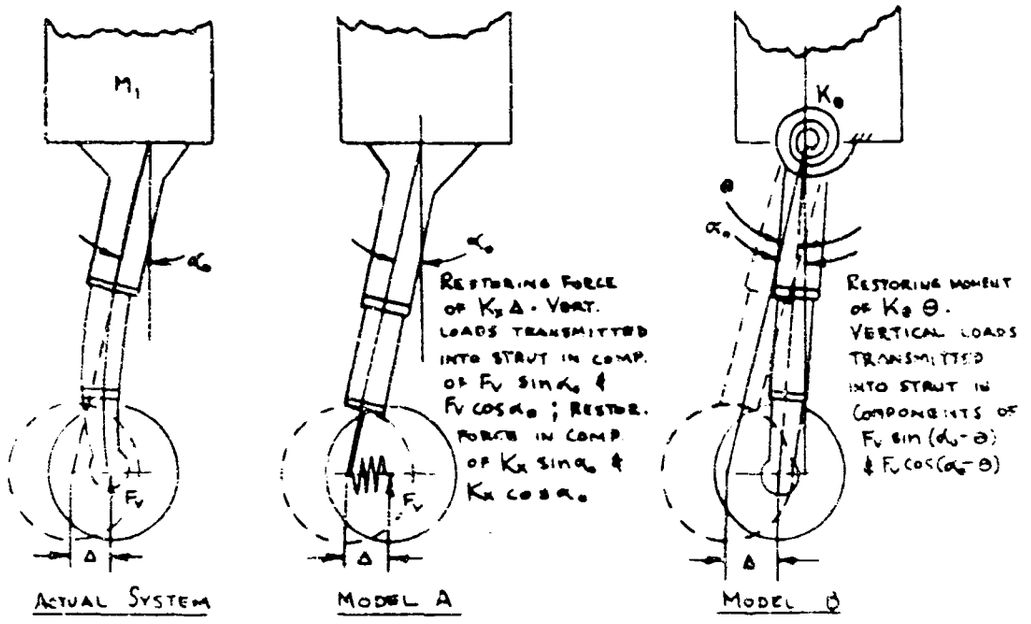

Figure 2-1. Landing Gear Bending Models

Tire Model

In addition to the above modifications, it was felt that an improvement in the tire model was necessary. The model given in the proposal consisted of a single nonlinear elastic element. This model has several drawbacks. For example, if the tire comes into contact with a bump of height h and the axle is forced to transverse a straight line patch parallel to the ground, the single spring tire model develops a force of $f(\delta_0 + h)$ where f is the nonlinear spring function and δ_0 is the initial tire deflection. However, in the actual tire, the force developed is much less than this quantity since the bump distorts far less of the footprint than a total footprint deflection of (h).

This deficiency suggests an improvement in the tire elasticity model. If the model is made up of a series of nonlinear elastic elements, then for normal tire loading all spring elements will be deflected, while for "bump" loading only the spring element in the vicinity

of the bump would be deflected. Thus the vertical load developed for the two cases would be more realistic in comparison to the actual tire load characteristics.

A second modification, which would also be necessary with the single spring tire model, is the conversion of the bump contour to an equivalent contour of equal height but greater length than the original bump. This is necessary in that the tire deflection is not exactly equal to the bump contour. Regions of the tire adjacent to the bump will be deflected even though no portion of the bump is actually contacting them. This is shown qualitatively in the figure below.

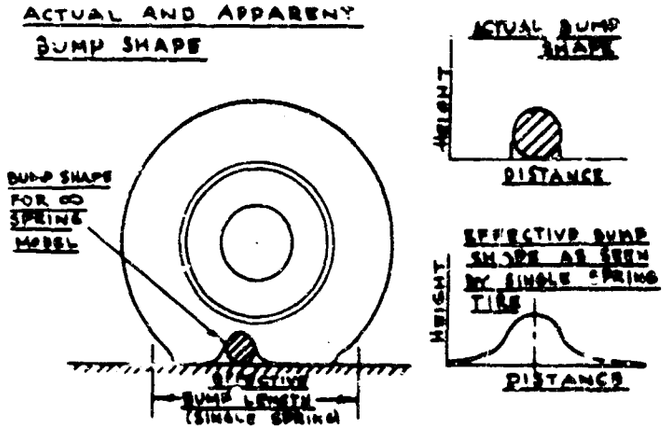

Figure 2-2. Actual and Apparent Bump Shape

The combination of the two features, multiple spring elements and effective bump contour, results in a model which describes the load deflection characteristics of the tire rather well for both the uniform tire deflection and the bump or localized tire deflection.

The model shown for the F4H-1 tire consisted of three spring elements located at ± 4.25 inches from the center and at the center of the tire footprint. Experiments with the tire were conducted to establish the load deflection characteristics of the tire for uniform tire deflection, localized tire deflection, and combinations of both. The bump shape and spring curves are shown in Figures 2-3 and 2-4. A comparison between experimental and mathematical model data is shown in Figures 2-5 and 2-6.

Computer Simulation Study

The F4H-1 main landing gear system was simulated on a Berkeley 1100 Analog Computer. The setup was such that the band-pass unit could be either wired into the system for formulation of the F4H-1 gear with band-pass, or disconnected to simulate the standard landing gear system.

Preliminary runs were made with the standard system to check the computer simulation against airplane drop test results. Run No.207 and Run No.212, Ref. McDonnell Memo 32-529, 17 ft./sec. and 21 ft./sec., three-point landing drops, respectively, were used for comparison with the computer results.

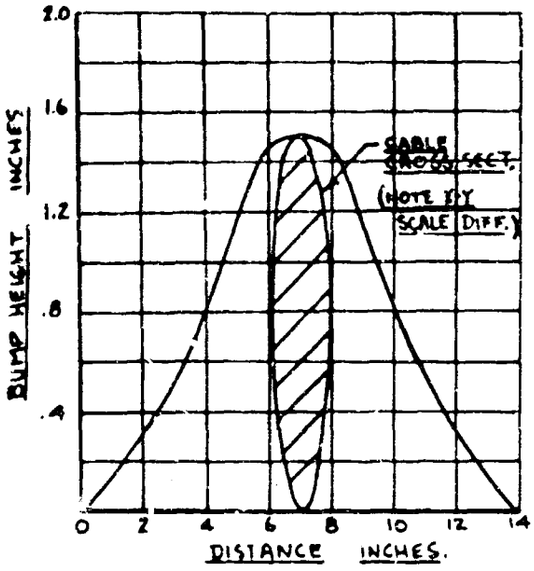

Figure 2-3. Bump Height Vs. Distance Curve

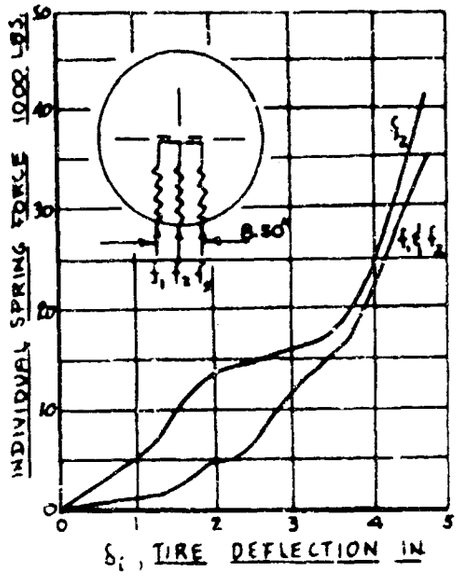

Figure 2-4. Tire Force-Deflection Curves

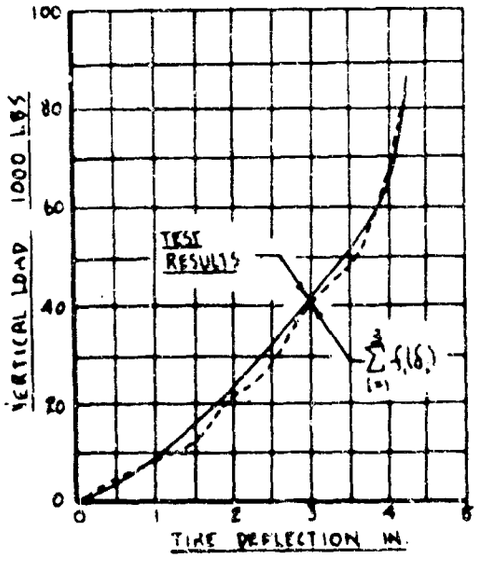

Figure 2-5. Tire Load-Deflection Curves

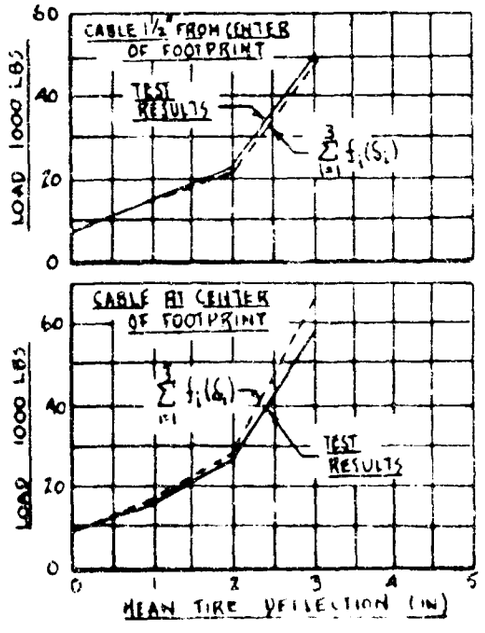

Figure 2-6. Tire Load-Deflection Curves

The following percent differences in load-stroke phenomena were obtained:

Run No.	Energy		%	Max. Load		%	Max. Stroke		%
	Airplane	Computer	Diff.	Airplane	Computer	Diff.	Airplane	Computer	Diff.
207	621,000	600,000	3.5	53,000	50,000	5.7	14.20	14.85	4.4
212	905,000	903,000	0.2	78,000	80,500	3.2	15.0	15.0	0.0

It was felt that the simulation was adequate and the study of the band-pass unit was begun.

A total of ten runs were made through which it was determined that the F4H-1 main landing gear was not adaptable to the band-pass unit. A sample run (Run No.5) is shown in Figure 2-7. Specifically it was found that the pressure signal to the band-pass unit lagged behind the input (the bump impact forces) to such a degree that the impact would be over with before there was any significant rise in the dynamic pressure of the strut. Thus even when the band-pass unit opened fully there was no reduction in impact loads.

Analysis of Computer Simulation Results

Through an analysis of the action of the F4H-1 landing gear it was determined that the excessive lag in the pressure buildup was due to the presence of the high pressure chamber in series with the orifice flow of the strut. The high pressure chamber of the F4H-1 main gear is a feature of the gear which allows the gear to be shrunk for retraction with relatively low loads. This is achieved by incorporating into the strut, in addition to a low pressure air chamber above the dynamic chamber, a high pressure air chamber below the dynamic chamber statically actuated by mechanical contact with the orifice support tube. This results, statically, in a stepped air curve. Up to fourteen inches of stroke, the static resistance of the strut is relatively small. At fourteen inches of stroke the high pressure chamber becomes operative and this chamber can support the static vertical load of the airplane. For retraction, therefore, the gear can be shrunk approximately fourteen inches using low shrinking loads.

Dynamically, however, the chamber can be actuated by the buildup of pressure in the strut. This provides two flow paths for the fluid in the dynamic chamber; first, through the orifice controlled by the metering pin and second, into the volume made available by the piston stroke of the high pressure chamber. This type of action results in the time lag previously mentioned.

It can be shown that the lag between the maximum pressure and the bump force at the tire is given approximately by

$$\Delta t_1 = \frac{\lambda}{2v}$$

for a gear of the F4H-1 type as long as

$$M\left(\frac{2\pi v}{\lambda}\right)^2 >> k$$

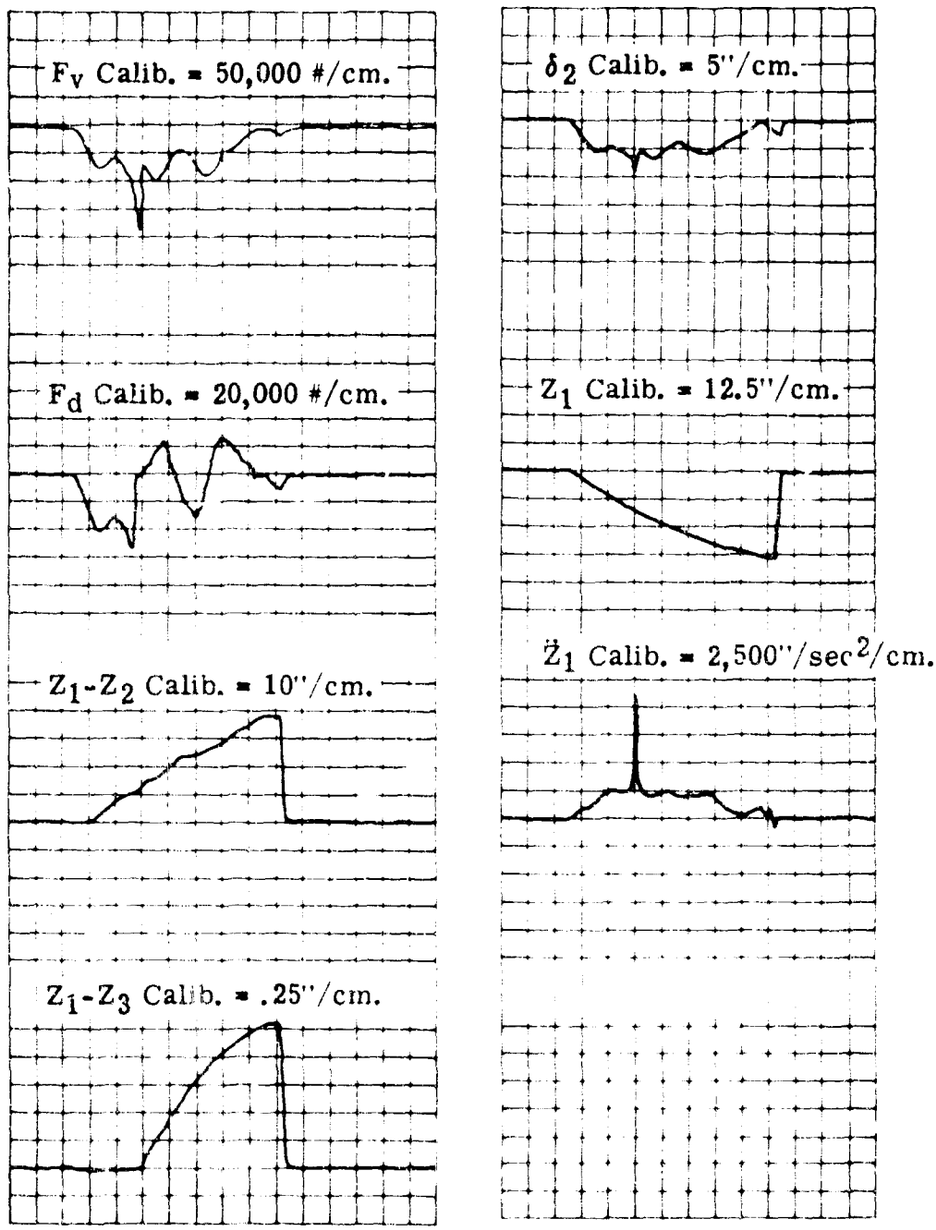

Figure 2-7. Computer Run N 5

where

Δt_1 = time lag
λ = wave length of bump as seen by tire
v = forward velocity of airplane
M = unsprung mass
k = effective spring rate of high pressure air chamber

In contrast to this, a conventional gear will have a time lag approximated by

$$\Delta t_2 = \frac{\lambda}{4V}\left[1 - 2 \arctan\left(\frac{c\,\lambda}{2\pi m v}\right)\right]$$

where

c = equivalent viscous damping coefficient of metering pin and orifice (average stroking force divided by average stroking velocity)

Applying the above equations to the F4H-1 main landing gear for a hypothetical bump

m = .720 lb.-sec.^{2}/in.
λ = 9.0 in.
v = 140 mph = 2460 in./sec.
c = 500 lb.-sec./in.
k = 10,000 lb./in. (average over 2 inches of high pressure chamber compression)

Thus the time between the reaching of the maximum load on the tire and the point of maximum buildup in pressure is

$$\Delta t_1 = \frac{1}{2}\frac{9.0}{2460} = .00183 \text{ seconds}$$

a conventional gear on the other hand would have a time lag of

$$\Delta t_2 = \frac{9.0}{4 \times 2460}\,(1 - 2 \arctan .405)$$

$$\Delta t_2 = .000212 \text{ seconds}$$

The actions of the two types of gears are shown qualitatively in Figures 2 and 2-9.

The analysis of the action indicated also that the time rate of change of the pressure for a gear of the F4H-1 type would lag the maximum impact force by approximately $\Delta t_1/2$ while in a conventional system the same item would lead the impact force. Thus a conventional system will anticipate high impact loads while the F4H-1 system will not.

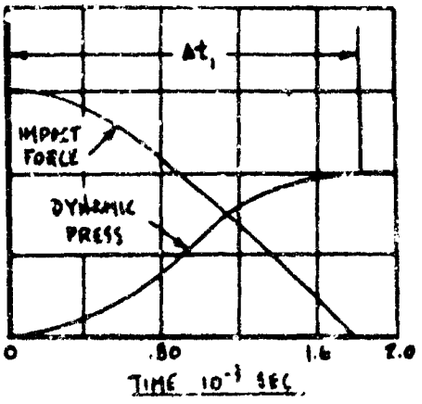

Figure 2-8. Gear Response

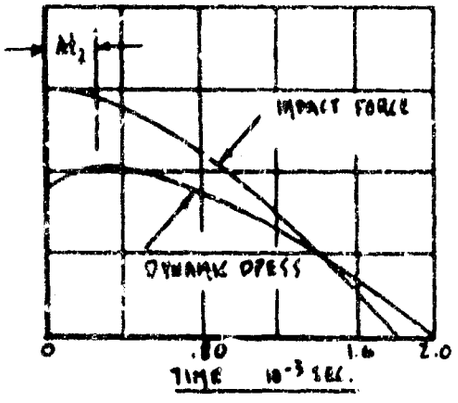

Figure 2-9. Gear Response

The expression for Δt_1 was checked against the computer results and it was found that the time lag on the computer simulation correlated well with the prediction. For example, the time lag found in Run No.5 was

$$\Delta t = .0040 \text{ seconds}$$

The pertinent data for this run is

$$\lambda = 22.5$$
$$v = 2550 \text{ in./sec.}$$

Thus

$$\Delta t_1 = \frac{1}{2}\frac{\lambda}{v} = .0044 \text{ seconds}$$

Checking

$$m\left(\frac{2\pi v}{\lambda}\right)^2 \text{ in comparison to } k$$

$$m\left(\frac{2\pi v}{\lambda}\right)^2 = 36.4 \times 10^4 \text{ lb./in.}, \qquad k = 1.0 \times 10^4 \text{ lb./in.}$$

Since the spring rate is considerably below the "inertia" term, the time lag should tend toward that given by the Δt_1 expression-which it does.

The comparison test of the inertia term to the spring rate term provides a useful check on whether or not the compressibility is significant if

$$m\left(\frac{2\pi v}{\lambda}\right)^2 >> k$$

Then the compressibility effect predominates

If

$$k >> m\left(\frac{2\pi v}{\lambda}\right)^2 ,$$

then the compressibility effect is insignificant.

It is interesting to note that a conventional strut has some fluid compressibility which would tend to duplicate the action of the F4H-1 high pressure chamber if the bulk modulus was too low. However, it is seen that

$$k_{fluid} = \frac{A_p^2 B}{v_o}$$

where

A_p = air piston area
B = bulk modulus of fluid
v_o = volume of strut lower chamber

For a typical main gear these quantities are of the following orders of magnitude

A_p = 15 in.^{2}
B = 300,000 lb./in.^{2}
v_o = 50 in.^{3}

Thus

k = 1.35×10^6 lb./in.

which is considerably above the "inertia" term magnitude previously calculated as 36.4×10^4 lb./in. A conventional gear would therefore tend toward the action predicted by the expression for Δt_2 which was derived on the bases of incompressible orifice flow in the strut.

Modification of F4H-1 Main Gear and Model

For purposes of the computer study of band-pass, it would be possible to modify the F4H-1 gear model to do away with the time lag previously discussed. Such a modification is shown in Figure 2-10. Here it is seen that the motion of the high pressure piston has essentially been uncoupled from the dynamic pressure of the strut. Compression of the high pressure chamber takes place only when there is mechanical contact between the metering pin support tube and the piston of the high pressure chamber. This type of action

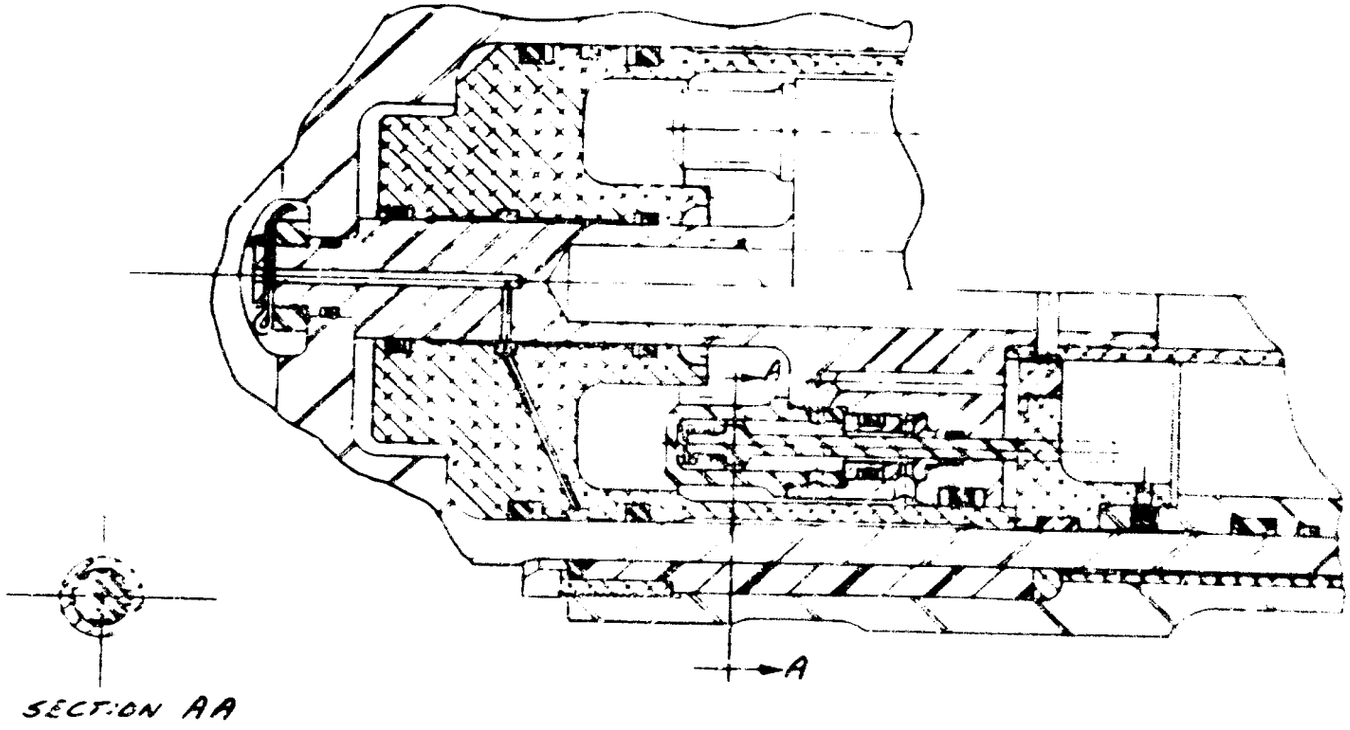

Figure 2-10. Proposed Blocking Valve For F4H MLG Band-Pass Shock Strut

converts the F4H-1 gear to a conventional system in net effects. The high pressure chamber simply causes a stepped air curve for the strut while a conventional strut has a smooth air curve corresponding approximately to the isothermal air compression process.

The above modification would require a redevelopment (analytically) of the metering pin since it substantially affects the energy absorbing characteristics of the gear. Furthermore, if simulation of present airplane-drop characteristics is desired, it is possible that several metering pins would have to be analytically developed for the modified gear.

CONCLUSIONS AND RECOMMENDATIONS

It was concluded from the computer results that a band-pass unit will not function properly in the F4H-1 main gear. The inability of the band-pass unit to function was traced to the presence of the high pressure air chamber in series with the strut orifice flow.

Based on analytical studies of a conventional system it was concluded that a conventional gear should not have this same difficulty. The band-pass unit should be able to anticipate the high load from bump impact due to its sensitivity to the rate of pressure buildup in the dynamic pressure chamber of the strut.

Based on studies of the F4H-1 gear structure, it was determined that mechanical changes in the gear could be made to eliminate the time lag effect of the high pressure chamber. Such changes would require a "paper" redesign of the pin configuration to duplicate airplane characteristics.

It was recommended that the band-pass development program be continued using another more conventional landing gear system, such as the A3J-1 or the F9F main gear, rather than a modified F4H-1 main gear. The simulation achieved in this study was felt to be sufficient to warrant a more extensive analytical study of the band-pass principle, as applied to the landing gear shock strut, than that originally proposed. Such an extension would allow the detailed study of the loads transmitted into the wheel and unsprung mass by bump impact in addition to the study already proposed in which band-pass was to be evaluated on only the net improvement it provided in the loads transmitted to the airframe proper. In addition, miscellaneous exploratory studies such as that undertaken to improve the tire model, were felt to be in order.

SECTION III

TECHNICAL DISCUSSION - NORTH AMERICAN A3J-1 MLG THEORETICAL STUDIES

The general objectives of this phase of the program were achieved by a program combining pure analytical, experimental, and analog computer methods. In summary, the program was as follows:

1. Development of a simplified mathematical model of the band-pass mechanism.
2. Linearized study of the above model.
3. Analog computer study of this model.
4. Tire model investigations.
5. Study of the complete landing gear system with and without band-pass by analog computer simulations.

DEVELOPMENT OF A SIMPLIFIED MATHEMATICAL MODEL OF THE BAND-PASS MECHANISM

In Bendix Report VP-1030, the model set up to study the band-pass mechanism adapted to an airplane main landing gear system consisted of a five-degree of freedom nonlinear dynamical system. Although such a model is necessary for detailed load and motion determinations, it is not highly suitable to study the details of the band-pass system itself. This is due to two factors. First, the complexity of the system makes it impossible to reduce the resulting pressure build-up and associated motions to simple expressions in which the influence of the band-pass parameters is apparent. Secondly, the complexity of the system requires an extensive computer setup (approximately seventy-five amplifiers plus eleven function generators and associated equipment) which in turn requires considerable time and diligence to assure correct results. For these two reasons, a simplified model was sought to help determine the influence of the parameters associated with the band-pass mechanism on the output of the system. The output of the system was considered to consist of tire vertical load, dynamic chamber hydraulic pressure, main mass vertical acceleration, etc.

Since all of these outputs were ultimately related to the dynamic chamber hydraulic pressure, the first simplification in concept consisted of localizing the over-all effect of the band-pass mechanism to its effect on the dynamic chamber pressure. The second

simplification had to do with input to the system. For the complete landing gear system, the input consists of an obstruction on the runway surface. Here again the net effect of this from the standpoint of its effect on the band-pass system was a sudden relative movement between the outer cylinder and the piston. Thus, the second simplification consisted of reducing the input to a sinusoidal stroke of the shock strut. Further simplification was achieved by noting that the incremental stroke of the shock strut during bump impact was small, thus changes in the orifice size due to metering pin movement would be small; and changes in the air pressure in the struts upper chamber would be small since this is also a function of stroke. Still further simplification was achieved by noting that the total bump impulse was small due to its short time duration. Therefore, changes in the main mass' motion during bump impact would be small. Thus the feedback from the dynamic strut pressure to the main mass' motion could be eliminated.

These simplifications result in the reduction of the system to that of a single degree of freedom. Although some of the simplifications are broad, they are based on both the initial band-pass studies of the F4H-1 main gear, and on experimental experience on main-gear drop tests. With reasonable stroke input, the results of the simplified study from the standpoint of the band-pass parameter effects agree very well with later studies using the complete five-degree of freedom system.

A schematic of the band-pass mechanism is shown in Figure 3-1A. Figure 3-1B is a free body diagram of the simplified system. The simplifications mentioned above are reflected in the motions and pressures shown in the free body diagram.

The fluid flow from the dynamic chamber takes place through three areas. The first is the main metering orifice, the second is through the inlet to the band-pass control chamber, and the third is the variable valve area opened by the stroke of the band-pass plunger. Volume is gained in the dynamic chamber by both the fluid compression and by the upward movement of the band-pass control plunger. The continuity equation is therefore

$$A_{P_1}(\dot{Z}_1 - \dot{Z}_2) - \frac{V_D}{B}\dot{P}_1 - A_{P_3}(\dot{Z}_1 - \dot{Z}_3) = C_D A_0 \sqrt{\frac{2}{\rho}(P_1 - P_2)} + C_D A_V \sqrt{\frac{2(P_1 - P_2)}{\rho}} + C_D A_{0B}\sqrt{\frac{2(P_1 - P_3)}{\rho}} - C_D A_{0S}\sqrt{\frac{2(P_2 - P_3)}{\rho}} \quad (1)$$

The term $C_D A_{0S}\sqrt{\frac{2(P_2 - P_3)}{\rho}}$ is to account for a relief valve, to allow free flow into the dynamic chamber, when P_2 becomes greater than P_1. For bump impact during landing impact, P_1 is considerably greater than P_2 at all times so that this term is zero and does not enter into the problem. It should also be noted that the square root notation used above is shorthand for the inverted square root function and should be interpreted as $|\Delta P|^{1/2}(\Delta P)^{-1}$.

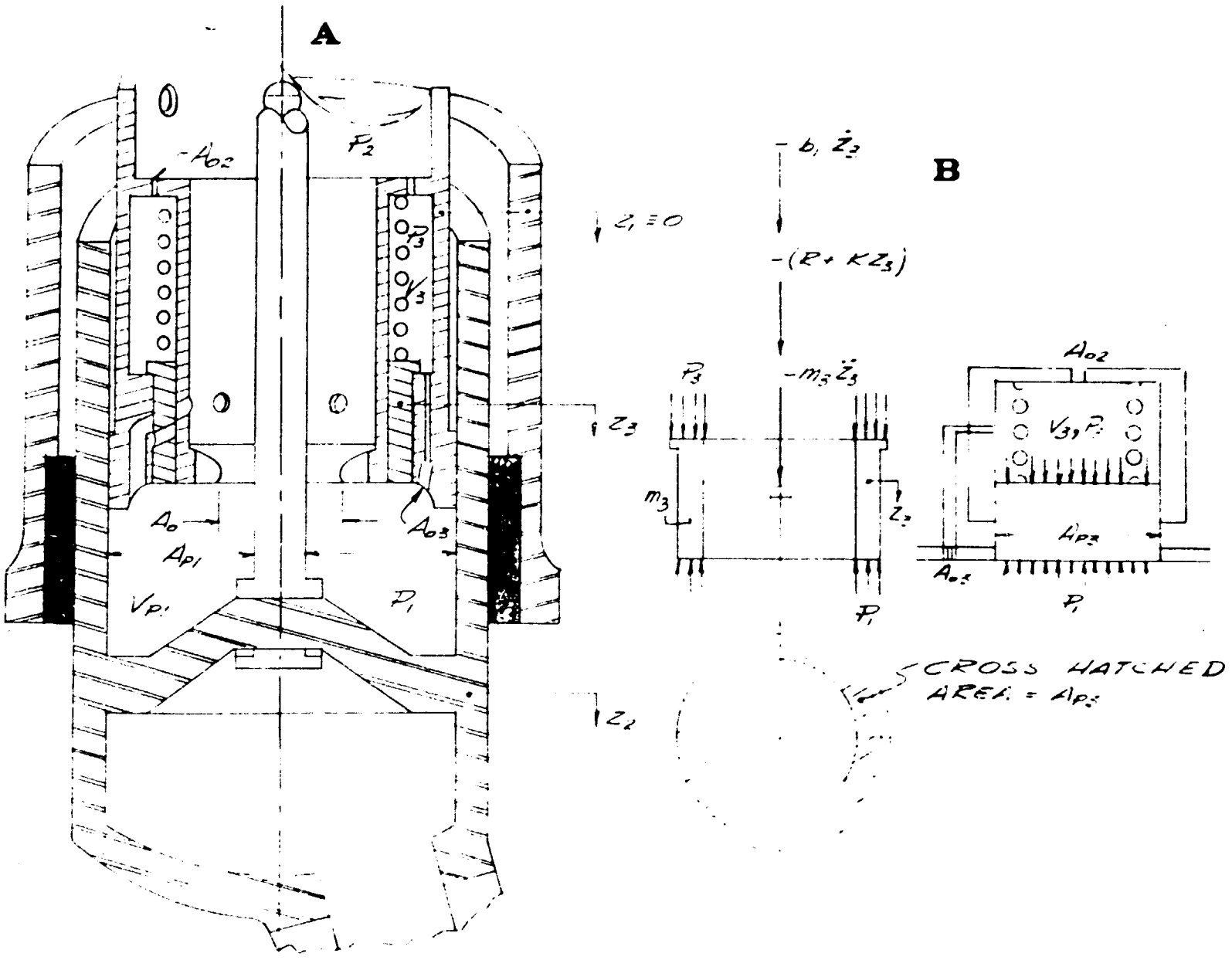

Figure 3-1. Schematics and Free Body Diagram Low Pass Hydraulic Band-Pass Filter Installed in Main Landing Gear Shock Strut

The compatibility of the flow into and out of the band-pass control chamber is defined by

$$A_{P3}(\dot{Z}_1 - \dot{Z}_3) - \frac{V_{P3}}{\beta}\dot{P}_3 + C_D A_{03}\sqrt{\frac{2(P_1 - P_3)}{\rho}} = C_D A_{02}\sqrt{\frac{2(P_3 - P_2)}{\rho}} \qquad (2)$$

The summation of forces acting on the band-pass valve plunger is given by

$$m_3\ddot{Z}_3 = b_1(\dot{Z}_1 - \dot{Z}_3) + K_S(Z_1 - Z_3) + A_{P3}(P_3 - P_1) + R \qquad (3)$$

Where R is the spring preload of the control chamber spring. It should be noted that K_s must be considered nonlinear to account for plunger valve bottoming. This is accomplished by considering K_s as very large for positive $(Z_1 - Z_3)$ and the normal spring rate for negative $(Z_1 - Z_3)$.

With the simplifications mentioned previously these equations reduce to

$$A_{X1}\dot{Z}_2 + \frac{V_D}{\beta}\dot{P}_1 - A_{P3}\dot{Z}_3 + C_D A_0\sqrt{\frac{2(P_1 - P_3)}{\rho}} - C_D A_V Z_3\sqrt{\frac{2(P_1 - P_3)}{\rho}} + C_D A_{03}\sqrt{\frac{2(P_1 - P_3)}{\rho}} = 0 \qquad (4)$$

$$A_{X3}\dot{Z}_3 + \frac{V_{P3}}{\beta}\dot{P}_3 - C_D A_{03}\sqrt{\frac{2(P_1 - P_3)}{\rho}} + C_D A_{02}\sqrt{\frac{2(P_3 - P_2)}{\rho}} = 0 \qquad (5)$$

and the equation of motion of the valve plunger becomes

$$m_3\ddot{Z}_3 + b\dot{Z}_3 + K_S\dot{Z}_3 + A_{P3}(P_1 - P_3) - R = 0 \qquad (6)$$

Equations (4), (5), and (6) constitute the equations of motion of the simplified model of the band-pass mechanism. Using the above equations, two studies were conducted. The first consisted of the linearization of the above equations so as to reduce them to being amenable to analytic solution. The second study consisted of the analog computer solution of the equations. The linearized solution is covered in Bendix Report No. SH-61-2, and only the results will be covered here.

RESULTS OF LINEARIZED ANALYTICAL STUDY OF SIMPLIFIED MODEL

The null pressures are the pressures obtained for a fixed value of $\dot{Z}_2$ when Z_3 and $\dot{Z}_3$

are zero. These constitute the pressures about which perturbations caused by the motion of the band-pass valve take place. The most important of these null pressures is $(P_1 - P_3)_0$ which determines the amount of preload necessary to prevent opening of the valve for normal landing impact stroke velocities. This pressure also differentiates the hydraulic band-pass filter from a normal poppet valve. A normal poppet valve would be acted upon only by the pressure P_1. The band-pass valve will remain closed even though P_1 exceeds the preload of the valve since the pressure P_3 counteracts the P_1 pressure. The null $P_1 - P_3$ pressure is given by

$$(P_1 - P_3)_0 = \frac{A_{P1} \dot{Z}_2^2}{\frac{2C_d^2}{\rho}\left[A_o - \frac{A_{03}}{\left[1 + \left(\frac{A_{03}}{A_{02}}\right)^2\right]^{1/2}}\right]^2 \left[1 + \frac{A_o^2}{A_{02}^2}\right]} \tag{7}$$

The null $P_1 - P_2$ pressure is given by

$$P_1 - P_2 = \frac{A_D^2 \dot{Z}_2^2}{\frac{2C_d^2}{\rho}\left[A_o + \frac{A_{03}}{\left[1 + \left(\frac{A_{03}}{A_{02}}\right)^2\right]^{1/2}}\right]^2} \tag{8}$$

The time solution for the dynamic chamber pressure is given by

$$P_2 = \frac{\rho}{2} \Delta Z_2 \omega \left[K_1 e^{-\lambda_1 t} \sin \omega t + \right.$$
$$\left. + K_2 \cos \omega t + K_3 + K_4 e^{-\lambda_2 t} + K_5 e^{-\lambda_3 t} \right] \tag{9}$$

where

ρ = mass density of hydraulic

ΔZ_2 = perturbation in stroke input

ω = frequency of half sine bump input

The remaining constants depend on the roots of the characteristic equation and the roots of the cubic numerator of the ΔP_1 transfer function.

$$s^4 + \left(\frac{\beta}{\alpha} + 2\zeta\omega_n\right)s^3 + \left(\frac{\gamma}{\alpha} + \omega_n^2\left[1 + \frac{A_{P3}^2}{3K_S}(V_{P1} + V_{P3})\right] + \frac{\beta}{\alpha}2\zeta\omega_n\right)s^2$$

$$+ \left\{\frac{\gamma}{\alpha}2\zeta\omega_n + \frac{\omega_n^2}{\alpha}\left[\beta + \frac{C_S A_{P3} a_v V_{P3}}{3K_S} + \frac{A_{P3}^2}{K_S}(C_3 + C_n)\right]\right\}s$$

$$+ \frac{\omega_n^2}{\alpha}\left(\gamma + \frac{C_S a_v A_{P3} C_3}{K_S}\right) = 0$$

where

$$\omega_n^2 = \frac{K_S}{M_3}$$

$$\zeta = b_1 / 2\sqrt{K_S M_3}$$

$$c_1 = \frac{\sqrt{\frac{2}{\rho}}\, C_D (A_0)_0}{2\sqrt{(P_1 - P_2)_0}}$$

$$c_2 = \frac{\sqrt{\frac{2}{\rho}}\, C_D A_{03}}{2\sqrt{(P_1 - P_3)_0}}$$

$$c_3 = \frac{\sqrt{\frac{2}{\rho}}\, C_D A_{02}}{2\sqrt{(P_3 - P_2)_0}}$$

$$c_4 = \frac{\sqrt{\frac{2}{\rho}}\, C_D a_v (z_3)_0}{2\sqrt{(P_1 - P_2)_0}}$$

$$\zeta = \sqrt{\frac{I_z}{\rho}}\, C_{2D}\sqrt{\quad}$$

$$C_6 = C_3 + C_2$$

$$C_7 = C_1 + C_4$$

$$\omega = \frac{V_{D1}\, V_{D2}}{B^2}$$

$$\gamma = \frac{1}{2}\left[V_{D3}(C_5 + C_7) + C_6 V_{D2}\right]$$

$$\delta = C_5 C_2 + C_6 C_7$$

The roots of the characteristic equation must be computed. For systems similar to that investigated, the roots of the characteristic equation will consist of two real roots and one set of complex conjugates. These roots are denoted as

$$-a_1 \;,\; \cdots i \;,\; -a_4 \pm b_4 i$$

The cubic numerator is

$$s^3 + \left(\frac{C_6 B}{V_{D3}} + 2\zeta\omega_n\right)s^2 + \left[\left(1 + \frac{A_{D2}}{V_{D2}} \cdot \frac{B}{C_2}\right)\omega_n^2 + \frac{C_6 B}{V_{D2}}\, 2\zeta\omega_n\right] s$$

$$+ \frac{C_6 B}{V_{D3}}\,\omega_n^2 \;=\; 0$$

The roots of this equation are

$$-a_3 \;,\; -a_2 \pm b_2 i$$

In terms of the above constants and roots, γ_7 thru γ_{10} are defined as follows

$$\gamma_7 = \left[\frac{(a_4^2 + \omega^2)\left[(a_3 - a_4)^2 + b_4^2\right]\left\{\left[(a_5 - x_5)^2 + b_5^2 - b_4^2\right]^2 + 4b_4^2(a_5 - x_5)^2\right\}}{b_4^2(a_1 - a_3)^2 + b_4^2\left[(a_2 - a_4)^2 + b_4^2\right]\left[(x_4^2 - \omega^2 - b_4^2)^2 + 4x_4^2 b_4^2\right]} \right]^{1/2}$$

$$\gamma_8 = \left\{ \frac{(a_3^2 + \omega^2)\left[(a_5^2 + b_5^2 - \omega^2)^2 + 4a_5^2\omega^2\right]}{(a_1^2 + \omega^2)(a_2^2 + \omega^2)\left[(a_4^2 + b_4^2 - \omega^2) + 4x_4^2\right]^2} \right\}^{1/2}$$

$$\gamma_9 = \frac{(a_2 - a_1)\left[(a_3 - x_3)^2 + b_3^2\right]}{(a_3 - a_1)\left[(x_4 - a_1)^2 + b_4^2\right](a_2^2 + \omega^2)}$$

$$\gamma_{10} = \frac{(a_3 - a_2)(a_5 - x_5)\left[(a_5 - x_5)^2 + b_5^2\right]}{(a_1 - a_2)\left[(a_4 - x_4)^2 + b_4^2\right](x_5^2 + \omega^2)}$$

$$\psi_1 = \theta_1 + \theta_2 + \theta_3 - \theta_4 - \theta_5 - \theta_6$$

$$\theta_1 = TAN^{-1}\left(\frac{-b_4}{-a_4}\right)$$

$$\theta_2 = TAN^{-1}\left(\frac{-b_4}{a_3 - a_4}\right)$$

$$\theta_3 = TAN^{-1}\left[\frac{-2b_4(a_5 - x_4)}{(a_5 - a_4)^2 + b_5^2 - b_4^2}\right]$$

$$\theta_4 = TAN^{-1}\left(\frac{-b_4}{a_1 - a_4}\right)$$

$$\theta_5 = TAN^{-1}\left(\frac{-b_4}{a_2 - a_4}\right)$$

$$\theta_6 = TAN^{-1}\left(\frac{2b_4 a_4}{a_4^2 + \omega^2 - b_4^2}\right)$$

$$\psi_2 = \theta_7 + \theta_8 - \theta_9 - \theta_{10} - \theta_{11}$$

$$\theta_7 = TAN^{-1}\frac{\omega}{a_3} \; ; \quad \theta_8 = TAN^{-1}\left(\frac{2a_2\omega}{a_2^2 + b_2^2 - \omega^2}\right)$$

$$\theta_9 = TAN^{-1}\frac{\omega}{a_1} \; ; \quad \theta_{10} = TAN^{-1}\frac{\omega}{a_2}$$

$$\theta_{11} = TAN^{-1}\left(\frac{2a_6\omega}{a_6^2 + b_6^2 - \omega^2}\right)$$

The valve movement is given by

$$\Delta Z_3(t) = K_3 \Delta Z_2 \omega \left[\gamma_{11} e^{-a_6 t} SIN(b_6 t - \psi_3) + \gamma_{12} COS(\omega t + \psi_4) + \gamma_{13} e^{-a_1 t} + \gamma_{14} e^{-a_2 t}\right] \quad (10)$$

where

$$K_3 = \frac{B A_{P1} A_{P3}}{V_{P1} M_3}$$

$$\gamma_{11} = \left\{\frac{(a_6^2 + b_6^2)\left[(a_6 - a_6)^2 + b_6^2\right]}{b_6^2\left[(a_1 - a_6)^2 + b_6^2\right]\left[(a_2 - a_6)^2 + b_6^2\right]\left[(a_6^2 + \omega^2 - b_6^2)^2 + 4a_6^2 b_6^2\right]}\right\}^{1/2}$$

$$\gamma_{12} = \left[\frac{(a_6^2 + \omega^2)}{(a_1^2 + \omega^2)(a_2^2 + \omega^2)\left[(a_6^2 + b_6^2 - \omega^2) + 4a_6^2\omega^2\right]}\right]^{1/2} \quad (11)$$

$$\gamma_{13} = \frac{(-a_1)(a_6 - a_1)}{(a_2 - a_1)\left[(a_6 - a_1)^2 + b_6^2\right](a_1^2 + \omega^2)}$$

$$\gamma_{14} = \frac{(-a_2)(a_6 - a_2)}{(a_1 - a_2)\left[(a_6 - a_2)^2 + b_6^2\right](a_2^2 + \omega^2)}$$

$$\theta_3 = \theta_1 + \theta_{12} - \theta_7 - \theta_8 - \theta_9$$

$$\theta_{12} = TAN^{-1}\left|\frac{-a_2}{a_4 - a_1}\right| \qquad (11)$$

$$\theta_9 = \theta_{13} - \theta_{14} - \theta_{10} - \theta_{11}$$

$$\theta_{13} = TAN^{-1}\left|\frac{\omega}{\alpha_6}\right|$$

As an example of the application of the above equations, a comparison between analog computer results and the results calculated from the linearized solution is shown in Figure 3-2. The linearized results shown in this figure are based on Equation (9) with high frequency terms dropped. This is discussed in more detail in the report covering the linearized study.

ANALOG COMPUTER STUDY OF SIMPLIFIED MODEL

A series of studies on an analog computer were carried out using the simplified model of the band-pass shock strut. The procedure used in this study was to prescribe to Z_2 a steady velocity simulating the stroke velocity of the strut during landing impact, plus a half-wave sinusoidal displacement simulating the additional stroke occuring during simultaneous landing and bump impact. The magnitude of the stroke was determined on a somewhat empirical basis. It was first determined that a full one-and-one-half inches of half-wave sinusoidal stroke would result in unrealistically large loads. This is, of course, to be expected since the gear stroke caused by bump impact is reduced in the actual gear by both the wheel and tire deformation, and by the slight upward movement of the main mass. It was known from the original studies on the F4H-1 gear that a severe bump impact would raise the internal pressure of the strut about 15 percent over the pressure obtained in a limit drop. Using this concept plus data from A3J-1 main gear drop tests conducted at Bendix (Ref. 4), a realistic sinusoidal stroke was obtained as an input to the system.

The steady strut-stroke velocity was selected to duplicate dynamic chamber pressures obtained during the same limit drops for a main metering orifice area equal to the average area in the total stroke. The combination of orifice area and steady-stroke velocity was later varied in the parameter variation studies.

Nominal data for the study was as follows:

$A_0 = .45$ in.^{2}

$A_{02} = .001$ in.^{2}

$A_{03} = .010$ in.^{3}

A_{p1} = 20.428 in.^{2}

A_{p3} = .785 in.^{2}

a_v = 10 in.^{2}/in.

b = value to yield 10 percent critically damped system

k = 100 lb./in.

M_3 = .00035 lb. sec.^{2}/in.

R = 100 lb.

V_{p1} = 200 in.^{3}

V_{p3} = 3.0 in.^{3}

Z_2 = 125 in. sec. (steady stroke velocity)

Z_2 = .141 in.

The results of this study are shown in Figures 3-3 thru 3-8. Figure 3-3 shows the analog computer time solutions for the nominal case given above. Figures 3-4 and 3-5 are two runs for which the valve motion became unstable and are discussed below in the parameter variations discussion. Figures 3-6, 3-7, and 3-8 are results of the parameter variation study in terms of the maximum pressure rise caused by the bump impact and the maximum valve stroke.

Figure 3-6A shows the effect of volume changes in the dynamic chamber of the shock strut. Here it can be seen that the net pressure rise caused by the bump impact is insensitive to volume changes. However, the plunger valve stroke is influenced -- dropping off as the volume of the dynamic chamber is increased. At first the results appear to be contradictory. That is, with decreased stroke, it would seem that the incremental pressure rise should increase since there is less opening of the orifice area between the dynamic chamber and air chamber of the strut. However, it is to be noted that an increase in volume also corresponds to a drop-off in the spring rate of the fluid so that there is a larger shock-absorbing capability in the fluid. This counterbalances the lowered orifice resistance caused by the larger orifice opening. The over-all effect of volume change is an important aspect of the parameter variation study since the fluid volume of the dynamic chamber does vary with stroke. The valve instability found at the lower dynamic chamber volumes put a serious limitation on the other parameters of the band-pass unit. For example, it can be seen that an improvement in the total pressure rise could be gained by reducing the outlet orifice area and the inlet orifice area down to perhaps 6×10^{-4} in.^{2} and 6×10^{-3} in.^{2}, respectively. However, this also would lead to a marginally stable system for the nominal dynamic chamber volume of 200 in.^{3}. Further, it would lead to a highly unstable valve motion when the strut was compressed

(text continued on page 3-17)

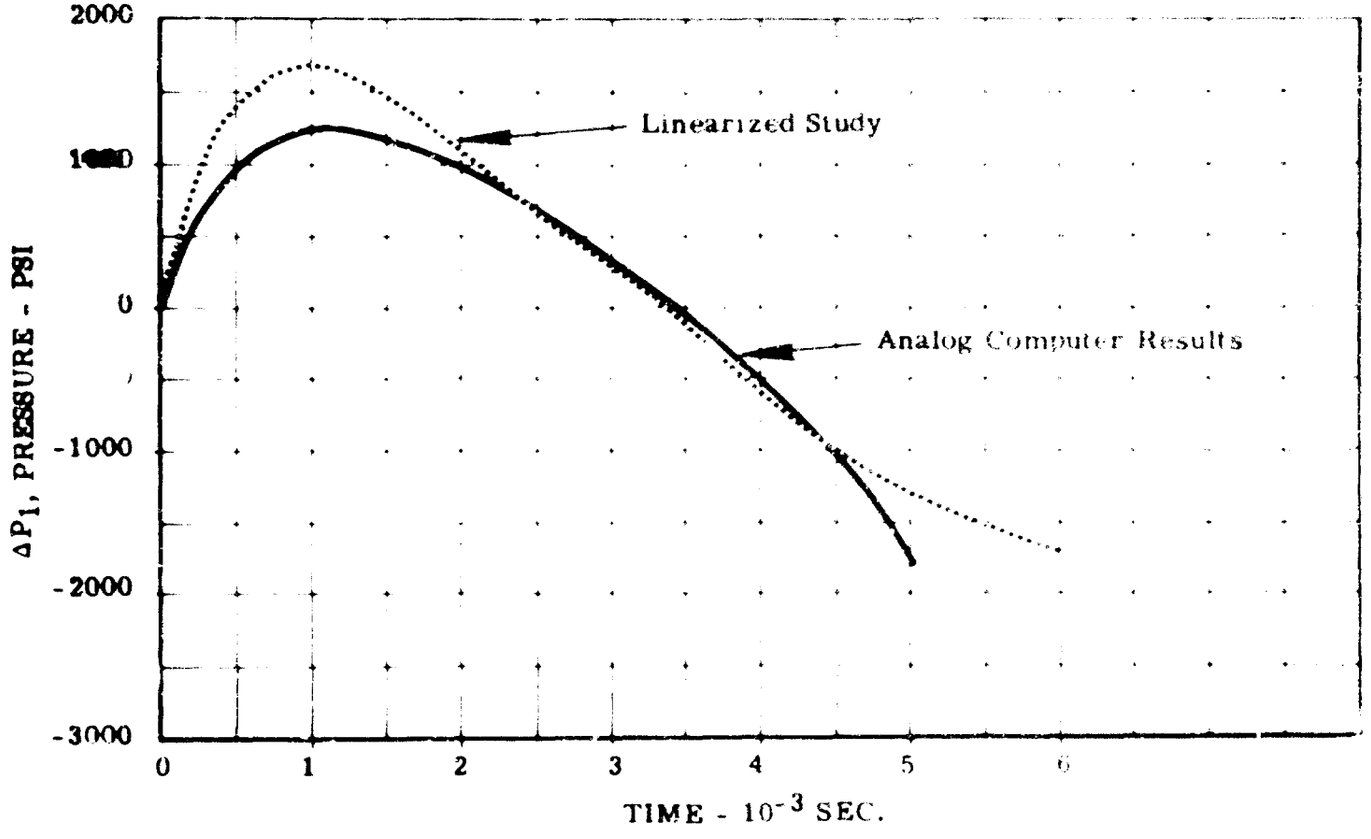

Figure 3-2. Comparison of Results of Linearized Study and Analog Computer Results

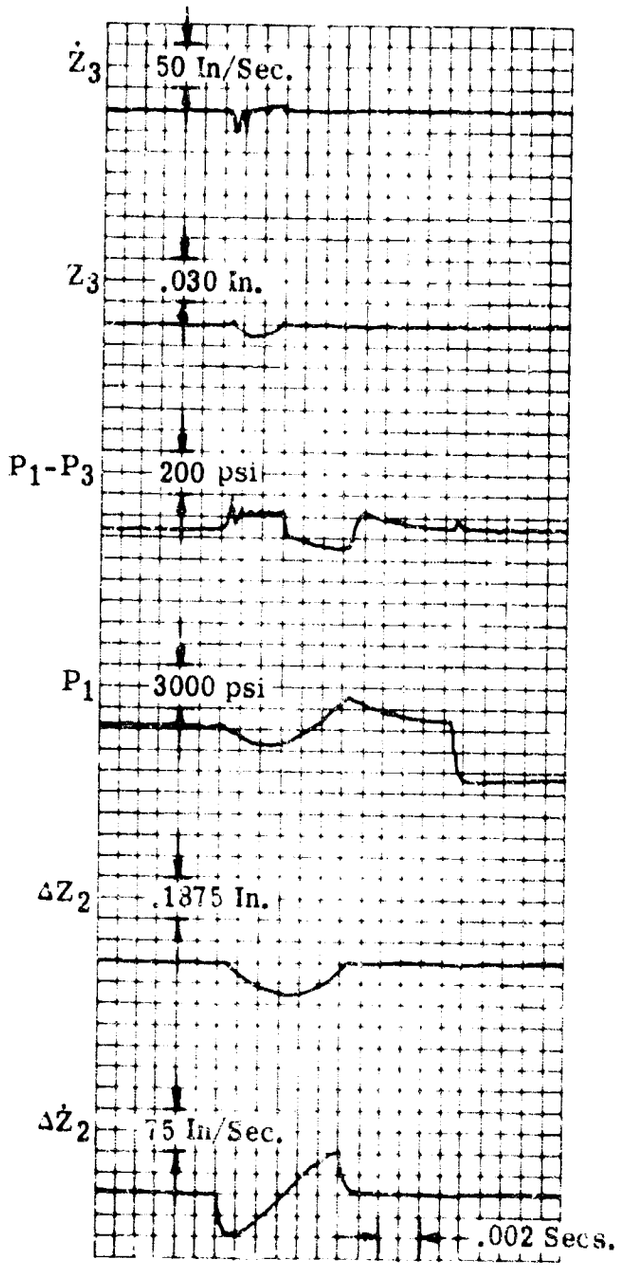

Figure 3-3. Computer Results Simplified Model Nominal Case

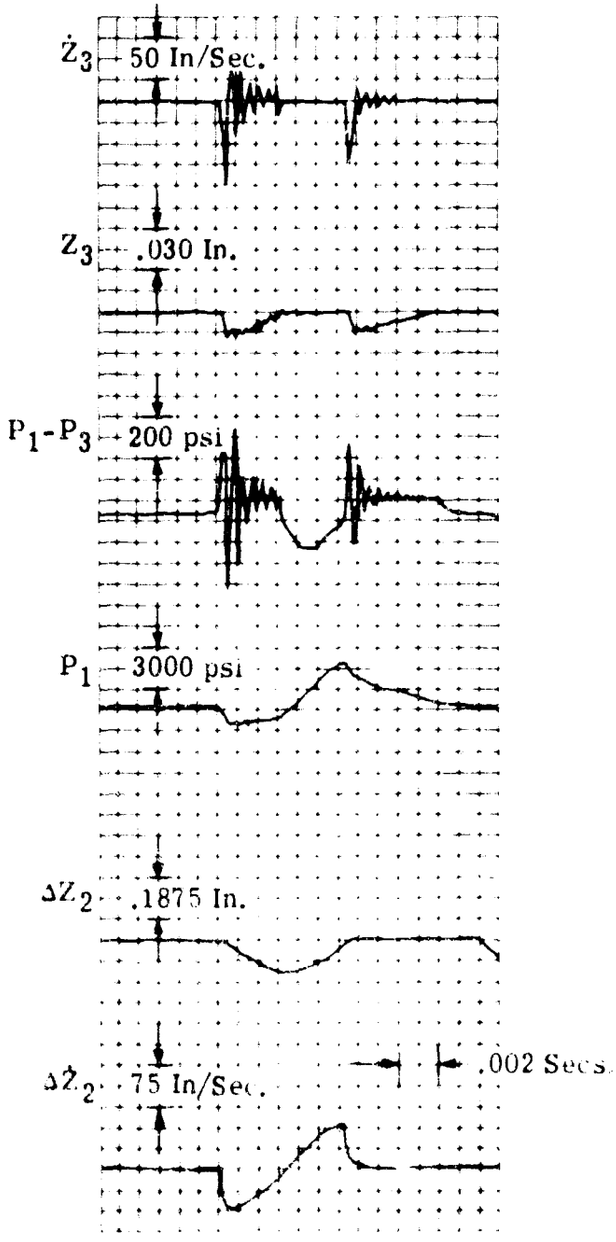

Figure 3-4. Computer Results Simplified Model $V_{p1} = 50$ in.^{3}

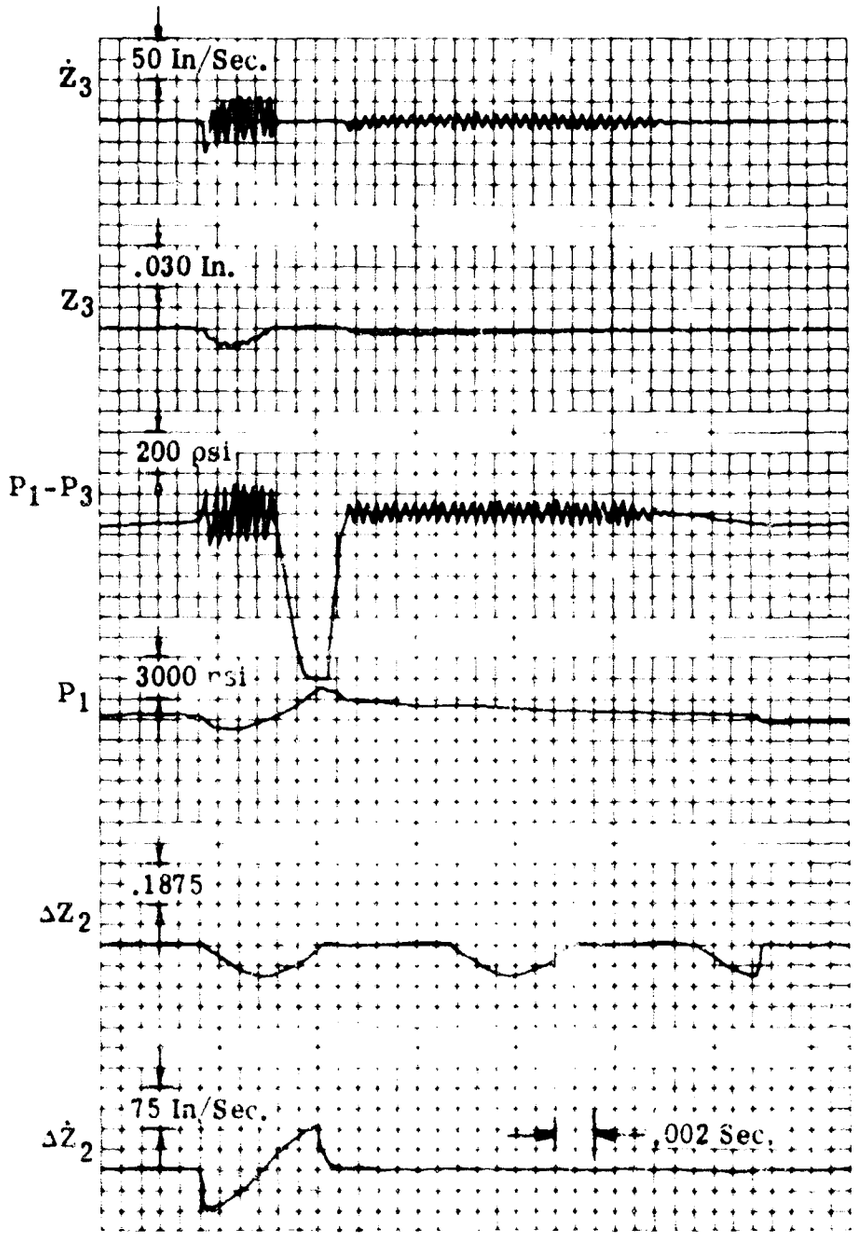

Figure 3-5 Computer Results - Simplified Model

A_{O2} = .000143 in.^{2} A_{O3} A_{O2} = 10.0

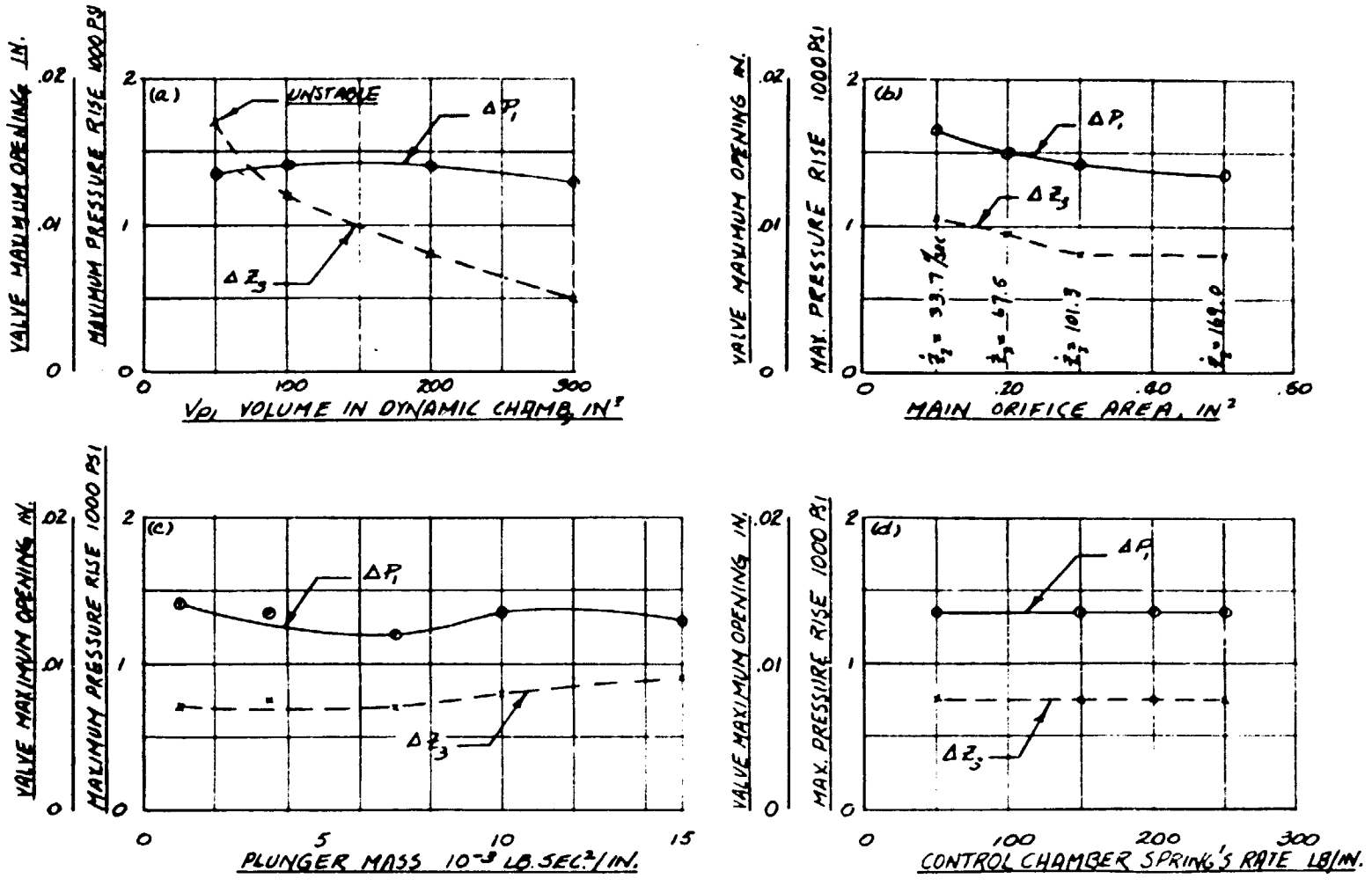

Figure 3-6. Parameter Variation Studies Simplified Band-Pass Shock Strut Model Analog Computer Solutions

to any volume below -- say 150 in.^{3}. Since such reduced volume on the dynamic chamber does take place in actual gear operation, it limits the amount of improvement that can be made by any other parameter variations which improve the net pressure rise in the strut during impact and, at the same time, results in a marginally stable valve.

To illustrate the general nature of the instability encountered with reduced dynamic chamber volume, the computer time solution for the case marked unstable in Figure 3-6A is shown in Figure 3-4.

The second parameter variation study was carried out to find the effect of changes in the main orifice area which in the actual strut would vary due to the variable area of the metering pin. The results of this study are shown in Figure 3-6B. Since the pin is designed to yield high efficiency in the load stroke curve, low areas will, in general, correspond to low stroke velocities and large orifice areas to higher stroke velocities. For this reason, the stroke velocity was varied along with the orifice area to maintain a near constant null P_1 pressure and thus simulate normal landing impact conditions. The variations in the stroke velocity for each particular orifice area are noted in Figure 3-6B.

From Figure 3-6B it can be seen that the net pressure rise and valve stroke are relatively insensitive to the main orifice area. A design based on average orifice area and average piston stroke velocity should, therefore, accommodate the whole range of stroke velocities and orifice areas encountered in going from an extended to a compressed shock strut, providing cognizance is taken of the critical stability condition encountered with the low dynamic chamber volume associated with the compressed and near compressed shock strut.

The effect of plunger valve mass is shown in Figure 3-6C. Here it can be seen that the incremental pressure rise and the valve stroke are relatively insensitive to the plunger mass. Some slight improvement could be made over the nominal case by an increase of the mass to the vicinity of 7×10^{-3} lb. sec.^{2}/in. which appears to be a minimum point on the ΔP_1 function. The relative insensitivity of the output on the valve mass allows considerable latitude on its design and, if necessary, it could be designed by strength and size considerations without appreciably affecting the output of the band-pass unit. This is true over a limited range of mass values. Figures 3-9A and 3-9B show the computer time solutions for the two extreme mass values, 1×10^{-3} and 15×10^{-3} lb. sec.^{2}/in., respectively. Here it can be seen that the smallest mass value is tending toward valve instability although the slight valve flutter is not yet large enough to be reflected in the P_1 pressure and is only evidenced in the differential pressure across the valve area ($P_1 - P_3$). The largest mass value results in a quite stable valve but it can be seen that the time delay between the beginning of strut sinusoidal stroke and plunger valve movement has increased slightly. A careful measurement on the records indicated a time delay approximately 15 percent greater than the time delay found with smallest mass. The valve stroke is also less abrupt for the large mass case. The small mass case has practically a step on the valve stroke, while the large mass case builds up to its maximum stroke in practically a sinusoidal fashion.

It can be seen that there are limitations on the mass of the plunger valve in both the high and low directions. Low mass values tend toward instability, whereas high mass

values tend toward sluggish valve motion (although the maximum mass studied still gave sufficiently small time delay between the beginning of piston stroke input and the beginning of plunger valve stroke). The natural frequency of the plunger valve should be well above the range of input frequencies resulting from bump impact. The frequency of the valve's motion can be determined from the mass and the compressibility of the fluid in the band-pass control chamber. This is discussed below.

The fourth item considered in the parameter variation studies was the effect of the control chamber spring rate. Here the preload was kept constant at 100 pounds while the spring rate was varied from 50 to 250 pounds per inch. The results of this study are shown in Figure 3-6D. Here it can be seen that the spring rate had no effect whatsoever on either the incremental pressure rise or the plunger valve stroke. The four computer time plots further showed that there was practically no change in any of the other phenomena such as the variation of plunger position with time or the variation of the pressure on the strut dynamic chamber with time. Surprisingly, the frequency of the transient valve motion showed only a very slight increase (on the order to 5 percent) in going from the 50 pound per inch rate to the 250 pound per inch rate. If the frequency of the valve's motion were determined by the spring rate of the control chamber spring and the mass of the plunger valve, such a change in spring rate would result in a 224 percent increase in frequency. The spring rate of the control chamber spring plays only a small part in the value of the natural frequency of the valve's motion.

The natural frequency of the valve's motion is determined almost entirely by the compressibility of the fluid in the control chamber, the volume of that chamber, the valve, and the valve mass. The natural frequency is given by,

$$f_n = \frac{1}{2\pi}\sqrt{\frac{KV + \beta A p_3^2}{V_3 M_3}} \qquad (12)$$

Since KV is small in comparison to BAp_3^2 the effect of the spring rate is negligible.

This fact is convenient since it simplifies the problem of spring design to that of obtaining the correct preload. Within practical ranges, rate has no effect on the performance of the band-pass system.

At this point, it is appropriate to discuss the problem of valve instability since it is related to the action of the fluid in the band-pass control chamber. The whole action of the band-pass system depends upon a rather delicate pressure balance between the dynamic chamber of the shock strut and the control chamber of the band-pass mechanism. The delicate nature of this balance is apparent when it is noted that pressure differences on the order of 120 psi are sufficient to open the band-pass unit while normal dynamic chamber pressures are in the vicinity of 4000 psi for a 20 ft./sec. landing impact. Thus, only a 3 percent variation in the P_3 pressure can upset the balance and either open the band-pass unit fully or close it completely, depending upon the direction of the variation. In order to maintain P_3 close to P_1, and at the same time not allow the leakage of fluid through the control chamber orifices to reduce P_1 excessively during normal landing impact, the ratio between the inlet orifice and the outlet orifice must be large and the outlet orifice must be very small.

During bump impact, therefore, the increased flow into the control chamber and the flow incurred due to the upward movement of the plunger valve is not accommodated by the small outlet orifice and the fluid simply compresses slightly. Once the plunger has reached its maximum upward movement, the fluid begins to expand and sends the piston downward and, in severe instability, may completely close. The cycle then repeats itself until an equilibrium position is found by the plunger valve.

The valve instability is heightened by several factors. First, if the inlet orifice to the band-pass unit is small, the drop-off of P_3 pressure with increased stroke due to bump impact is excessive. The valve movement is thus accelerated too rapidly and the result is excessive overshoot of both the $P_1 - P_3$ pressure and the valve movement. A small volume of fluid in the dynamic chamber of the strut also leads to instability since with low fluid volume there is little cushioning of the input to the band-pass mechanism between the shock strut piston and the orifice plate. That is, there is greater fluid flow into the band-pass control chamber due to the smaller amount of fluid compression in the strut dynamic chamber with low dynamic chamber volume.

A third factor heightening the instability is a small value of A_{02} (the control chamber outlet orifice area). This is due to the fact that with small outlet flow, fluid compression is increased. High values of valve gain and the rate of orifice area increase with valve stroke also lead to a more unstable system. With increased valve gain, a given amount of valve movement will cause larger pressure fluctuations in the dynamic chamber and therefore in the control chamber. Increased pressure fluctuations in turn result in a longer time for the valve to reach its equilibrium.

These are the physical reasons for the instability of the valve. It is unfortunate, but also typical, that most of the parameter extremes which cause instability also improve the valve performance from the standpoint of reduced incremental pressure rise in the strut's dynamic chamber. This is true within limits since severe instability will bring about a rapid reclosing of the valve, thus increasing the incremental pressure rise. The instability brings into play another consideration in valve design. The valve cannot be designed exclusively by that combination of parameters which brings about a minimum pressure rise in the dynamic chamber (minimum load transferred to the main mass of the airplane).

Returning to the parameter variation studies, the fifth item considered was the valve preload. Valves were studied where the preload ranged from 35 psi to 200 psi. The results of this study are shown in Figure 3-7A.

The lowest value of preload shown in Figure 3-7A corresponds to the null $(P_1 - P_3)$ pressure differential for the steady stroke velocity of 125 in. sec. Preloads below this value will result in the valve opening during the landing impact, thus preventing the shock strut from absorbing the landing impact energy.

It can be seen that valve preload has a large influence on the pressure rise during bump impact. The preload should be designed as close as possible to the maximum null $(P_1 - P_3)$ pressure differential expected during landing impact. Since maximum expected stroke velocities can be predicted, and since the orifice area vs. stroke is known, the

$(P_1 - P_3)$ pressure differential can be calculated from Equation (7) for the band-pass design.

The sixth item considered was the orifice area ratio A_{o3}/A_{o2}. The results of this study are shown in Figure 3-7B. It can be noted that the value of A_{o3}/A_{o2} affects the null $(P_1 - P_3)$ pressure (see Equation 7) and that it is necessary to vary the preload in addition to the inlet-to-outlet orifice area ratio to obtain results which can be compared.

Figure 3-7B indicates that a low value of A_{o3}/A_{o2} is desirable to obtain a low pressure rise in the strut's dynamic chamber during bump impact, but two other considerations come into play which limit the amount this ratio can be reduced. The first is the stability of the valve's motion. Pressure improvement can be obtained by a reduction in A_{o3} and A_{o2} simultaneously, or by holding A_{o2} fixed and reducing A_{o3} but not by increasing A_{o2}. Reduction in A_{o3} heightened the instability as noted previously. The second factor is preload. Decreasing the ratio A_{o3}/A_{o2} increases the preload necessary to maintain the valve closed for normal landing impact. High preload presents a design problem due to space and area limitations within the control chamber.

The seventh item considered was the control chamber outlet orifice area A_{o2}. The results of this study are illustrated in Figure 3-7C. The ratio A_{o3}/A_{o2} was held fixed in this study so that the nominal preload of 100 pounds applies for each case. Figure 3-7C shows that a decrease in A_{o2} decreases the pressure rise in the strut dynamic chamber during bump impact. However, this also leads to valve instability. The marked instability of the valve motion when A_{o3}/A_{o2} is reduced to .000143 in.^{2} is indicated by the computer time solution shown in Figure 3-5.

The eighth item considered in the parameter variation study was the valve cross-sectional area A_{p3}. The results of this study (See Figure 3-7D) indicate some improvement on the dynamic chamber pressure rise with reduced area. This was due to the reduction in the spring rate of the fluid compression of the control chamber, which allowed larger motion of the plunger valve for a given input. A larger overshoot of the $(P_1 - P_3)$ pressure differential was noted with the reduced area, but no appreciable change in stability (number of cycles of transient valve motion) was noted in going from the two extremes of .5 and 1.5 in.^{2} on A_{p3}. This is mentioned because later studies with the complete landing gear system showed marked instability in the valve motion for the reduced A_{p3} when the volume of the dynamic chamber was at near minimum. A similar result was obtained with increased V_3. An increase in V_3 is similar to a decrease in A_{p3} in that it also decreases the spring rate of the fluid column in the band-pass control chamber.

The ninth item considered in the parameter variation study was the effect of the valve gain -- valve gain being defined as the rate of orifice area increase with plunger valve stroke. The results of this study are shown in Figure 3-8. Decreased valve gain causes a rise in the pressure in the strut dynamic chamber simply because it decreases the amount of area increase between the strut's dynamic chamber and the air chamber. Increased valve gain, while decreasing the pressure rise in the dynamic chamber of the strut, tends toward unstable valve operation for reasons previously discussed. Maximum

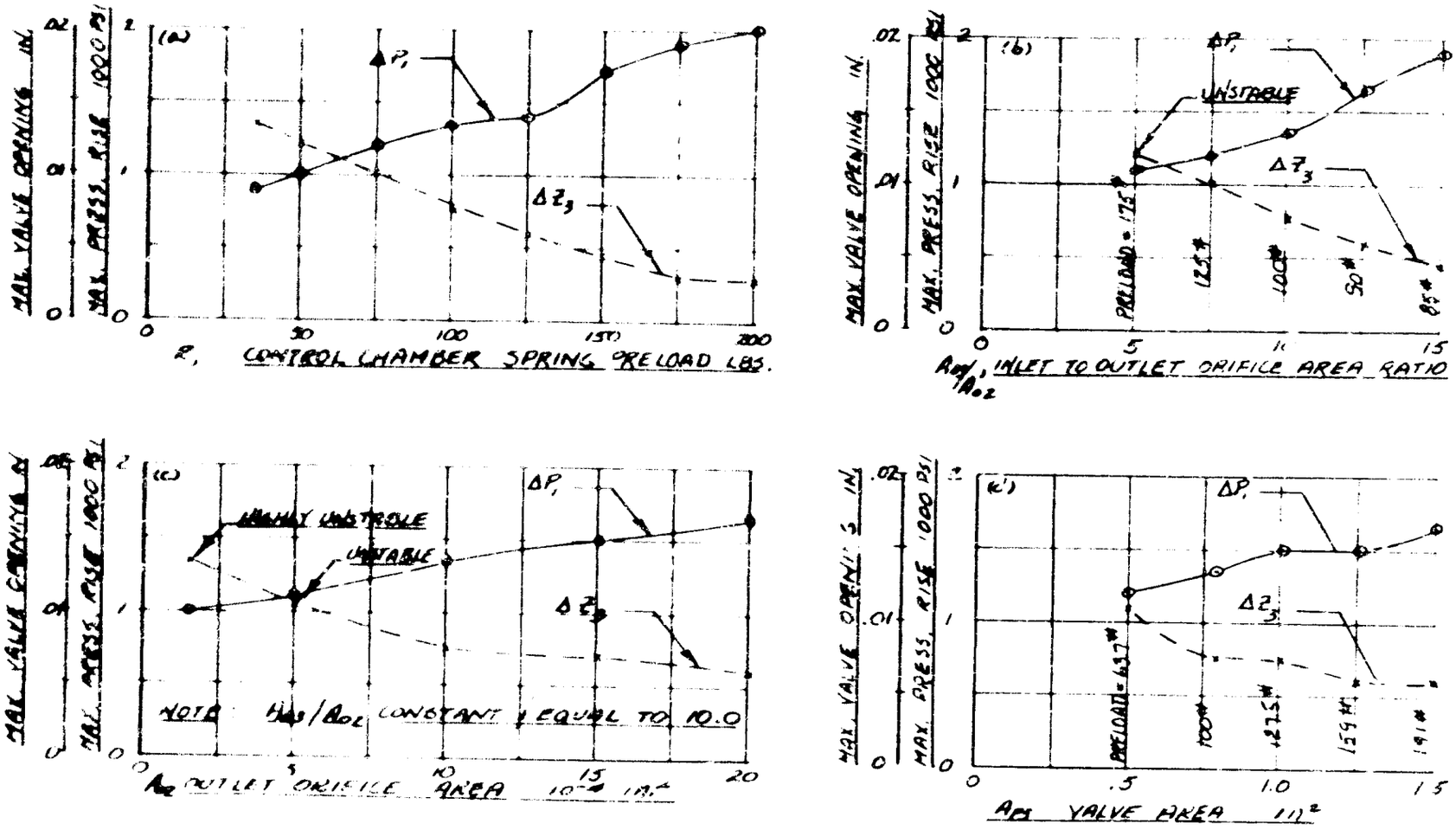

Figure 3-7. Parameter Variation Studies Simplified Band-Pass Shock Strut Model; Analog Computer Solutions

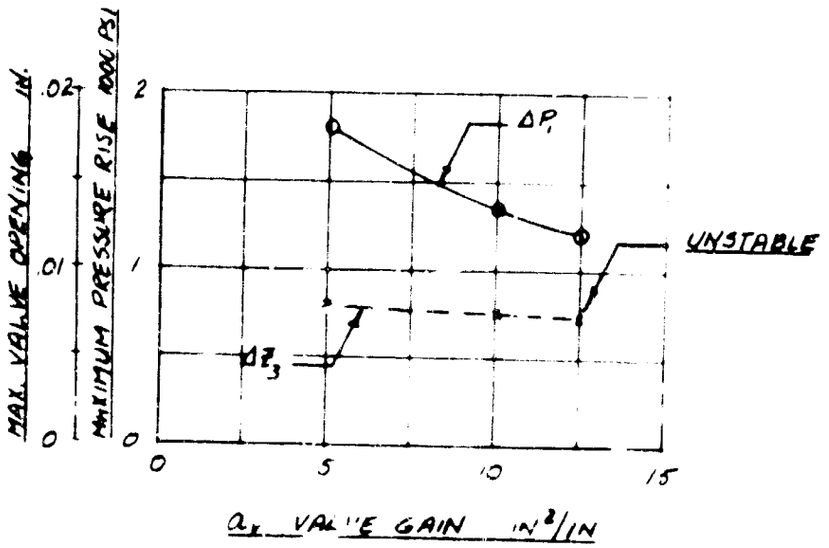

Figure 3-8. Parameter Variations Studies Simplified Band-Pass Shock Strut Model Analog Computer Solutions

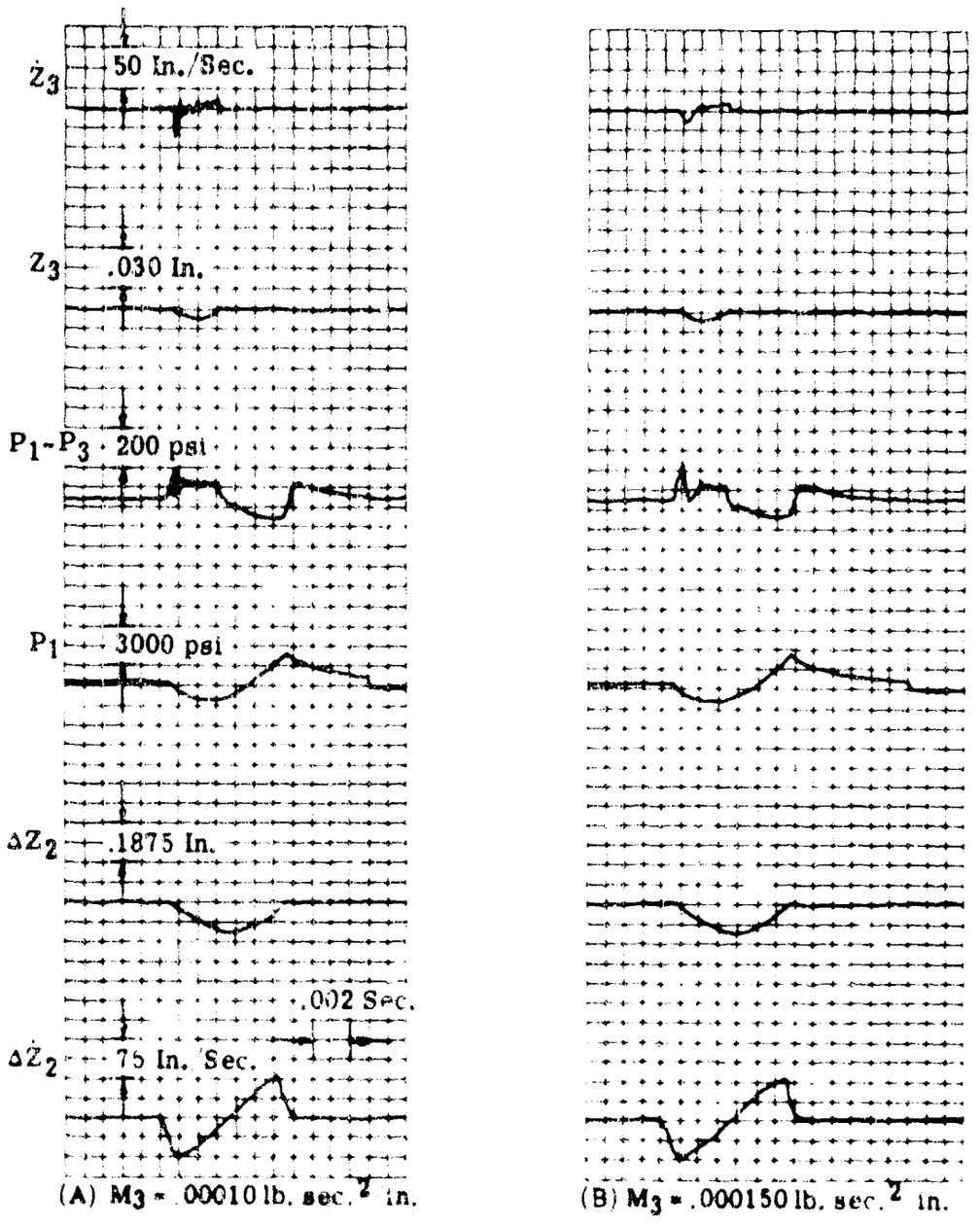

(A) M_3 = .00010 lb. sec.^{2} in. (B) M_3 = .000150 lb. sec.^{2} in.

Figure 3-9 Computer Results Simplified Model

allowable valve gain appears to be in the vicinity of 10 in.^{2}/in. Such a gain would result in marginal stability for the low dynamic chamber volume encountered in the compressed or near-compressed strut condition.

SUMMARY AND CONCLUSIONS FROM STUDIES OF SIMPLIFIED BAND-PASS SHOCK STRUT MODEL

1. The optimum set of values for the parameters associated with the band-pass mechanism is controlled by the interaction of three factors: first, the pressure rise in the dynamic chamber of the shock strut, or equivalently, the load transmitted to the main mass of the airframe; second, the valve stability; and third, size and space limitations imposed by the dimensions of the shock strut.

2. The performance of the band-pass mechanism is relatively insensitive to main orifice area, plunger mass, and the spring rate of the control chamber spring. For the system in question, the optimum mass appears to be 7 x 10^{-3} lb. sec.^{2}/in. but variations from 2 to 11 lb. sec. ^{2}/in. could be taken without appreciably affecting the performance of the valve. Spring rate has practically no effect on valve performance and the spring can be designed on a preload basis only.

3. Low dynamic chamber volume results in valve instability. The valve should be designed on the basis of the minimum volume of the strut's dynamic chamber.

4. The inlet to outlet orifice area ratio of the band-pass control chamber should be as low as possible, but not so low as to lead to instability or excessively large required preload. A balance of factors yields a value between 8 and 10 for this ratio.

5. Control chamber spring preload (R) should be made as close as possible to the maximum (P_1 - P_3) pressure differential times the valve area A_{p3}. The present design requires a preload of 50 lbs. or more to preclude opening of the valve on a limit drop. Excessive preload reduces the effectiveness of the band-pass mechanism.

6. The outlet orifice area should be made as small as possible, but not so small as to result in valve instability. For A_{03}/A_{02} ratio of 10 the A_{02} orifice area could possibly be reduced as low as 7.5 x 10^{-4} in.^{2} but for A_{03}/A_{02} reduced to 8, A_{02} could only be reduced to 10 x 10^{-4} in.^{2}. Further reduction would result in valve instability.

7. Valve area should be designed low. (Later studies show that lowering this quantity tends toward instability in the near-compressed strut, as does an increase in the control chamber volume.) The nominal value of .785 in.^{2} appears to be near optimum.

8. Valve gain should be as high as possible without resulting in instability. A value of between 10 and 11 in.^{2}/in. appears to be near maximum for the present configuration.

9. With a band-pass mechanism designed by the latter criteria, a reduction of approximately 50 percent in the magnitude of bump impact loads transmitted to the airframe during simultaneous landing impact and bump impact could be achieved. The maximum pressure rise in the impact considered in the simplified analysis was 2400 psi during impact without a band-pass unit, while with a band-pass unit the load was reduced to 1200 psi.

MATHEMATICAL MODEL OF COMPLETE LANDING GEAR SYSTEM WITH BAND-PASS

Free body diagrams of the complete landing gear system are shown in Figure 3-10. The summation of forces in the vertical direction on the main mass gives

$$M_1 \ddot{Z}_1 + F_L + P_2 (A_{p2} - A_{p1}' - A_{p6}) + P_1 A_c - M_1 g \cos\alpha_0 + F_f = \text{[illegible]} \quad (13)$$

where

where	M_1	=	main mass supported by one landing gear
	F_L	=	lift force on main mass
	P_1	=	gage pressure within dynamic chamber of shock strut
	P_2	=	gage pressure within air chamber of shock strut
	F_f	=	friction drag between piston and outer cylinder of the shock strut
	A_{p1}	=	area encompassed in I.D. of piston
	A_{p1}'	=	A_{p1} less the cross-sectional area of the orifice support tube
	A_{p2}	=	area encompassed in I.D. of outer cylinder less the cross-sectional area of the orifice support tube
	A_{p6}	=	area between inner and outer cylinder
	A_c	=	cross-sectional area of piston walls at upper bearing point
	α_0	=	inclination of gear (positive as shown in Figure 3-10)

The summation of forces in the vertical direction on the piston yields

$$m_2 \ddot{Z}_2 + F_{V1} \cos\alpha_0 - P_1 A_{p1} - P_2 A_c - m_2 g \cos\alpha_0 - F_f = \text{[illegible]} \quad (14)$$

since

$$F_{V1} = F_V + m_A \ddot{Z}_2 \cos\alpha_0 \quad (15)$$

then equation (14) can be written as

$$M_2 \ddot{Z}_2 + F_V \cos\alpha_0 - P_1 A_{p1} - P_2 A_c - M_2' g \cos\alpha_0 - F_f = \text{[illegible]} \quad (16)$$

where	m_2	=	mass of shock strut piston and associated parts
	m_A	=	mass of wheel, brake, tire and associated parts
	M_2	=	$(m_2 + m_A \cos^2\alpha_0)$
	M_2'	=	$(m_2 + m_A)$

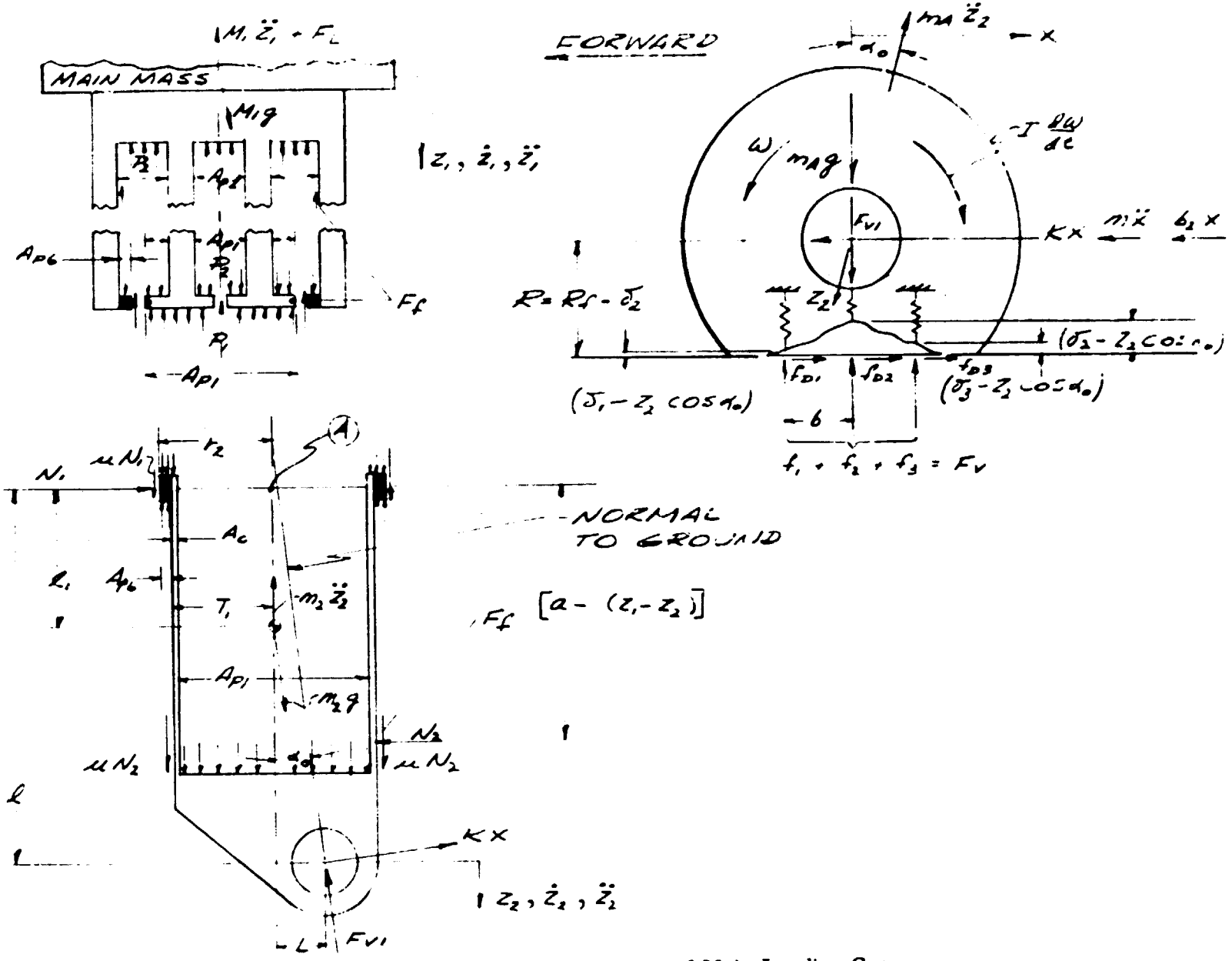

Figure 3-10. Free Body Diagrams of Main Landing Gear

F_{v1} = vertical (to ground) load on piston
F_v = vertical load on tire

The pressure P_2 results from the compression of the air in the shock strut air chamber and is a function of the stroke, $(Z_1 - Z_2)$.

$$P_2 = f(Z_1 - Z_2) \tag{17}$$

Considering the free body diagram of the shock strut piston, the summation of moments about point (A) yields

$$\mu N_1 r_2 - \mu N_2 r_1 + m_1 g \cos(\theta) l - F_{v1} \sin(\theta) l$$

$$+ K X \cos(\theta) l + P_2 \cos(\theta) l - N_2 (Z_1 - Z_2 + Z_{02} + l_1 \sin(\theta)) L = 0 \tag{18}$$

where
μ = coefficient of friction between outer cylinder and piston
N_1 = normal load on upper bearing
N_2 = normal load on lower bearing
r_1 = radius to surface of lower bearing
r_2 = radius to surface of upper bearing
l = length from center of upper bearing to center of axle
l_1 = length from center of upper bearing to center of gravity of piston
L = trail length
K = spring rate of strut in aft direction

From the same free body diagram the summation of forces normal to the strut centerline gives

$$K X \cos(\theta) + N_1 - N_2 + m_2 g \cos(\theta) - F_{v1} \cos(\theta) = 0 \tag{19}$$

From the free body diagram of the wheel the summation of forces in the horizontal direction gives

$$m \ddot{X} + b_2 \dot{X} + K X + m_A \ddot{Z}_2 = H_{fric} + F_{D1} + F_{D2} + F_{D3} \tag{20}$$

where
m = effective lumped mass of wheel, brake, tire, axle, and shock strut at axle for fore and aft motion considerations

c = damping coefficient associated with fore and aft motion
f_{Di} = drag forces on tire footprint (i = 1, 2, and 3)

The frictional force, F_f, between the outer cylinder and the piston is given by

$$F_f = \mu N_1 + \mu N_2 \frac{\dot{z}_1 - \dot{z}_2}{|\dot{z}_1 - \dot{z}_2|} \tag{21}$$

It can be noted that the tire has been divided into three springs. The original concept given in Reference 5 was to use only one nonlinear elastic element to represent the force deflection characteristic of the tire. As explained in Reference 6, this would not be sufficient to represent the true tire characteristics for both bump impact and landing impact. The model finally arrived at consisted of three equally spaced nonlinear springs. The bump shape was also modified to allow deflection of more than one spring when the bump was at the center of the tire footprint. Tests conducted on the F4H-1 tire are covered in Reference 7 together with the derived force deflection characteristics of the three springs and the modified bump shape.

Similar spring functions were derived for the A3J-1 main gear, wheel and tire making use of the load deflection shapes derived in Reference 7 and experimental data on the flat plate load deflection characteristic of a 36 x 11 24-ply type VII tire. The derived spring functions are given in the data section of this report.

The deflection of each spring is given by

$$z_1 = h\left(\int v\,dt - x + c\right) + z_2 \cos\alpha_0 \tag{22}$$

$$z_2 = h\left(\int v\,dt - x\right) + z_2 \cos\alpha_0 \tag{23}$$

$$z_3 = h\left(\int v\,dt - x - b\right) + z_2 \cos\alpha_0 \tag{24}$$

where h = bump shape, a function of $\left(\int v\,dt - x - b\right)$ etc.
v = forward velocity of airplane
b = spring spacing

Since the spring spacing is symmetrical with respect to the footprint centerline, the forward spring function is identical to the aft spring function so that only two functions are used to describe the tire force deflection characteristics. The fore and aft spring functions are designated g_1 (δ_1) and g_1 (δ_3) and the center spring function is designated g_2 (δ_2).

Thus $f_1 = g_1(\delta_1)$ (25)

$f_2 = g_2(\delta_2)$ (26)

$f_3 = g_1(\delta_3)$ (27)

The total vertical force at the tire footprint is

$$F_V = f_1 + f_2 + f_3 \tag{28}$$

Taking the summation of moments acting on the wheel gives

$$I\dot{\omega} = f_{D1} - \bar{r}_2 f_D + f_{D2} + f_{D3} - f_1 e + f_3 e \tag{29}$$

Hete it can be noted that the drag forces were all assumed to have a lever arm of $R_f - \delta_2$ which is only approximately true since ℓ_1 and δ_3 will in general be different that δ_2. However, for wheel moment calculations, the difference between $R_f - \delta_1$ and $R_f - \delta_2$ etc. will be a second order effect which can be neglected.

The drag forces, f_{D1}, are determined by two different sets of equations. The particular set to be used depends upon whether the tire is rolling or sliding.

Tire sliding is defined by the following equation

$$S_L = (V - \dot{x}) - \omega R_f - \bar{r}_2 \tag{30}$$

where S_L = sliding velocity

when $S_L \neq 0$ (tire sliding) then f_{D1} is given by

$$f_{D1} + f_{D2} + f_{D3} = \mu_T (f_1 + f_2 + f_3) \frac{S_L}{|S_L|} \tag{31}$$

where μ_T = sliding coefficient of friction between tire and runway surface

when $S_L = 0$

$$f_{D1} + f_{D2} + f_{D3} = \frac{I}{R_f - \bar{r}_2} \cdot \frac{d}{dt}\left(\frac{V - \dot{x}}{R_f - \bar{r}_2}\right) - f_{30} - f_{20} \tag{32}$$

until such time that

$$\left|f_{D1} + f_{D2} + f_{D3}\right| - \left|\mu_T f_1 + \mu_T f_2 + \mu_T f_3\right| > \epsilon \tag{33}$$

where ϵ is a small quantity, ideally zero.

Once the above condition becomes true, then f_{D1}, f_{D2}, f_{D3} are determined from Equation (31).

The latter set of equations together with the previously derived relationships, Equations (1), (2), and (3), constitute the equations of motion of the complete main landing gear system, including band-pass. It should be noted that in Equation (1) the volume of the dynamic chamber, V_{P1}, is not constant but is a function of $(Z_1 - Z_2)$. Likewise, the main orifice area, A_O, is also a function of $(Z_1 - Z_2)$ as determined from the metering pin contour. Both of these functions are given in the data section of this report.

NUMERICAL DATA - A3J-1 MAIN LANDING GEAR SYSTEM

Numerical data for the A3J-1 main landing gear and the nominal band-pass unit is as follows:

Masses and Moments of Inertia

M_1	=	main mass of airplane per gear	53.4 lb.sec.^{2}/in.
m_2	=	mass of inner cylinder and associated parts	.311 lb.sec.^{2}/in.
M_3	=	mass of band-pass plunger	.00035 lb.sec.^{2}/in
m_A	=	mass of wheel,brake,tire,fork,axle and associated parts	.594 lb.sec.^{2}/in.
M	=	effective lumped mass at axle for fore and aft motion considerations	.723 lb.sec.^{2}/in.
I	=	polar moment of inertia of rotating parts (wheel,tire,brake rotors, and associated parts)	80.0 lb.in.sec.^{2}

Spring Rates

k_s	=	spring rate of control chamber spring	100 lb./in.
k_x	=	fore and aft spring rate of strut	14,340 lb./in.

Areas

A_{p1}	=	inside area of inner cylinder	20.428 in.^{2}
A_{p1}'	=	inside area of inner cylinder minus area of orifice support tube	17.855 in.^{2}
A_{p2}	=	inside area of outer cylinder less orifice support tube	27.072 in.^{2}
A_{p3}	=	band-pass plunger valve cross-sectional area	.785 in ^{2}
A_{p6}	=	area between I.D. of outer cylinder and O.D. of inner cylinder	3.467 in.^{2}
A_c	=	wall area of inner cylinder	5.629 in.^{2}
A_o	=	main orifice area (see curve)	

A_{o2}	=	outlet orifice area of band-pass control chamber	0.001 in.^{2}
A_{o3}	=	inlet orifice area of band-pass control chamber	0.010 in.^{2}
A_{o5}	=	orifice area of dump valve	.300 in.^{2}

Lengths

L	=	mechanical trail	4.38 in.
l	=	length from center of upper strut bearing to axle centerline	55.04 in.
l_1	=	distance from center of upper bearing to center of gravity of shock strut piston	34.0 in.
a	=	distance between centers of strut bearings in fully compressed position	29.86 in.
R	=	radius of tire during rolling	15.00 in.
R_f	=	free radius of tire	18.38 in.
r_1	=	outside radius of inner cylinder	2.875 in.
r_2	=	radius to surface of upper strut bearing	3.061 in.
b	=	half length of effective footprint	4.25 in.

Miscellaneous

ρ	=	mass density of hydraulic fluid	.000085 lb.sec.^{2} in.^{4}
B	=	bulk modulus of hydraulic fluid	250,000 psi
V_{p1}	=	volume of shock strut dynamic chamber	(see curve)
V_{p3}	=	volume of band-pass control chamber	3.0 in.^{3}
c_d	=	orifice discharge coefficient (for main metering orifice A_o, $c_d \cong 0.85$)	.60
μ	=	coefficient of friction of strut bearings	.05
μ_T	=	coefficient of friction between tire and runway	.55
α_o	=	strut angle of inclination (variable) nominally	0
b_1	=	damping coefficient associated with relative motion of band-pass valve (adjusted to give approximately 10% of critical damping)	
b_2	=	(See Figure 3-10B)	
R	=	preload of band-pass control chamber spring	50 lbs.
V	=	forward velocity of airplane (variable) nominally	2655 in. /sec.

ANALOG COMPUTER RUNS

Using the equations of motion derived for the complete landing gear system, a total of 132 simulated drop tests were made. Parameter variations in both the variable landing gear parameters and the band-pass mechanism's parameters were made to determine

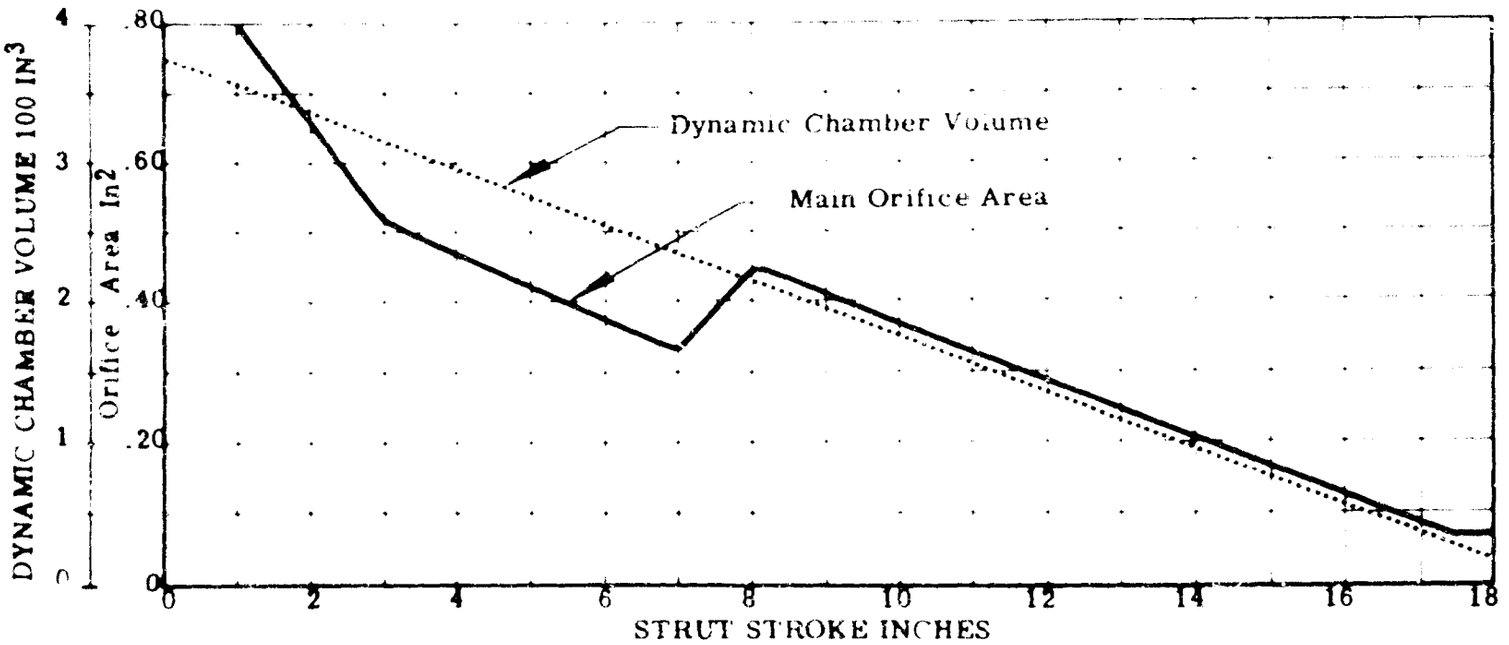

FIGURE 3-10A. Dynamic Chamber Volume and Main Orifice Area vs Stroke

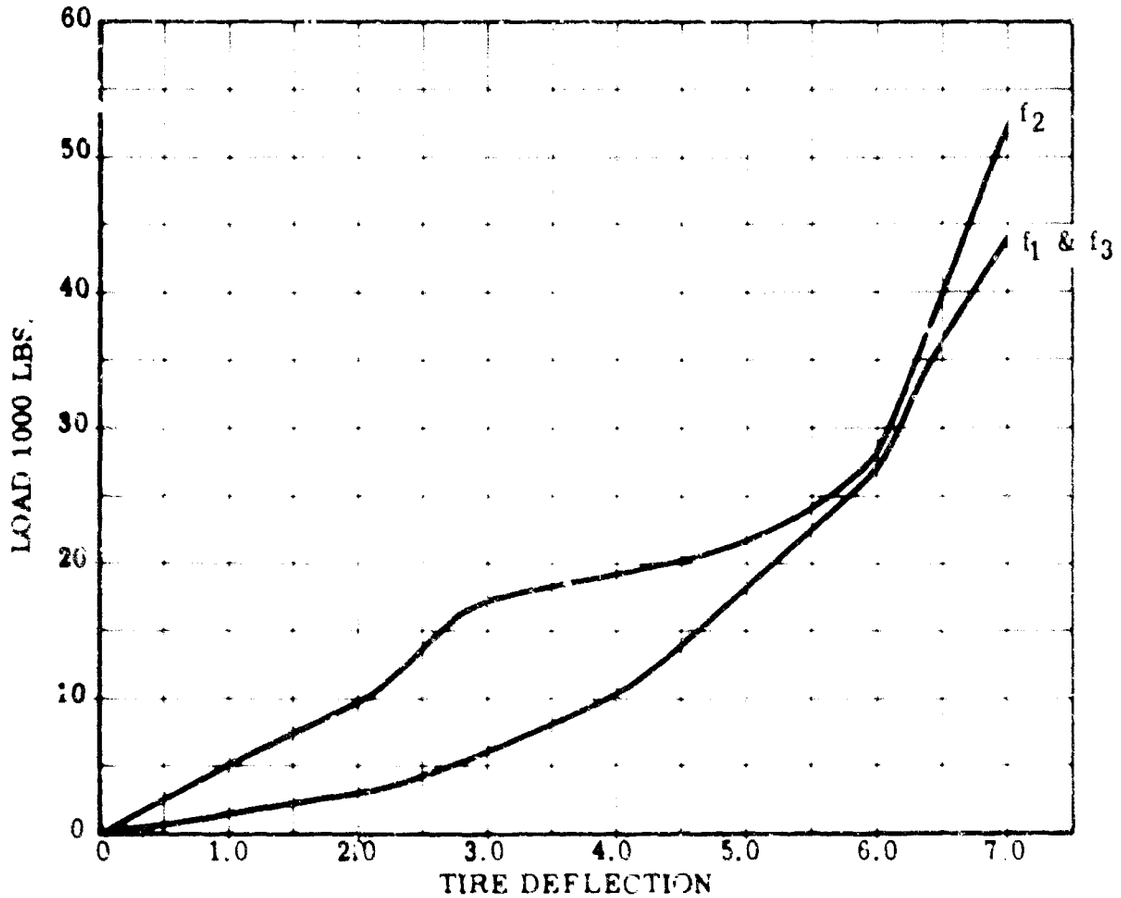

Figure 3-10B. Tire Force Deflection Functions Type VII-36 x 11-24 Ply

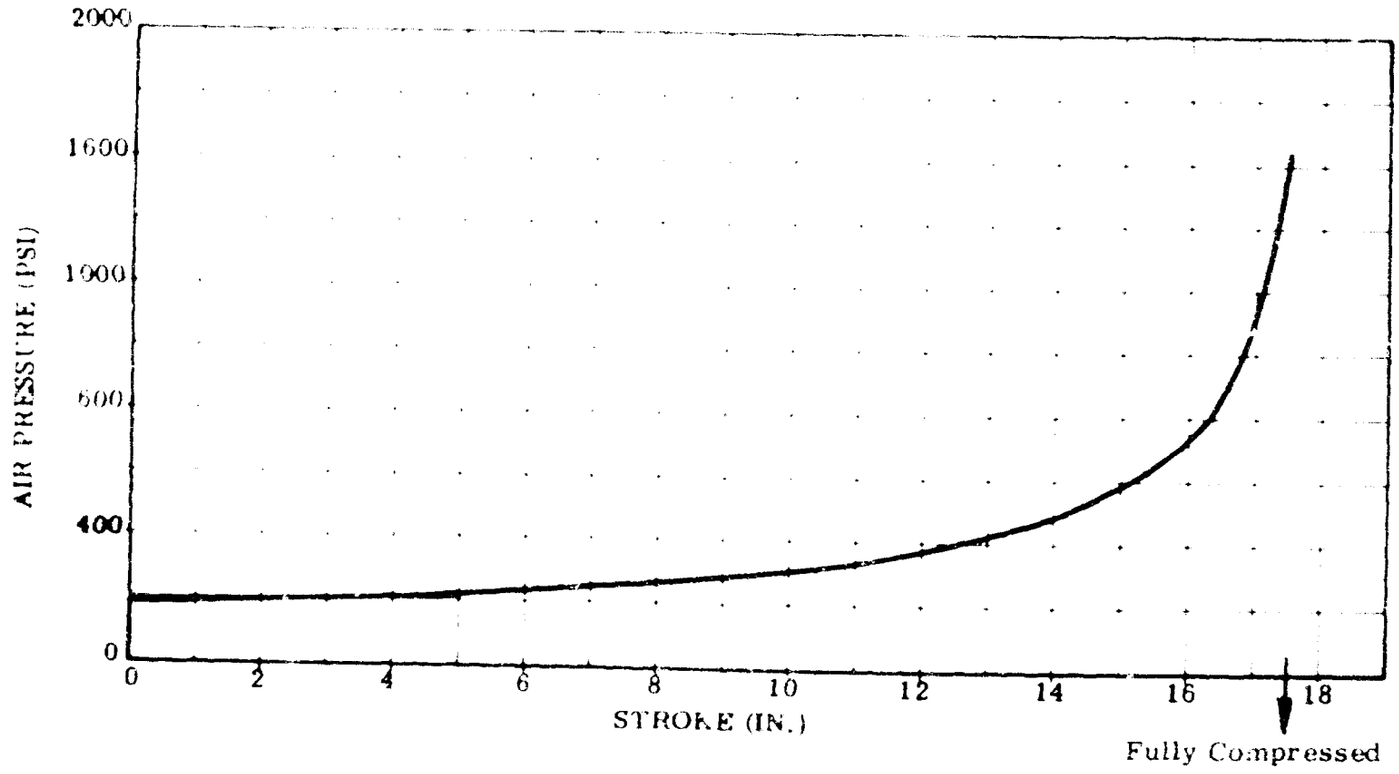

Figure 3-10C. A3J Main Gear Air Pressure vs Stroke

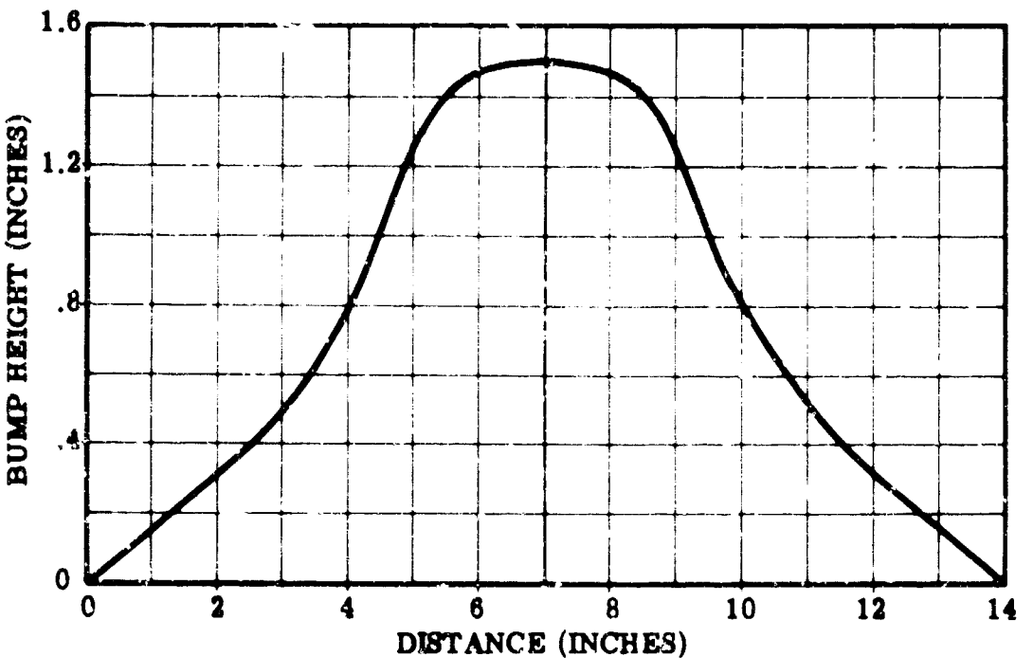

Figure 3-10D. Effective Bump Shape 1-1/2 Inch Cable

the over-all performance of the system with band-pass. The following is a tabulation of the computer runs:

(1) Comparison with standard drop test results
(2)-(10) Variations in sink speed 12, 14, 16, 18, 20, 21, 22, 23, 24 ft./sec.
(11)-(17) Variations in speed 2400, 2600, 2800, 3000, 3200, 3400, 3600 in./sec.
(18)-(19) Effect of strut inclination (18) same as (1). (19) $\alpha_2 = 5°$
(20)-(27) Same as (1) except impacts at 2, 4, 6, 8, 10, 12, 14, 16 inches of stroke
(28) Same as (27) but with nominal band-pass unit
(29) A_{o3} decreased to .005
(30) R_3 increased from 50 lbs. to 100 lbs.
(31) Same as (30) except bump brought in at 4 inches of stroke
(32) $A_{o3}/A_{o2} = 10$ (nominal) $\alpha_v = 20$
(33) Repeat of (28) except preload = 100 lbs.
(34) Repeat of (28)
(35) Repeat of (34)
(36) α_v changed to 20 $in.^2/in.$
(37) A_{p3} cut in half
(38) Unsprung mass decreased by factor of 3 A_{p3} returned to .785 $in.^2$
(39) Same as (38) with $\alpha_v = 10$ $in.^2$ in.
(40) Same as (38) with $\alpha_v = 10$ $in.^2$ in. Unsprung mass = 1 6 nominal
(41) Same as (38) with $\alpha_v = 10$ $in.^2$ in. Unsprung mass = 1 9 nominal
(42) Pot 013 increased from .1250 to .5000
(43) Step valve Upper A_{p3} = .785 2 R = 100
(44) Same as (1) except bump at 16 inches stroke - no band-pass
(45) With band-pass system - bump at 16 inches stroke, R = 100 lbs.
(46) Same as (45) R = 50 lbs.
(47) Same as (46) except $\alpha_v = 12.5$ $in.^2$ in.
(48) Same as (47) except $\alpha_v = 15.0$ $in.^2$ in.
(49) Same as (47) except b_3 increased by factor of 4
(50) Nominal b_3, v_3 decreased by factor of 5.0 ($\alpha_v = 15.0$ $in.^2$ in.)
(51) $\alpha_{v1} = 20.0$ $in.^2/in.$ same as (50) otherwise
(52) A_{o2} reduced to .0005 same as (51) otherwise
(53) v_3 returned to nominal value, $A_{o2} = .0010$ b_3 x 10.0 $\alpha_v = 15.0$
(54) b_3 x 20 $\alpha_{v1} = 15$ $A_{o2} = .00135$
(55) v_3 x 1 2 otherwise same as (54)
(56) v_3 x 2 otherwise same as (55)
(57) v_3 x 10
(58) b_3 x 20 $\alpha_{v1} = 20$)
(59) b_3 x 20 $\alpha_{v1} = 15$) } Not good computer problems
(60) b_3 x 20 $\alpha_{v1} = 15$ $A_{o2} = .00135$)
(61) b_3 x 20 $\alpha_v = 20$ $A_{o2} = .001$
(62) b_3 x 20 $\alpha_v = 15$ $A_{o2} = .001$
(63) b_3 x 20 $\alpha_v = 15$ $A_{o2} = .00135$
(64) b_3 nominal $\alpha_{v1} = 10$ $A_{o2} = .001$
(65) Nominal band-pass system bump at 2 in.
(66) 4
(67) 6

(68)	Nominal band-pass system	bump at 8 in.	
(69)		10 in.	
(70)		12 in.	
(71)		14 in.	
(72)		16 in.	
(73)	No band-pass	2 in.	
(74)		4 in.	
(75)		6 in.	
(76)		8 in.	
(77)		10 in.	
(78)		12 in.	
(79)		14 in.	
(80)		16 in.	
(81)	$A_{o3} = .0075$	8 in.	
(82)	$A_{o3} = .0075$	16 in.	
(83)	$A_{o3} = .0050$	8 in.	
(83-a)	$A_{o3} = .0050$	8 in.	100 lbs. preload
(84)	$A_{o3} = .0050$	16 in.	
(84-a)	$A_{o3} = .0050$	16 in.	100 lbs. preload
(85)	$A_{o2} = .0015$	8 in.	
(85-a)	$A_{o2} = .0015$	8 in.	100 lbs. preload
(86)	$A_{o2} = .0015$	16 in.	
(86-a)	$A_{o2} = .0015$	16 in.	100 lbs. preload
(87)	$A_{o2} = .0005$	8 in.	
(88)	$A_{o2} = .0005$	16 in.	
(89)	$v_3 = 5$ in.^{2}	8 in.	
(90)	$v_3 = 5$ in.^{2}	16 in.	
(91)	$v_3 = 1$ in.^{2}	8 in.	
(92)	$v_3 = 1$ in.^{2}	16 in.	
(93)	$A_{p3} = 1.0$ in.^{2}	8 in.	
(94)	$A_{p3} = 1.0$ in.^{2}	16 in.	
(95)	$A_{p3} = .50$ in.^{2}	8 in.	
(95-a)	$A_{p3} = .50$ in.^{2}	8 in.	30 lbs. preload
(96)	$A_{p3} = .50$ in.^{2}	16 in.	
(96-a)	$A_{p3} = .50$ in.^{2}	16 in.	30 lbs. preload
(97)	Preload = 35 lbs.	8 in.	
(98)	Preload = 35 lbs.	16 in.	
(99)	Preload = 65 lbs.	8 in.	
(100)	Preload = 65 lbs.	16 in.	
(101)	Preload = 80 lbs.	8 in.	
(102)	Preload = 80 lbs.	16 in.	
(103)	Preload = 100 lbs.	8 in.	
(104)	Preload = 100 lbs.	16 in.	

(105)	Sink speed = 12 ft./sec.)		bump at	4 in.
(106)	Sink speed = 12 ft./sec.)	With band-pass	↓	8 in.
(107)	Sink speed = 12 ft./sec.)			14 in.
(108)	Sink speed = 12 ft./sec.)			4 in.
(109)	Sink speed = 12 ft./sec.)	Without band-pass		8 in.
(110)	Sink speed = 12 ft./sec.)			14 in.
(111)	Sink speed = 23 ft./sec.)			4 in.
(112)	Sink speed = 23 ft./sec.)	With band-pass		8 in.
(113)	Sink speed = 23 ft./sec.)			16 in.
(114)	Sink speed = 23 ft./sec.)			4 in.
(115)	Sink speed = 23 ft./sec.)	Without band-pass		8 in.
(116)	Sink speed = 23 ft./sec.)			16 in.
(117)	v = 2300 in./sec.)			8 in.
(118)	v = 2300 in./sec.)			16 in.
(119)	v = 2700 in./sec.)			8 in.
(120)	v = 2700 in./sec.)	With band-pass		16 in.
(121)	v = 3100 in./sec.)			8 in.
(122)	v = 3100 in./sec.)			16 in.
(123)	v = 3500 in./sec.)			8 in.
(124)	v = 3500 in./sec.)			16 in.
(125)	v = 2300 in./sec.)			8 in.
(126)	v = 2300 in./sec.)			16 in.
(127)	v = 2700 in./sec.)			8 in.
(128)	v = 2700 in./sec.)	Without band-pass		16 in.
(129)	v = 3100 in./sec.)			8 in.
(130)	v = 3100 in./sec.)			16 in.
(131)	v = 3500 in./sec.)			8 in.
(132)	v = 3500 in./sec.)			16 in.

RESULTS OF ANALOG COMPUTER STUDY OF COMPLETE MAIN LANDING GEAR SYSTEM

The results of this study are shown partially in Figures 3-11 through 3-25. In general, the study indicated that the optimum configuration was quite close to the configuration arrived at by the simplified model studies. Further, it was found that although the band-pass unit could reduce the load transferred to the airframe and the dynamic chamber pressure as compared to an identical system not having the band-pass mechanism, it could not reduce the wheel and tire loads to any significant degree.

Run (1), the results of which are shown in Figure 3-11 in terms of tire vertical load vs. shock strut stroke, was carried out to check the degree of simulation achieved by the analog model of the landing gear system. The results indicate a close correlation

between the computer results and the actual drop test results obtained from Reference (4). Pressure fluctuations at the beginning of the stroke were not duplicated, but over-all shape, maximum stroke, and maximum vertical load do closely duplicate the results of the drop test. Similar correlation was obtained on drag load results. Differences between the drag load calculated on the computer, and drop test drag load, can be attributed mainly to the fact that the actual coefficient of friction between the tire and the drop test platform is variable whereas only a constant average coefficient of friction was considered in the analog computer simulation.

The effect of strut inclination was studied in runs (13) and (19). The results of these runs indicated that there was very little change in load-stroke phenomena for minor variations in the strut angle of inclination. For this reason, no further studies were carried out on the effect of strut inclination on the functioning of the band-pass shock strut mechanism. The load-stroke curves for these two runs are shown in Figure 3-12.

Runs (28) through (64) were miscellaneous exploratory runs. The purpose of these runs was to examine the effect of parameter variations carried out to alleviate the stability problem, and to maintain a high load reducing capacity of the band-pass unit.

Stability problems with the complete landing gear system were greater than those encountered in the simplified study. This was due primarily to the fact that the volume of the high pressure chamber of the strut could reduce to as low as 17.5 cubic inches at 18 inches of strut stroke. Figure 3-6A shows that such a volume would be expected to result in extreme instability problems. The lower preload (50 lbs.) would tend to alleviate this slightly, but parameter changes to increase dynamic chamber pressure attenuation, over that obtained with the nominal system, were found to be impractical due to the greater instability encountered with such changes. The computer results for a typical unstable condition are shown in Figure 3-13. This is the result of computer run (96) in which A_{p3} was reduced to .50 in.^{2}. The severity of the instability is indicated by the fact that the valve completely closed due to rebound of the compressed fluid.

Attempts were also made in these runs to alleviate valve instability by increasing the damping associated with the $Z_1 - Z_3$ motion. Practical increases in this damping term did little to the stability, however.

Following the initial exploratory runs, a series of runs were made to examine the functioning of the "optimized" band-pass shock strut over a range of variables normally encountered in service. This included:

1. Point of stroke at which bump impact occurred.
2. Variations in airplane sink speed.
3. Variations in airplane forward velocity at impact.

In addition, variations on several of the band-pass parameters were carried out to establish if any improvement in performance could be gained by slight changes in these parameters:

1. Control chamber inlet orifice size (A_{O3}).
2. Control chamber outlet orifice size (A_{O2}).

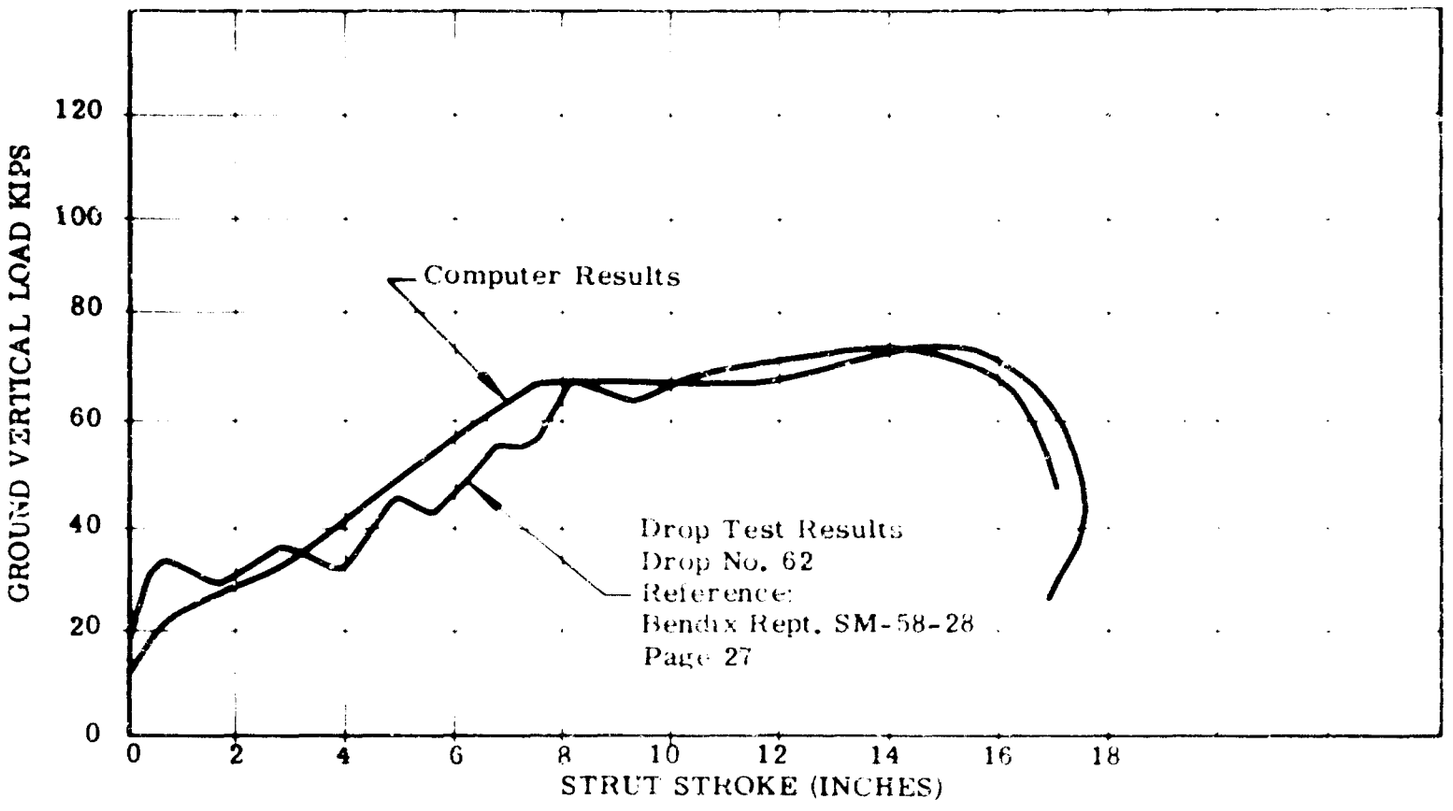

Figure 3-11. Comparison of Analog Computer Results and Drop Test Results
Ground Vertical Load vs Stroke

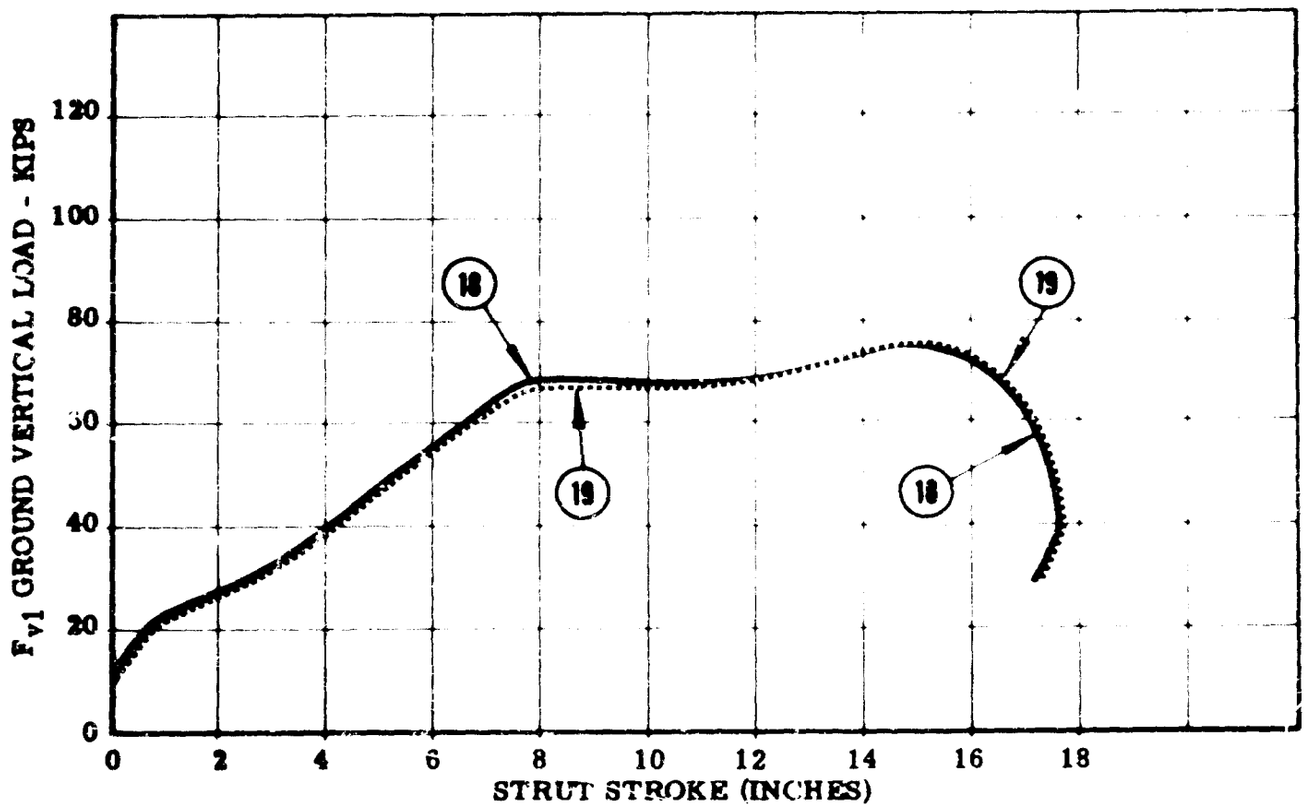

Figure 3-12. Effect of Small Strut Inclination

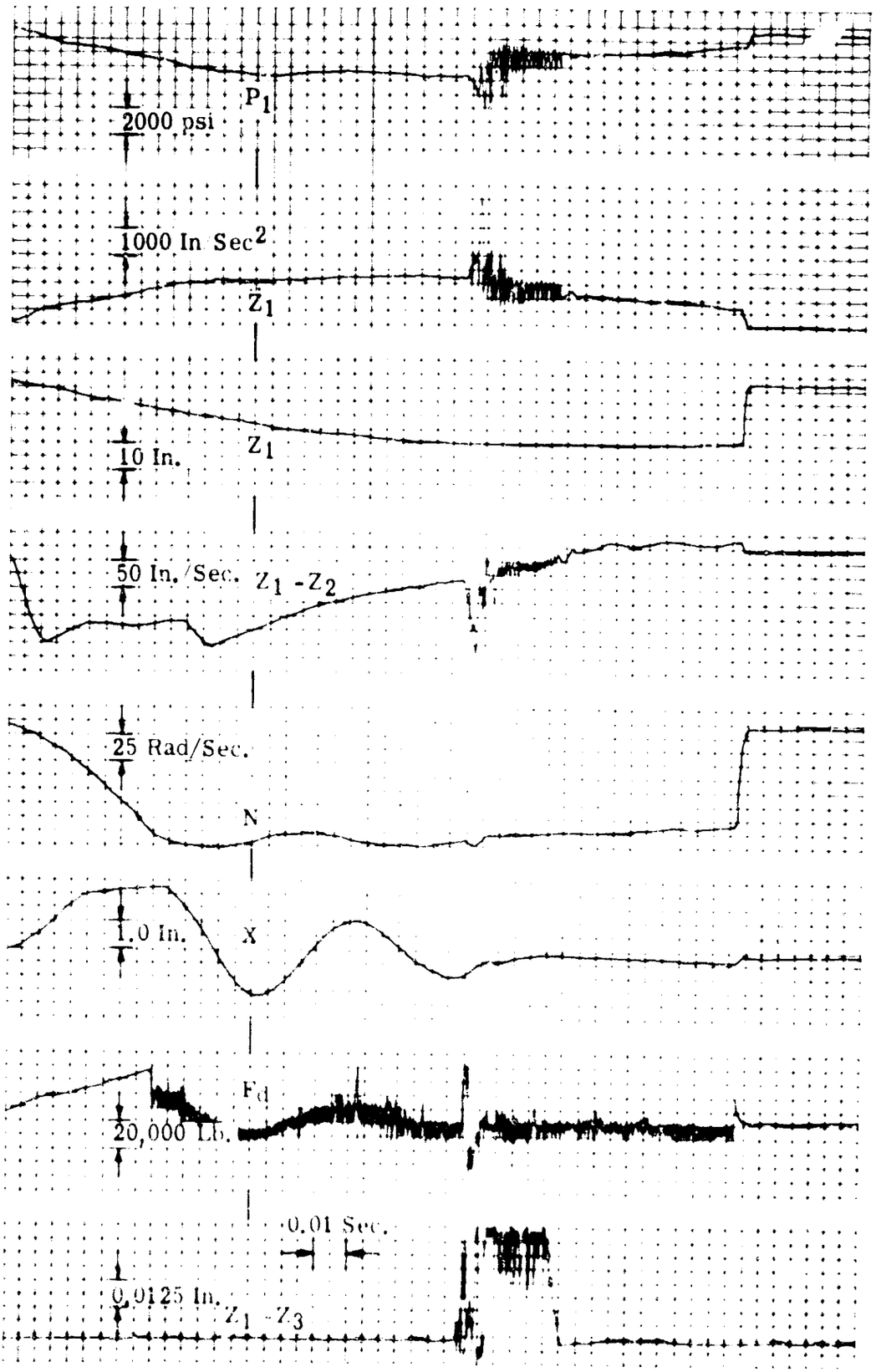

Figure 3-13. Run N[illegible]

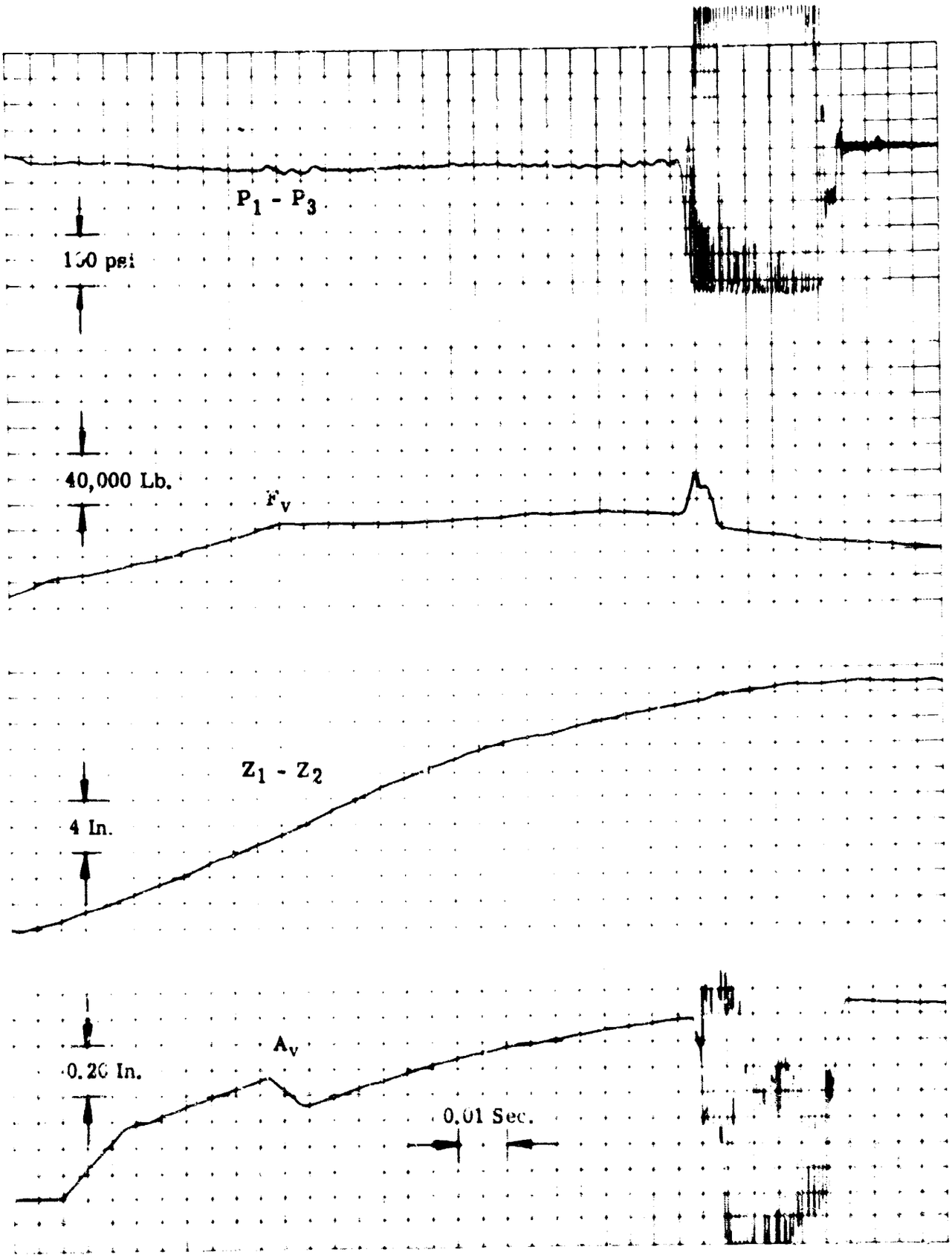

Figure 3-13A Run No. 96

3. Control chamber volume ($\forall_3$)
4. Plunger valve cross-sectional area (A_{p3})
5. Control chamber preload (R)

The effect of the particular instant of time during landing impact at which bump impact occurs is shown in Figure 3-14 and Figure 3-15. The complete computer results of these runs are given in Figures 16 through 31 in Reference 8.

Figure 3-14, in which the main mass acceleration vs. stroke is plotted, illustrates the improvement obtained by use of the band-pass mechanism. For low loads, those at two and four inches of stroke, the band-pass mechanism does little to improve the main mass acceleration due to the fact that the valve preload keeps the band-pass mechanism essentially closed. Once the vertical load has reached about 70,000 pounds, the band-pass mechanism begins to function effectively and main mass acceleration brought about by bump impact is considerably reduced. Figure 3-15 indicates that there is very little alleviation of the tire vertical load during bump impact through use of the band-pass mechanism.

The effect of airplane sink speed on the functioning of the band-pass unit is shown in Figures 3-16 and 3-17. These figures give the main mass acceleration and tire vertical load vs. stroke for Runs (105) through (116). The complete computer results of these runs are given in Figures 34 through 45 in Reference 8. Here, again it can be seen that the band-pass shock strut effectively reduces the loads transmitted to the main mass of the airplane when the vertical landing impact load is high. The series of drops at 12 ft. sec. sink speed show no improvement in bump impact loads due to the valve preload. On the other hand, the bump impact loads developed in the 23 ft. sec. drop show a slightly higher percentage reduction than those previously determined for the nominal sink speed of approximately 20 ft. sec.

The high sink speed drops also indicate that the 50-pound preload of the control chamber spring is sufficient to maintain the band-pass mechanism closed for the full range of sink speeds.

The effect of airplane forward velocity is shown in Figures 3-18 and 3-19. The first figure is the main mass acceleration vs. strut stroke for a forward velocity of 2300 in. sec. The second figure shows the same variables for a forward velocity of 3400. It can be seen that bump impact loads increase with velocity. The improvement gained by use of the band-pass mechanism is least for the lowest velocity at 16 inches of stroke. At the eight-inch stroke position, however, all three forward velocities, nominal, 2300 in. sec. and 3500 in. sec. result in approximately the same degree of improvement in the main mass acceleration.

As previously mentioned, parameter variation studies were carried out for A_{o3}, A_{o2}, $\forall_3$, A_{p3}, and R. Valve gain was not studied, since it was determined in the course of the miscellaneous exploratory runs that any slight increase in valve gain would result in instability at the near-compressed strut position. Valve mass and control chamber spring rate were found to have negligible effect within the range previously studied in connection with the simplified model.

(text continued on page 3-45)

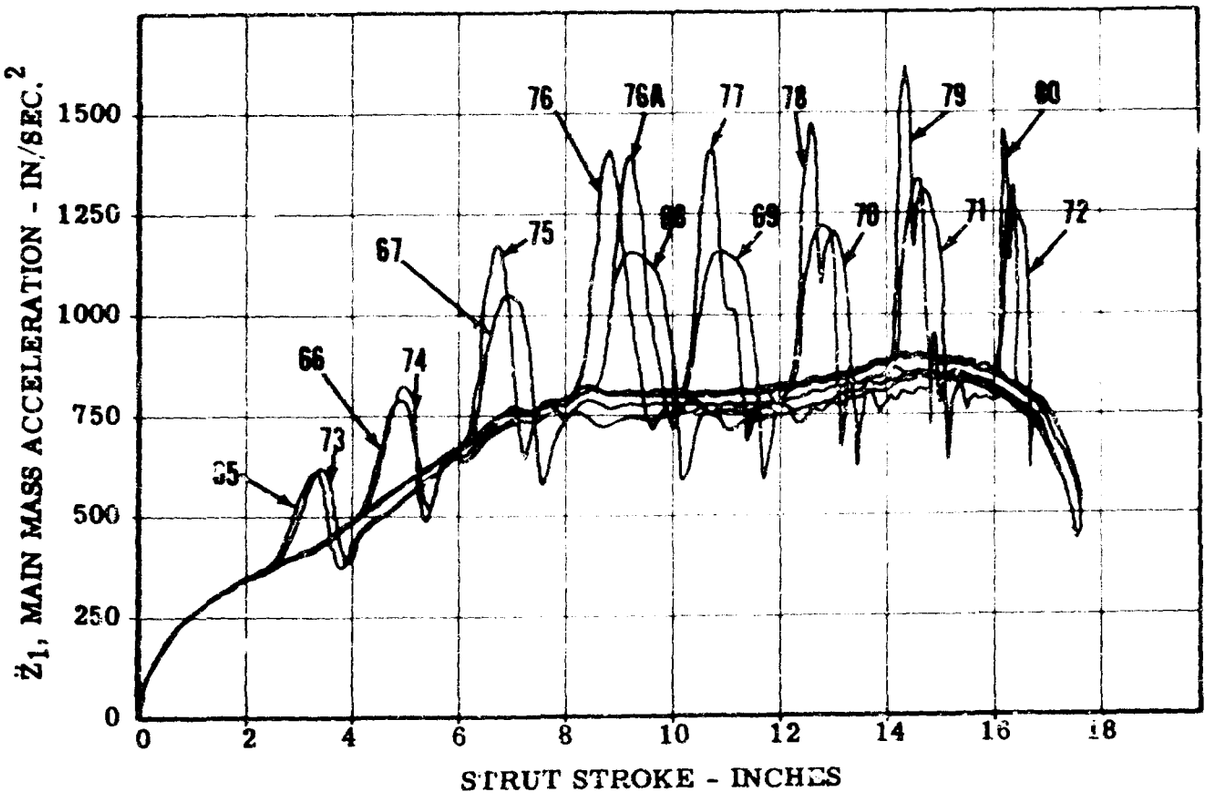

Figure 3-14. Main Mass Acceleration With and Without Band-Pass

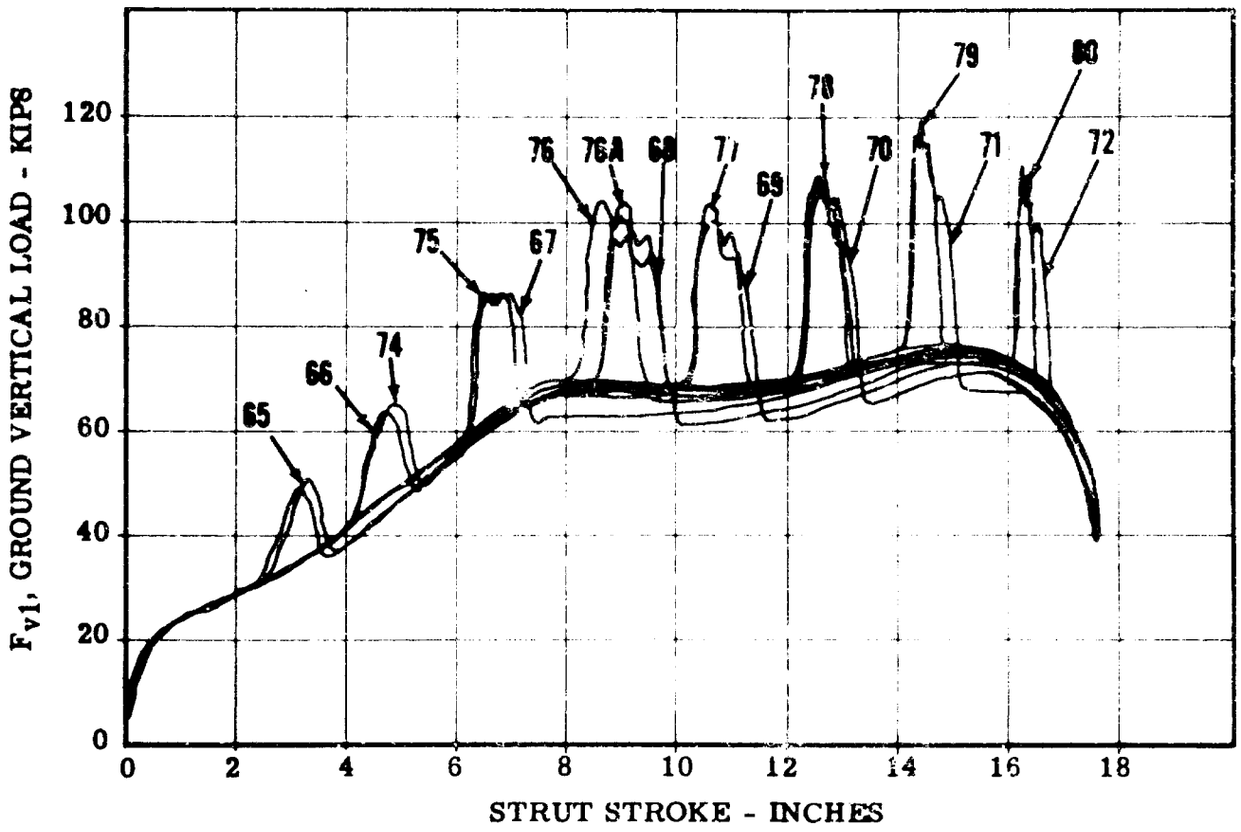

Figure 3-15. Ground Vertical Load With and Without Band-Pass

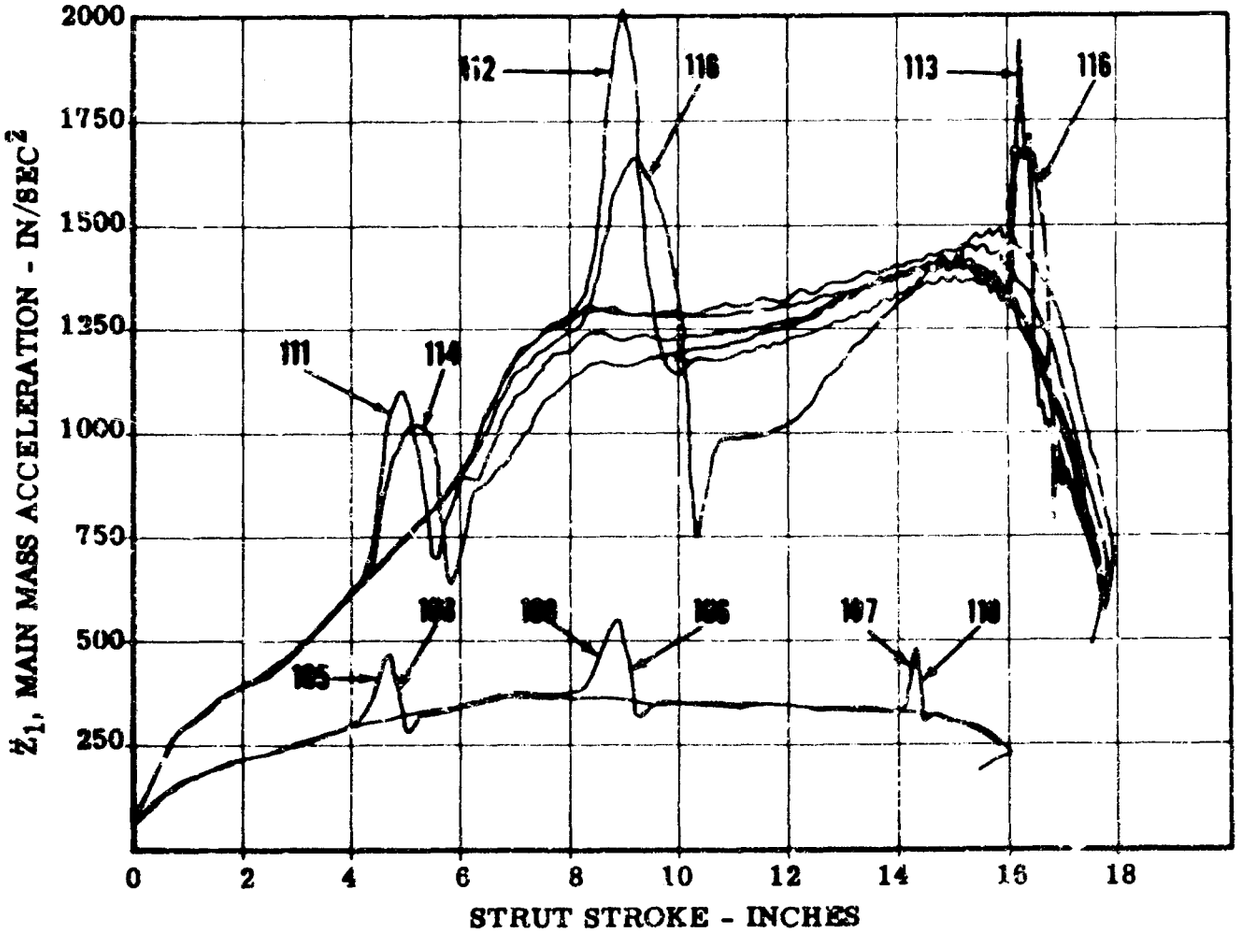

Figure 3-16. Effect of Sink Speed Main Mass Acceleration vs. Stroke With and Without Band-Pass

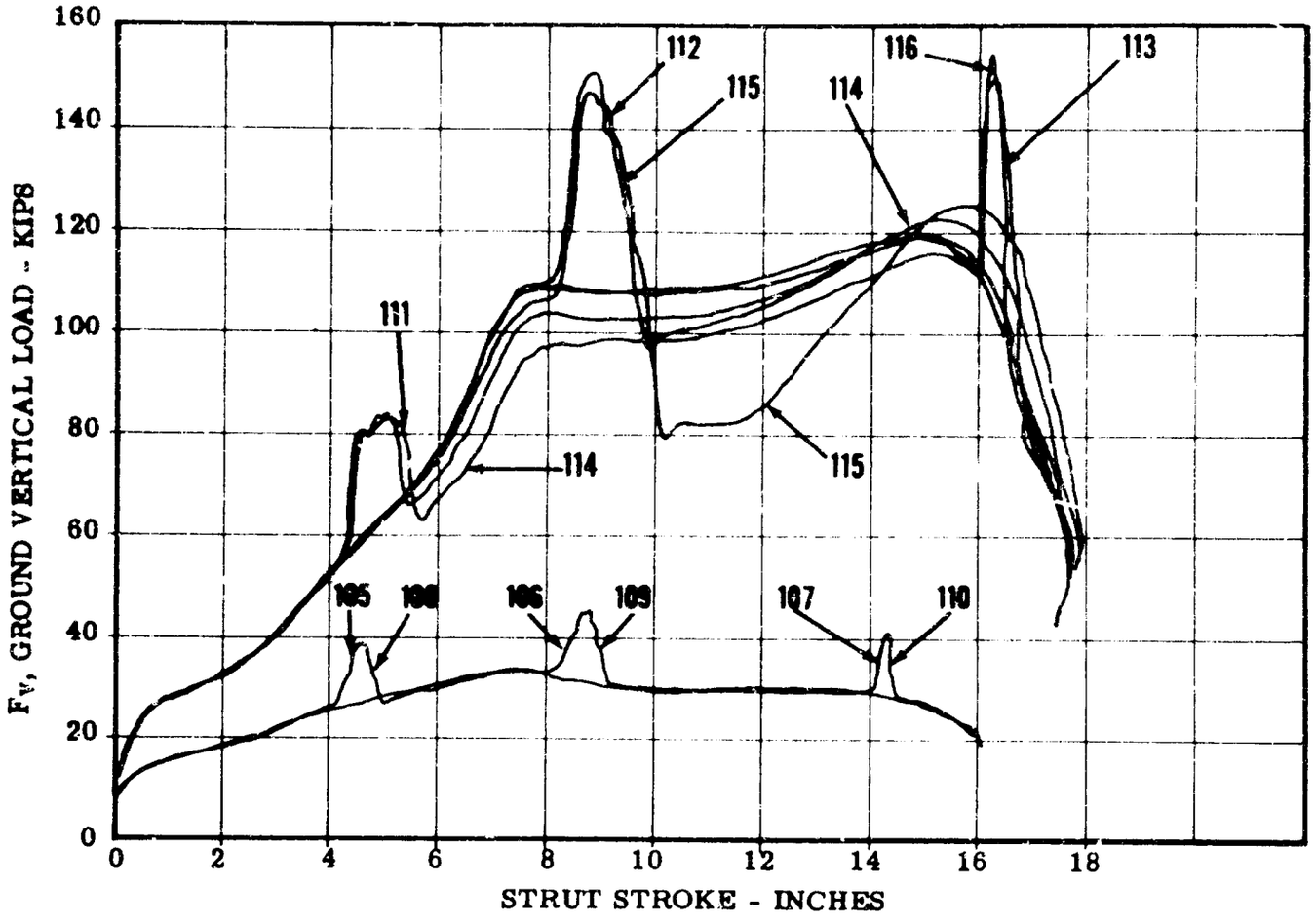

Figure 3-17. Effect of Sink Speed Ground Vertical Load vs. Stroke With and Without Band-Pass

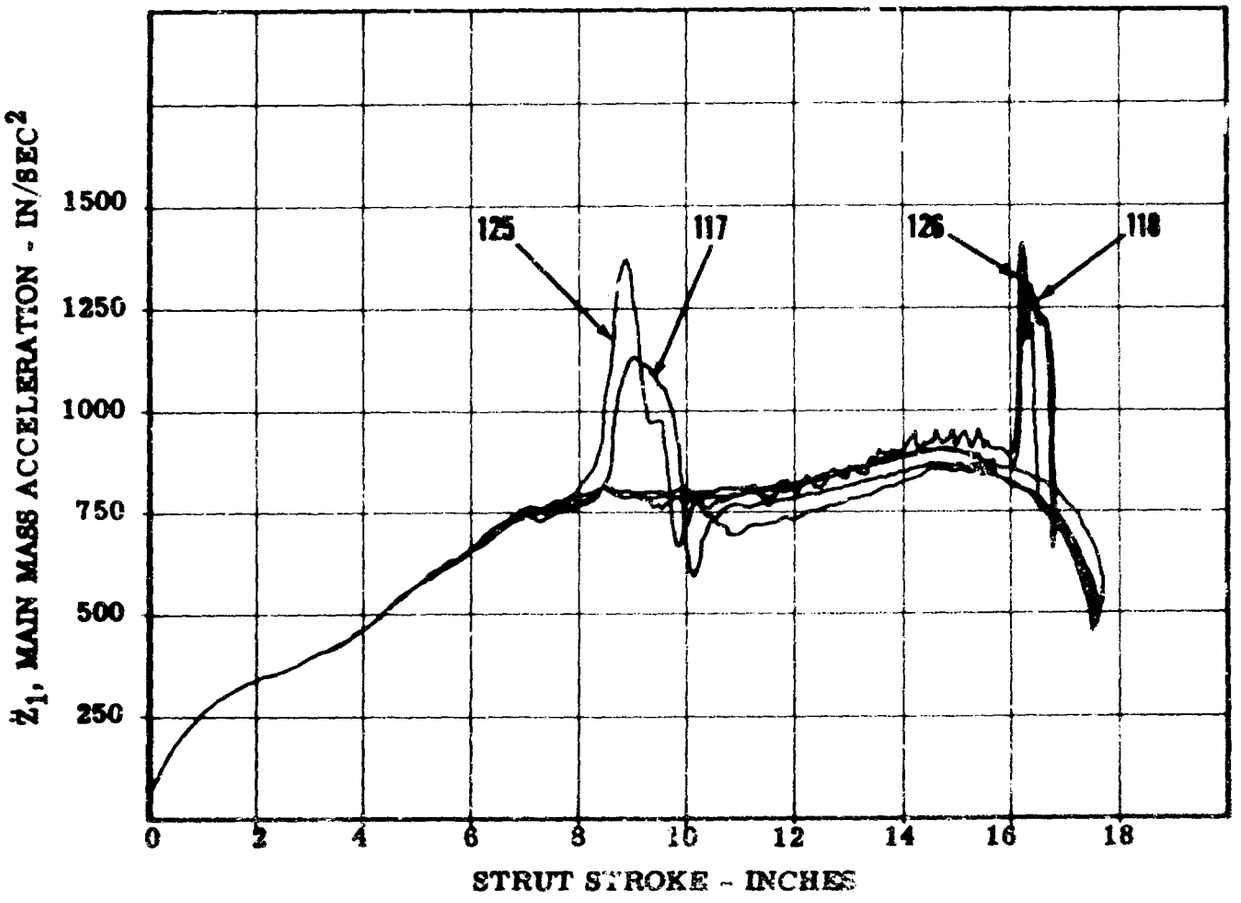

Figure 3-18. Effect of Forward Velocity-Low Velocity Impact

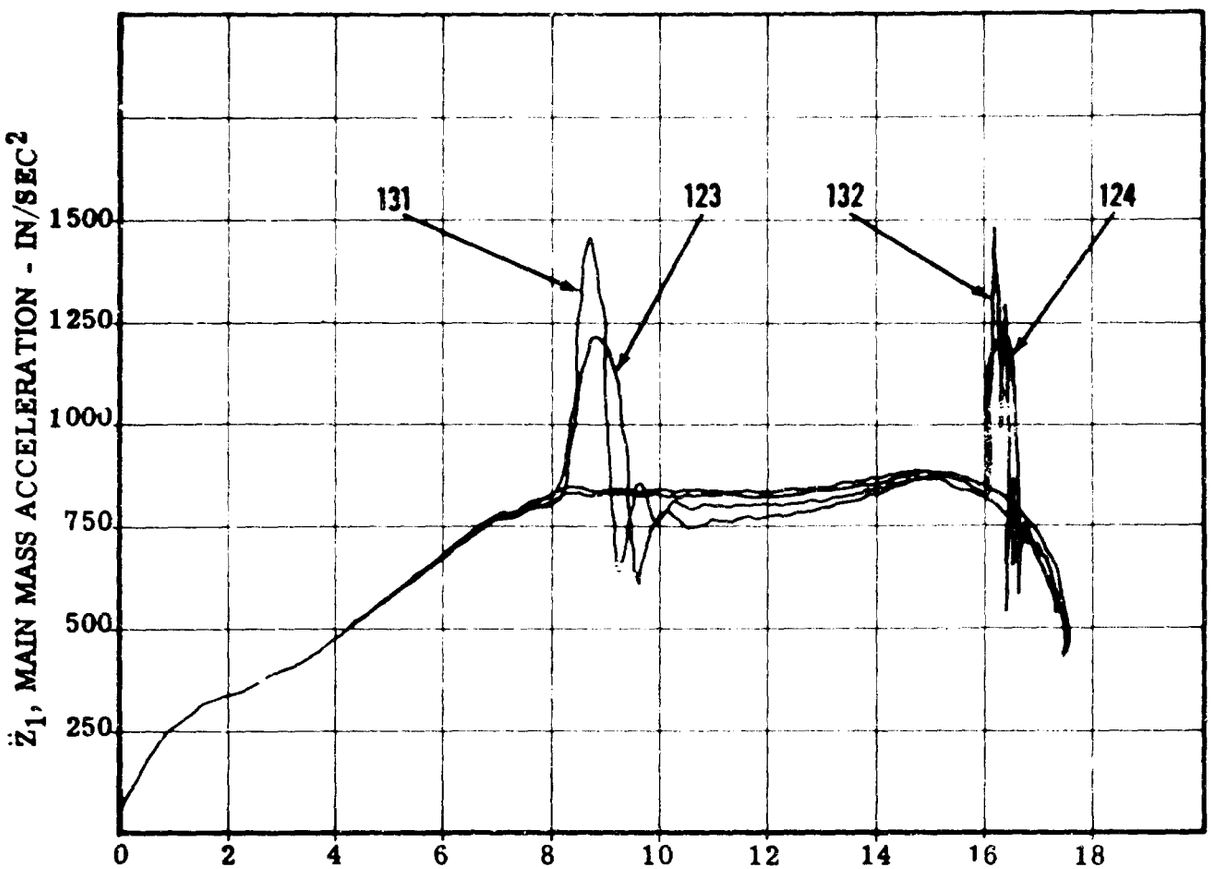

Figure 3-19. Effect of Forward Velocity-High Velocity Impact

The effect of A_{03} is shown in Figure 3-20, in which the main mass acceleration brought on by bump impact is plotted against A_{03}. Here, the ratio of A_{03} to A_{02} was not maintained fixed so that the smaller values of A_{03} would require a preload larger than the nominal value of 50 lbs. Therefore, runs were made with both 50 and 100 lb. preload at the lowest value of A_{03} (.005 in.^{2}). Comparison of the points for the bump impact, at eight inches of stroke, reveals the same general trend previously seen in Figure 3-7B. However, the points for the bump impact at 16 inches of stroke seem to violate previous contentions that decreases in A_{03} decrease the load transferred to the main mass, since the orifice size results in larger incremental main mass acceleration. The reason for this is the severe instability encountered with the combination of reduced inlet orifice area and reduced dynamic chamber volume. Extreme fluctuations in the P_1 pressure resulted from the valve instability thus increasing the main mass acceleration. The optimum value on A_{03} appears to be in the vicinity of .010 in.^{2}.

The effect of A_{02} on main mass incremental acceleration is shown in Figure 3-21. Since increasing A_{02} decreases A_{03}/A_{02}, higher preload is required for the higher values of A_{02}. The combined effect of increased A_{02} and increased preload at the larger values of A_{02} bring about higher loads for the bump impact occuring at 16 inches of stroke. Reducing A_{02} increases the ratio of A_{03}/A_{02} thus resulting in higher loads. The optimum value of A_{02} appears to be in the vicinity of .001 in.^{2}.

The effect of v_3 on main mass incremental acceleration is illustrated in Figure 3-22. Here the nominal value of 3.0 in.^{3} is near optimum. Increasing v_3 leads to instability and severe fluctuations in the dynamic chamber pressure. The 285 ft./sec.^{2} increase in the main mass acceleration for $v_3 = 5$, in Figure 3-22, is not precise since the computer overloaded during this instability, exaggerating the P_1 pressure fluctuation. However, the accelerations developed prior to saturation were considerably greater than those developed for $v_3 = 3.0$.

A similar effect is obtained by decreasing A_{p3}. The instability resulting from reducing A_{p3} to .50 in.^{2} is shown in Figure 3-13. Increasing A_{p3} to 1.00 in.^{2} alleviates the instability, but increases the main mass incremental acceleration. Figure 3-23 indicates that the value of .785 in.^{2} is near optimum for this parameter.

The effect of preload on the main mass incremental acceleration is shown in Figure 3-24. As expected, reducing preload decreases the main mass incremental acceleration. Reductions below 50 pounds cannot be tolerated however, since this would result in the band-pass valve opening for sink speeds in the vicinity of 23 ft./sec.

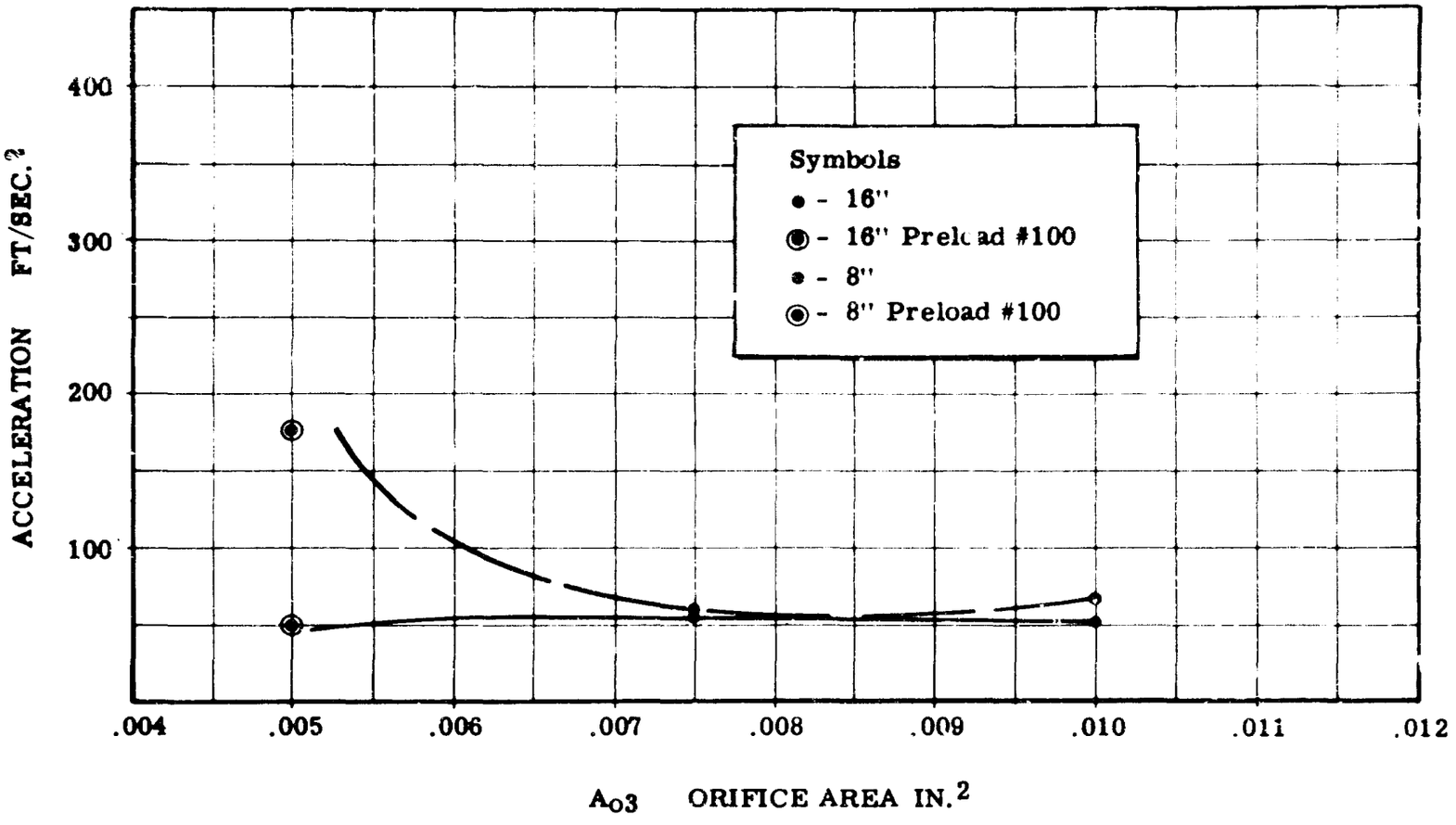

Figure 3-20. Parameter Variation Studies Analytical Investigation of Band-Pass Applied to North American A3J-1 Main Landing Gear Effect of A_{03} on Main Mass Incremental Acceleration

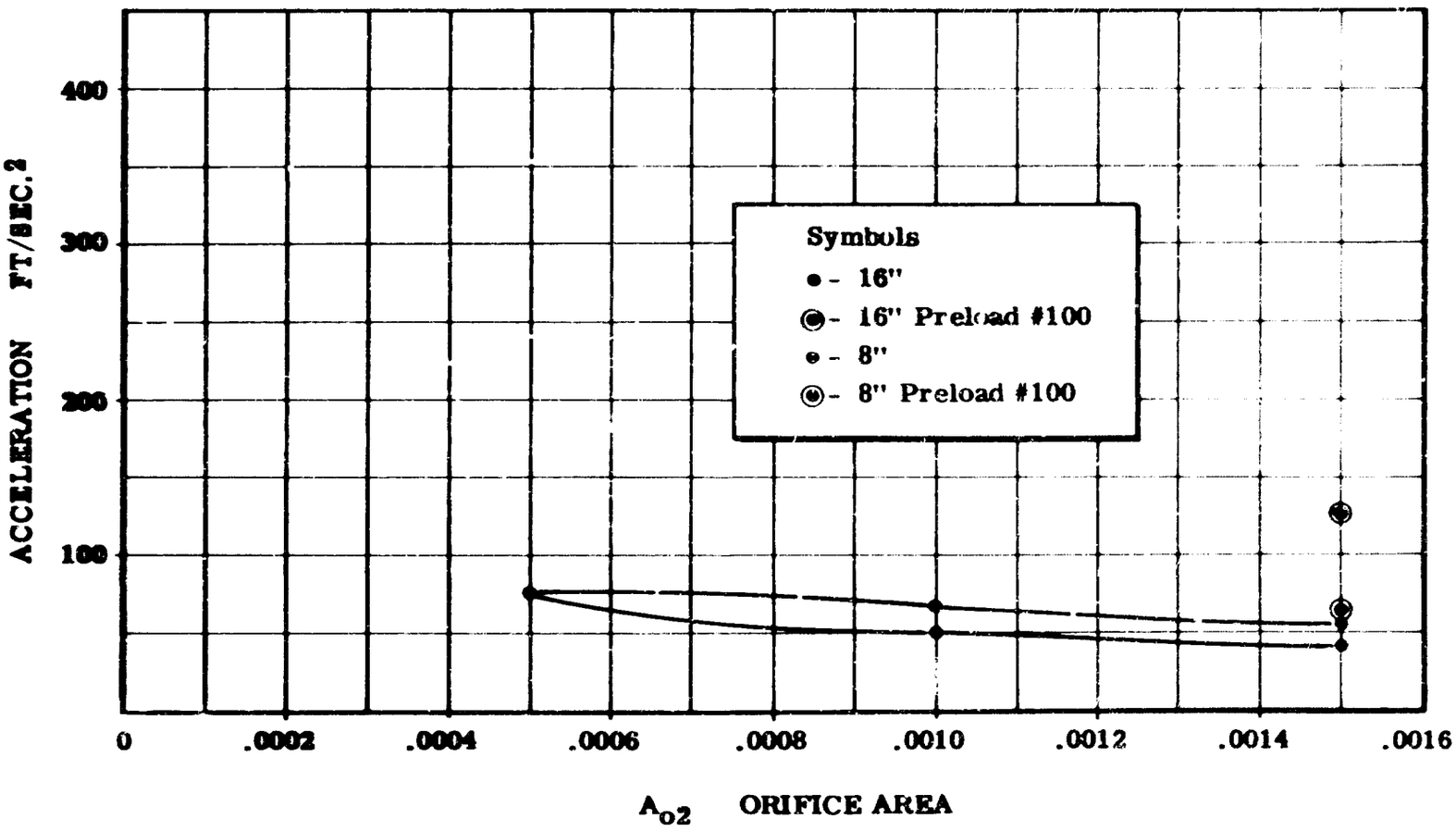

Figure 3-21. Parameter Variation Studies Analytical Investigation of Band-Pass Applied to North American A3J-1 Main Landing Gear Effect of A_{o2} on Main Mass Incremental Acceleration

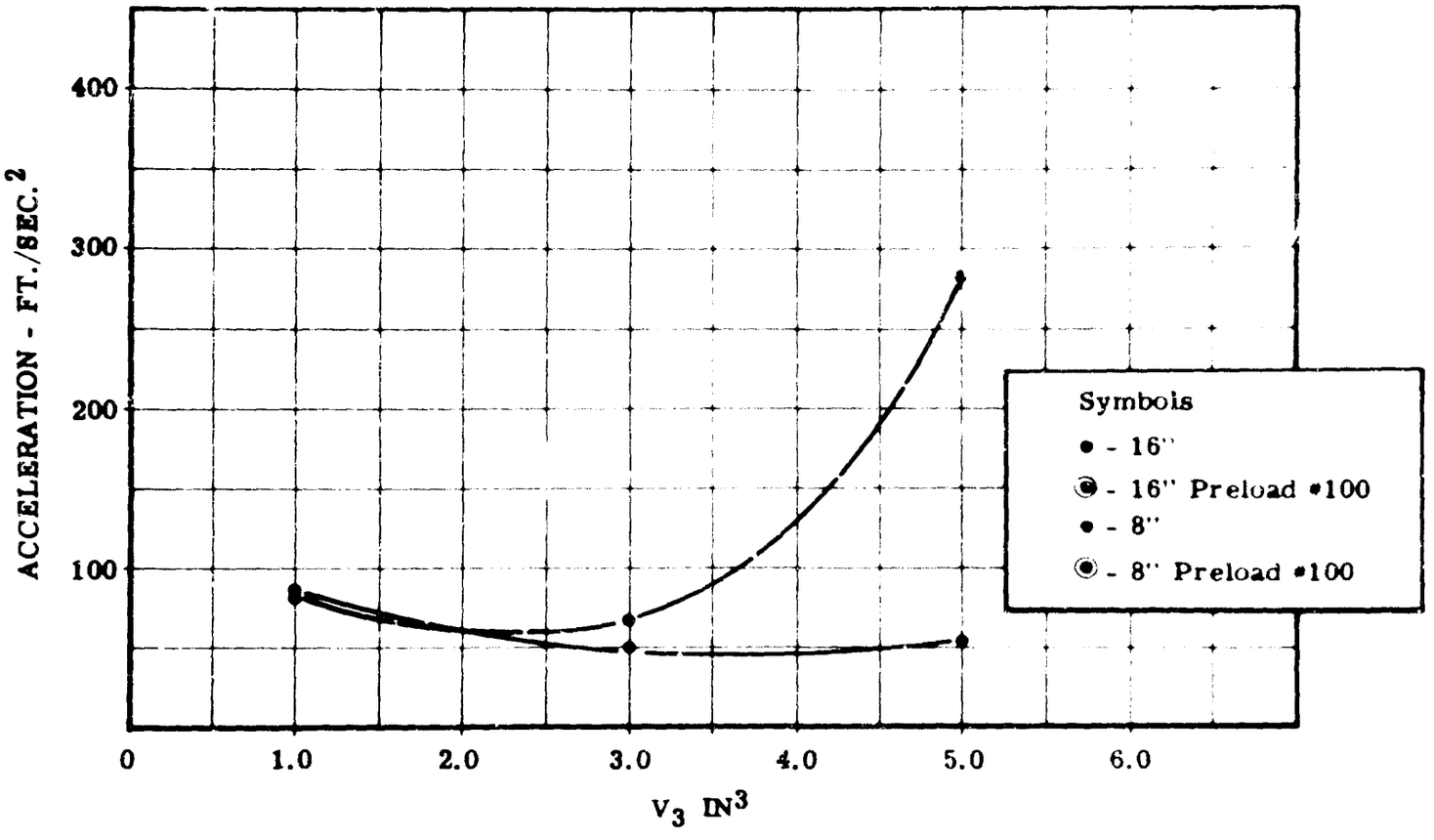

Figure 3-22. Parameter Variation Studies Analytical Investigation of Band-Pass Applied to North American A3J-1 Main Landing Gear Effect of V_3 on Main Mass Incremental Acceleration

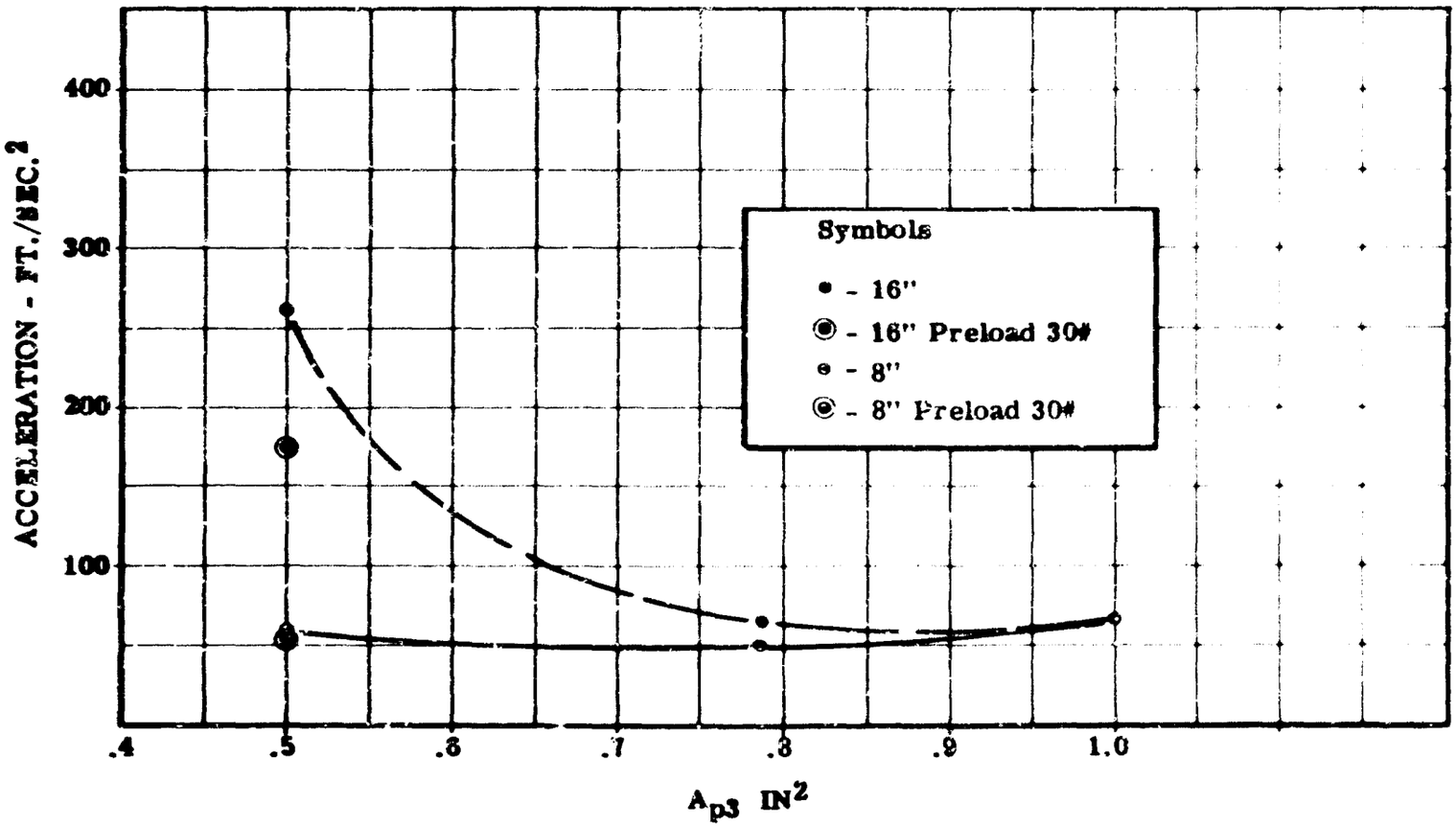

Figure 3-23. Parameter Variation Studies Analytical Investigation of Band-Pass Applied to North American A3J-1 Main Landing Gear Effect of A_{p3} on Main Mass Incremental Acceleration

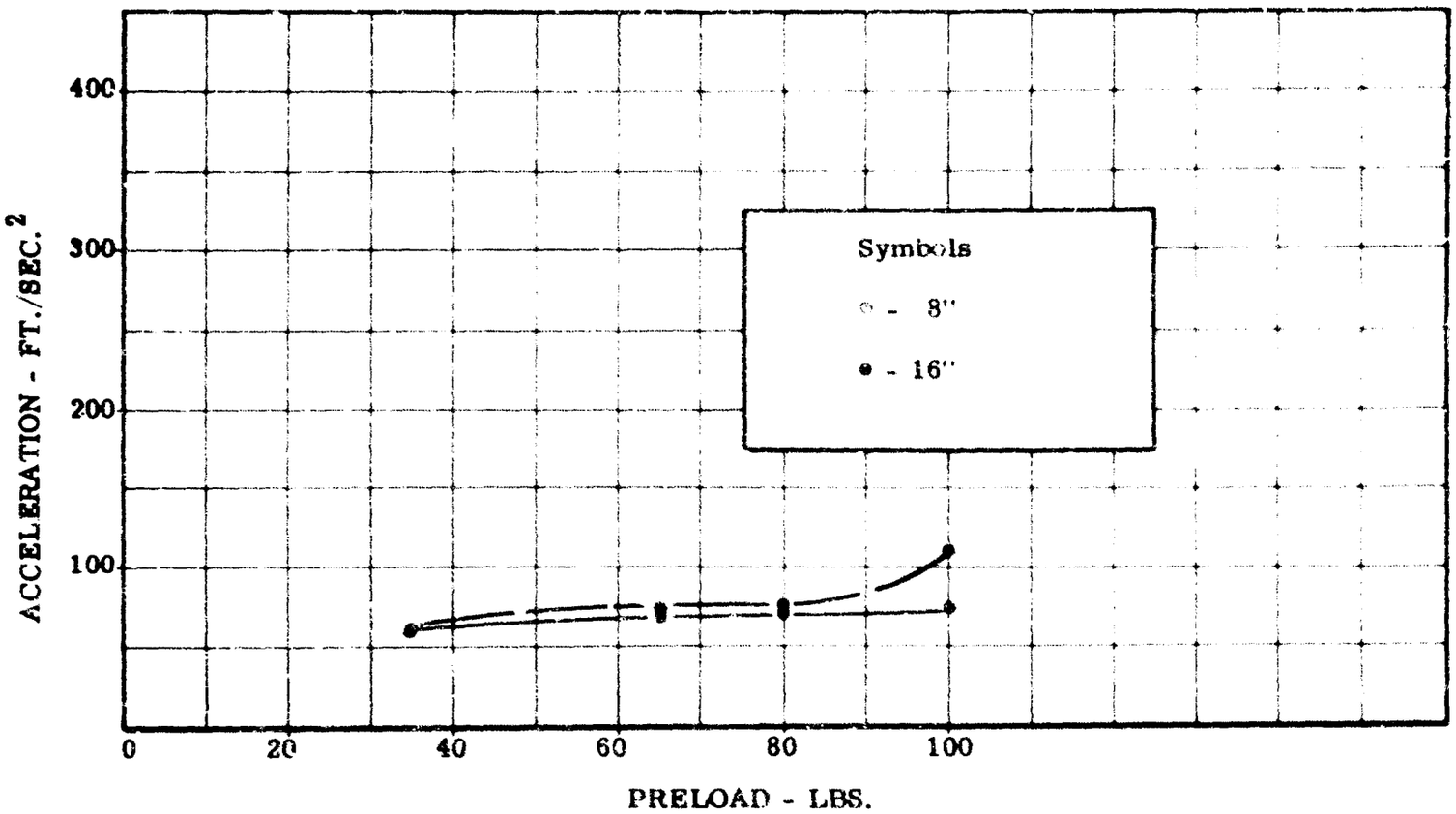

Figure 3-24. Parameter Variation Studies Analytical Investigation of Band-Pass Applied to North American A3J-1 Main Landing Gear Effect of Preloads on Main Mass Incremental Acceleration

GENERAL CONCLUSIONS FROM ANALYTICAL STUDY

1. A low pass hydraulic band-pass mechanism can be adapted to modern airplane landing gear shock struts to reduce the loads transmitted to the airframe. The load reduction that can be realized by such a device is on the order of 50 percent of those additional loads imposed by high frequency bump input occuring during landing impact.

2. A band-pass mechanism within the shock strut will not significantly reduce impact loads on the wheel and tire.

3. The design of a band-pass mechanism for any given landing gear application can be carried out using the simplified model derived in this study. Parameter adjustments to obtain near optimum performance of the unit based on the simplified model agree with those of the model of the complete landing gear system.

4. The natural frequency of the valve should be within the following range

$$12 < \frac{\lambda}{2\pi V}\sqrt{\frac{A_{p3}^2 B + K_s V_3}{V_3 M_3}} < 45$$

where λ = wave length of input bump load
v = forward velocity of airplane

5. Preload of the valve can be determined from Equation (7). Valve preload should be adjusted to a value slightly above that resulting from the highest stroke velocity during landing impact.

6. A band-pass mechanism for the A3J-1 shock strut should be designed to have the following numerical values for its parameters:

A_{o2} = .001 in.^{2}
A_{o3} = .010 in.^{2}
A_{p3} = .785 in.^{2}
α_v = 10.0 in.^{2}/in.
K_s = any value convenient
M_3 = .00035 to .00070 lb.sec.^{2}/in.
R = 50 lbs.

A preliminary design of such a valve is shown in Figure 3-25

7. The analytical study indicates that stability will be a limiting factor in design. If the stability question was not of concern, several of the above parameters could be adjusted to give greater attenuation of bump impact loads transmitted to the airframe. The problem of valve stability will have to be carefully examined in the experimental phase of the program.

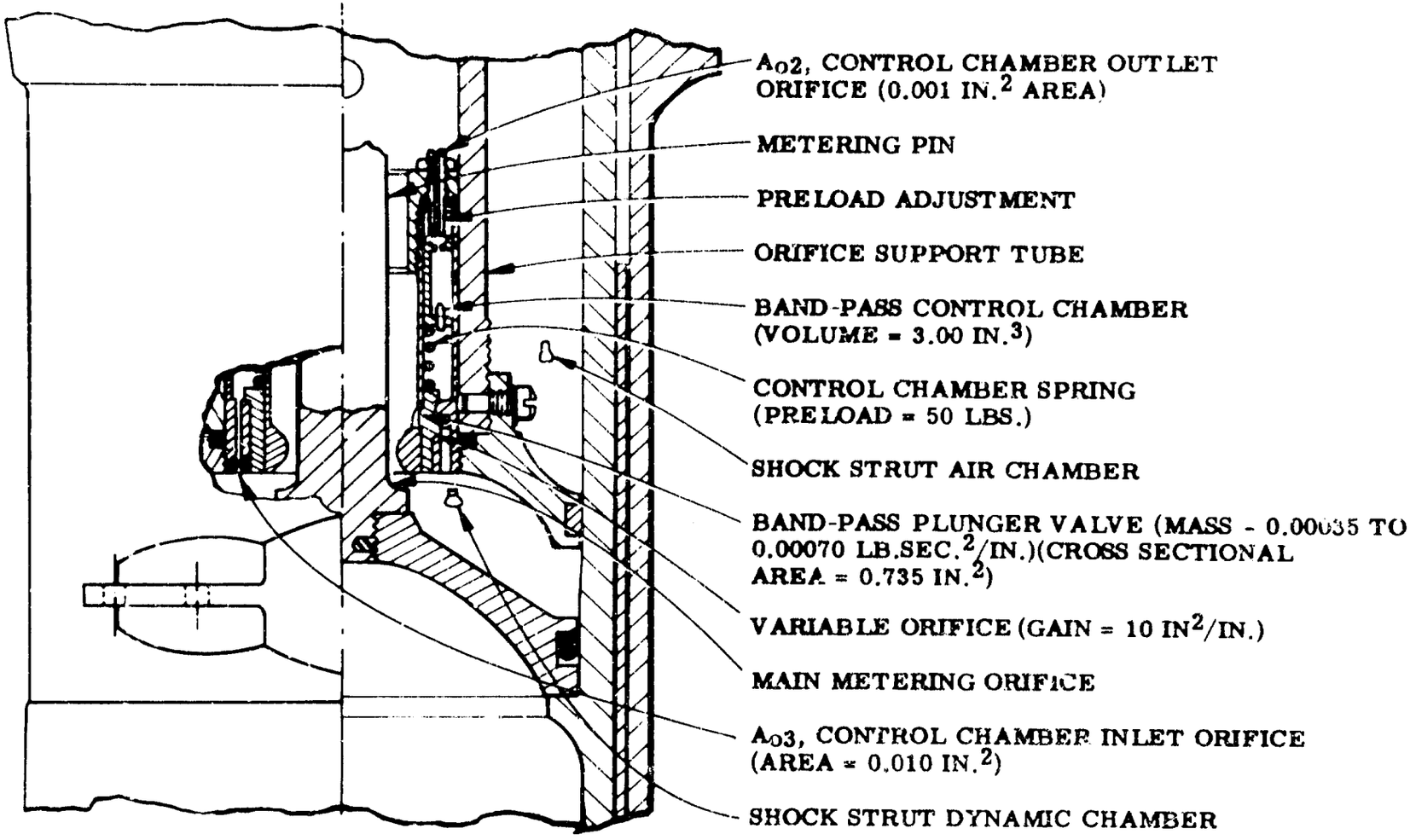

Figure 3-25. Preliminary Design of Band-Pass Unit Adapted to North American A3J-1 Main Landing Gear Shock Strut

SECTION IV

TECHNICAL DISCUSSION - EXPERIMENTAL PROGRAM

Test Request SDT-3528 was written to cover the experimental program. The theoretical program gave methods of design and optimization of a band-pass unit for application to any particular shock strut. The purpose of the experimental study was to confirm these methods by correlation with the computer program.

TEST SET-UP

The modified A3J-1 MLG was mounted in the drop tower above the 120 inch dynamometer. (See Figure 4-1). Spacial geometry at the attachment points simulated the actual installation of the landing gear in the aircraft. Safety cables were attached to the hoist used for raising and lowering the overhead platform. These cables were a safety feature providing means for raising the platform rapidly in case of failure of any part of the landing gear. These cables however, did limit the drop height to that providing a 19.6 foot per second impact velocity.

Two different types of cable throwing devices were used. The first was a steel tube with one end modified to hold the cable. The other end of the tube was pinioned so that the tube could swivel over the dynamometer wheel. Four inches of cable rested on this tube with the remaining cable overhanging the flywheel. The tube was spring loaded and held in place by a magnet. When a drop was made, the platform activated a switch which released the cable. Proper location of the switch determined the position of strut stroke at which time the cable would pass under the tire. This type device proved not too successful. The main problem was to develop sufficient force to force the cable segment between the tire and the flywheel. A second device was fabricated whereby the cable was pulled along two guide rods and under the tire by two aircraft shock cords. These shock cords, acting as springs, were stretched before the release of the drop rig. When a drop was made, the rig would throw a switch which released the cable. By moving the switch, the time at which the cable went under the tire could be altered.

This system, although workable, was not completely adequate. In retrospect such testing on a dynamometer flywheel is not recommended for the future.

SPECIMEN

The band-pass unit, Bendix Assembly Number RXD-18342, was designed for the North American A3J-1 Main Landing Gear. Detail drawings are numbered RXD-18343 through

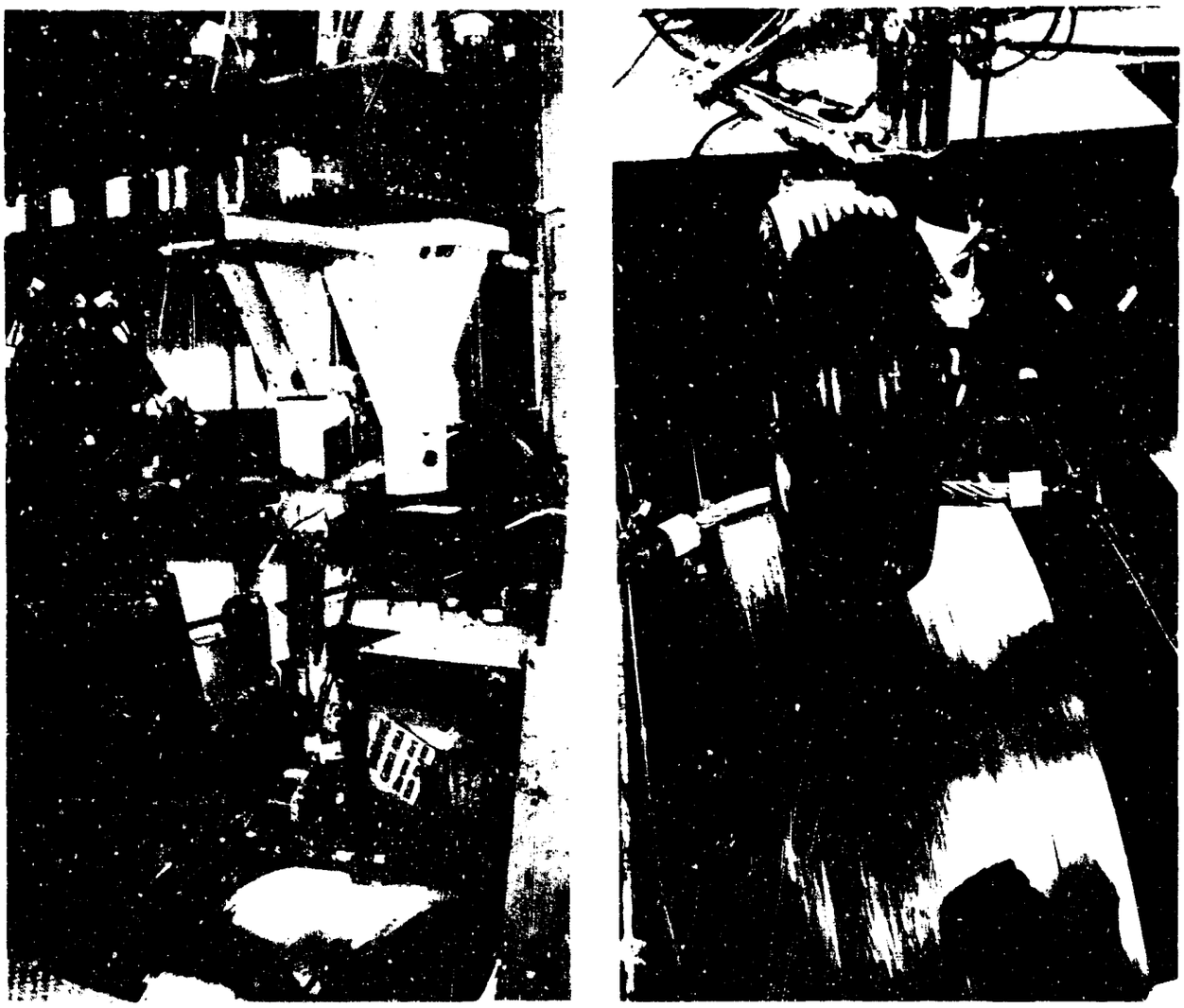

Figure 4-1. A3J-1 MLG Test Installation

RXD-16362. The orifice support tube was the only part of the A3J-1 strut that had to be modified in order to install the band-pass unit into the strut. The additional weight of the unit is approximately eight pounds.

The strut was a left hand main landing gear shock strut, Bendix Assembly Number 170687. The metering pin and orifice used had Bendix Part Numbers 170777 and 170764 respectively. This was the metering pin - orifice combination that was developed in the Bendix drop test and has the orifice area used in the analytical studies. Figure 4-2 shows the band-pass mechanism.

INSTRUMENTATION

A Consolidated Electrodynamics Corporation Recording Oscillograph, Type 5-114-P4 was used to obtain traces of vertical fork load, strut stroke, rig acceleration, unsprung mass acceleration, air pressure, hydraulic pressure, the pressure in the band-pass unit, the band-pass valve travel, and an indication of when the cable was underneath the tire. These were recorded with respect to time. The methods of picking up the individual parameters are described in the following paragraph.

Vertical Fork Load

Several strain gages were mounted on the fork and the output of gages measured for vertical load and for drag load. Two gages were wired in series to cancel out the interaction of drag load and the output of the gages recorded on the oscillograph. However, the vertical and drag loads applied during calibration were low in comparison to the drop loads experienced. Also, the effect of side load is unknown. For these reasons, the fork load was used as an indication of the relative loads and not a measure of the actual load.

Strut Stroke

A sliding contact on a wire was used to obtain an oscillograph trace of the strut stroke. The linearity trace was proven before the test was started. The stroke is calibrated by physically measuring the maximum stroke after each drop and equating this to the maximum deflection on the oscillograph.

Rig Acceleration

A Statham accelerometer was mounted on the rig near the center of gravity. This acceleration is linear for the range measured. A calibration of one 'g' can be measured during free fall for each record.

Unsprung Mass Accelerometer

A Statham accelerometer was mounted at the axle on the fork side of the strut. The calibration factor for this accelerometer is 100 g's.

Air Pressure

A precalibrated pressure capsule, was used to measure the air pressure. This capsule

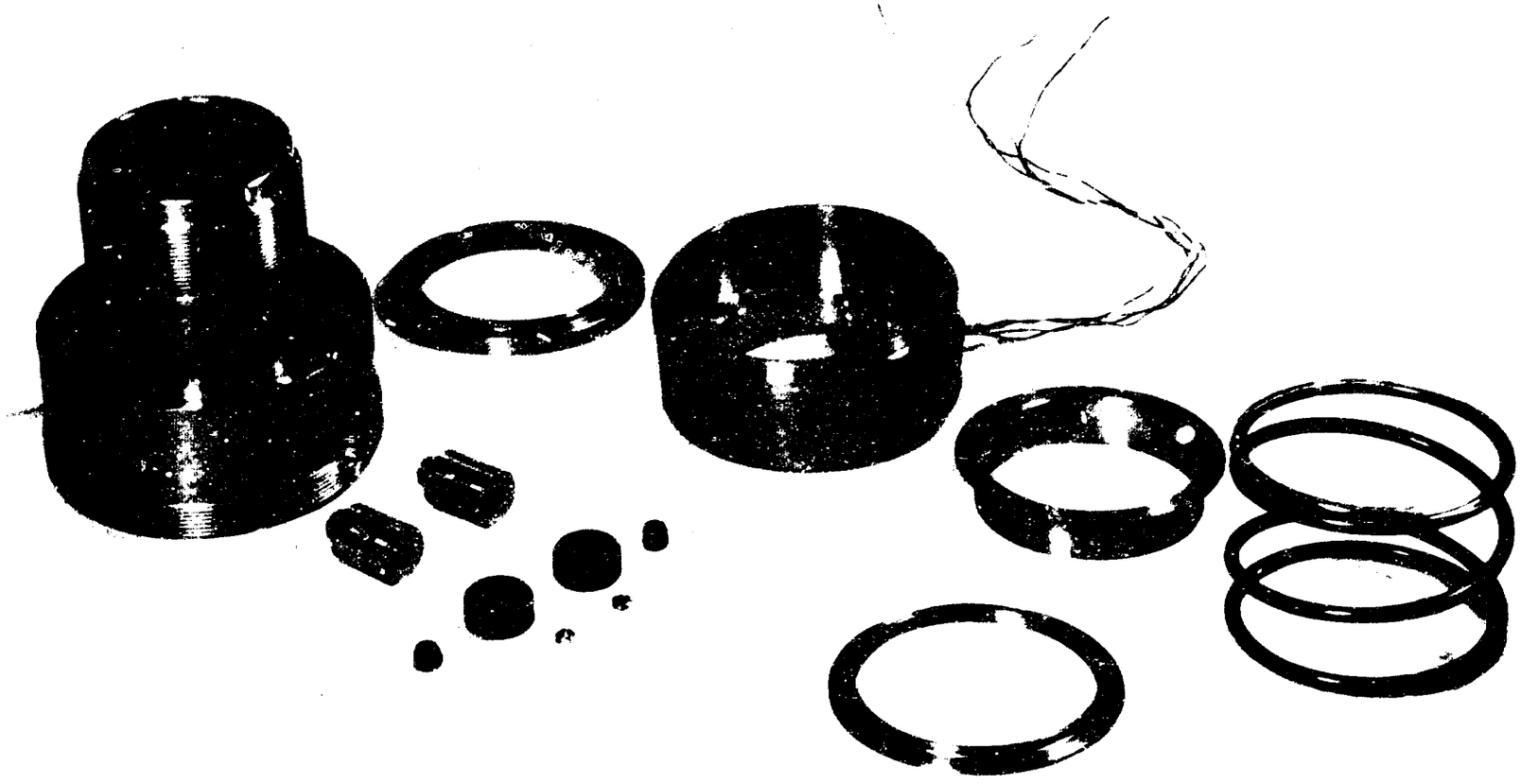

Figure 4-2. Band-Pass Mechanism

was mounted at the filler plug. Calibration of the capsule is linear and the calibration factor is 610 psi.

Hydraulic Pressure

The hydraulic pressure below the orifice was measured by drilling a hole in the metering pin diaphragm. A precalibrated pressure capsule was attached to the diaphragm at this opening to create a continuous passageway to the capsule. Calibration of the capsule was linear and the calibration factor is 3850 psi.

Internal Pressure in Band-Pass Unit RXD-18356

Part RXD-18356 was instrumented with strain gages to read hoop tension. The output of these gages was measured as a function of pressure. The calibration of these gages was linear and the calibration factor is 870 psi.

Band-Pass Valve Travel

The travel of the slide valves in the Band-Pass Unit was measured by using a Bently distance detector system. The sensing head is a pancake-wound coil which is loaded by the pressure of any conductive material. The distance the conductive material moves is determined by voltage change of the control unit. This is measured by galvanometer deflection on the oscillograph. The calibration of oscillograph deflection versus valve travel is in Figure 4-3.

Time of Cable Impact

A wire was attached to the cable that would break when the cable went under the tire. This broke the circuit to the oscillograph causing an abrupt galvanometer trace deflection.

TEST PROCEDURE

The gear with the band-pass unit installed was mounted as previously described. An extended strut air pressure of 186 psig was used for all drops.

A tire pressure of 250 psig and the band-pass unit blocked was used to start the test work. Initial drops were made at a low drop height and the drop height increased in increments using the cable for all drops. This was done to establish the size of the bump impact. Even though the cable was going under the tire at or near the peak load, the load increase due to the cable was small.

The bump impact would be worst, i.e. have higher load increase at or near a flat tire condition. Therefore, the tire pressure was reduced in 25 psi increments. At 175 psi tire pressure and 15 feet per second sink speed the incremental load increase due to the cable was significant.

The test program was continued and finished using 175 psi tire pressure.

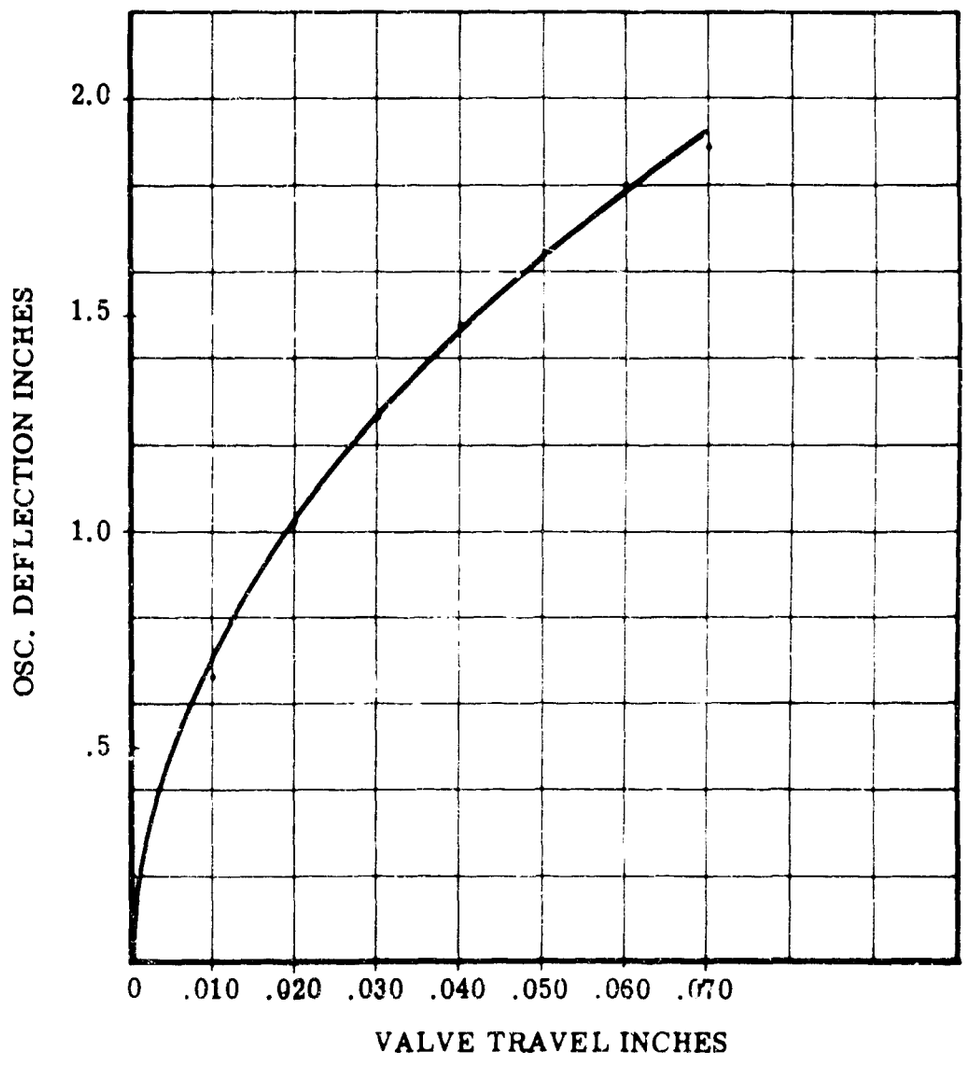

Figure 4-3. Band-Pass Valve Travel

An outline of the conditions and the drops made at those conditions follows:

I. Normal Strut Configuration (i.e. No Band-Pass Unit) Part II SDT-3528.

A. Without cable, (normal drops).

B. With cable.

Both made at 10, 12, 14, 15, 16, 17, 18 feet per second sink speed. Graphs of strut load versus stroke have been plotted for the above and appear on Figures 4-4 to 4-10.

II. Nominal Band-Pass Configuration Parts I and III SDT-3528 .001 outlet orifice, .010 Inlet Orifice, 60 pound preload on spring.

A. Without cable.

B. With cable.

Both made at 10, 12, 14, 15, 16, 17, 18 feet per second sink speed.

For Part I and II the lower drop heights, under 36.5 inches which is 14 feet per second vertical velocity, the cable impact load is small enough so that it is hard to distinguish normal variation of the load curve from the cable impact loads.

Graphs of strut load versus stroke have been plotted for the above and appear on Figures 4-11 to 4-16.

III. Parameter Changes - All drops at 17 feet per second made with and without cable.

A. Oil Volume Change Part VII SDT-3528.

1. Reduced 35% (Maximum change that could be accomplished).

2. Reduced 25%.

B. Nominal Oil Volume - Change inlet and outlet orifices so that the ratio of areas was 10. Part V SDT-3528.

1. .002 Inlet .0002 Outlet.
2. .005 Inlet .0005 Outlet.
3. .015 Inlet .0015 Outlet.
4. .020 Inlet .0020 Outlet.

C. Inlet orifice changed, outlet constant so ratio changed. Therefore spring preload had to be changed (Nominal .010, .001 60 lb.) Part VI SDT-3528.

1. Inlet .005, Outlet .001 (Nominal) Spring Preload 125 Pounds.
2. Inlet .015, Outlet .001 Spring preload 40 pounds.

(text continued on page 4-25)

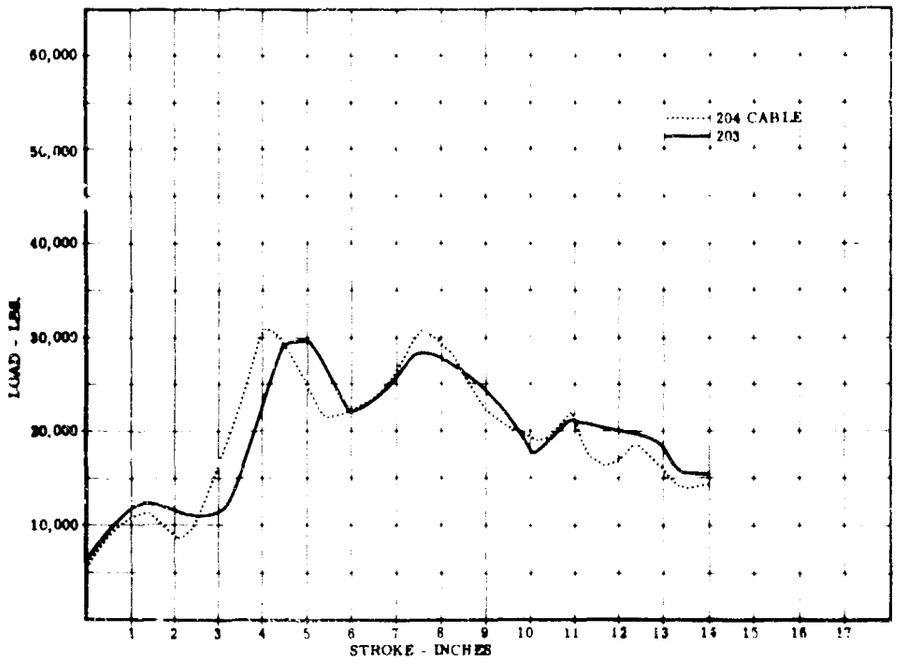

Figure 4-4. Band-Pass Test, A3J-1 MLG, Drop Height - 18.7 Inches, Band-Pass Inoperative

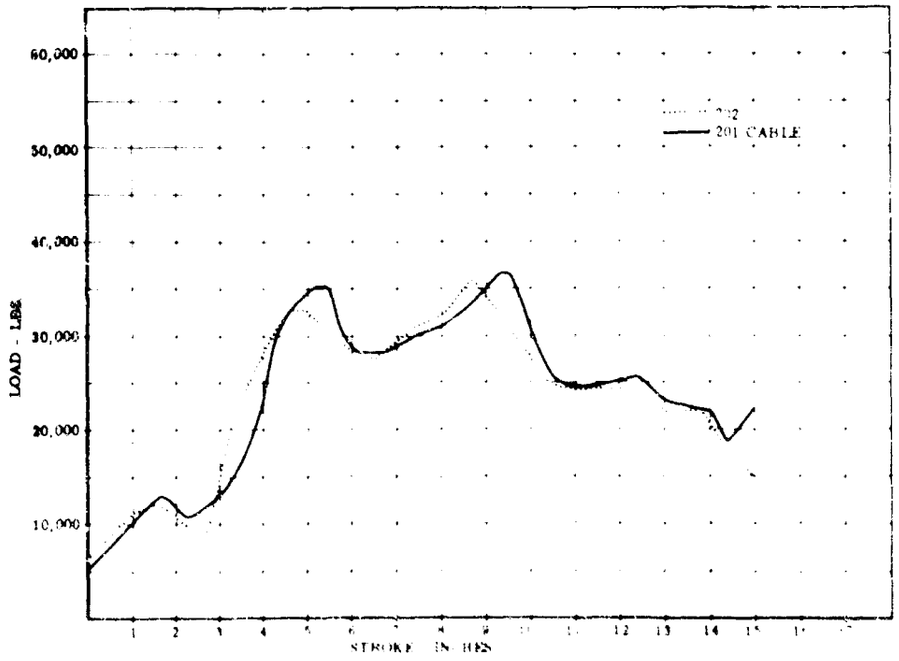

Figure 4-5. Band-Pass Test, A3J-1 MLG, Drop Height - 27 Inches, Band-Pass Unit Inoperative

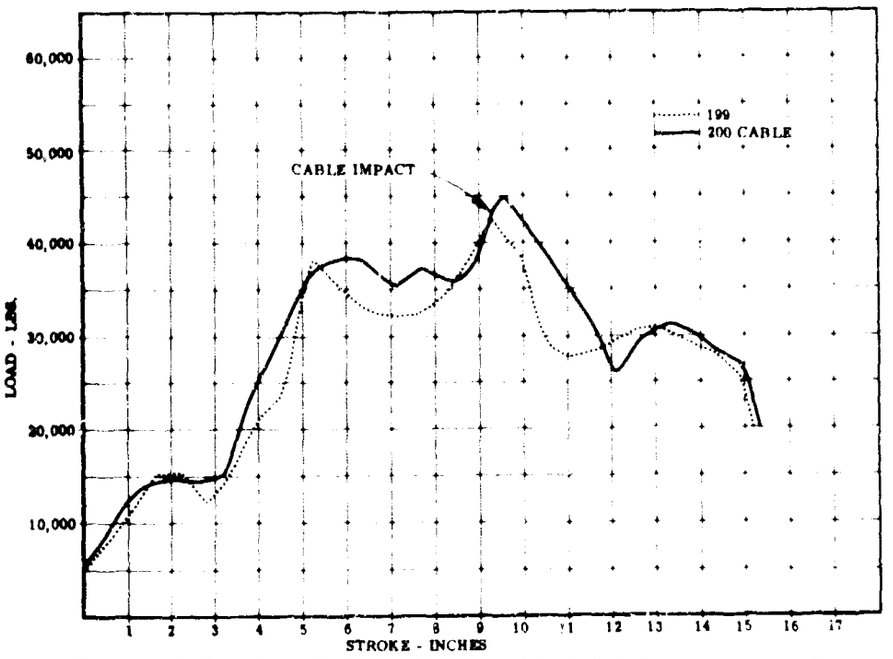

Figure 4-6. Band-Pass Test, A3J-1 MLG, Drop Height - 36.5 Inches, Band-Pass Unit Inoperative

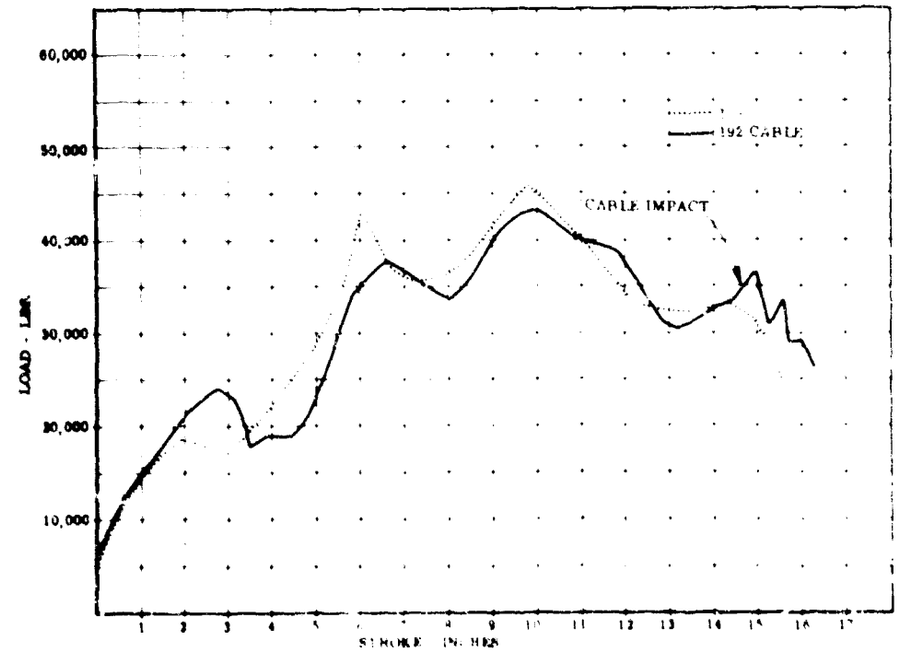

Figure 4-7. Band-Pass Test, A3J-1 MLG, Drop Height - 42 Inches, Band-Pass Unit Inoperative

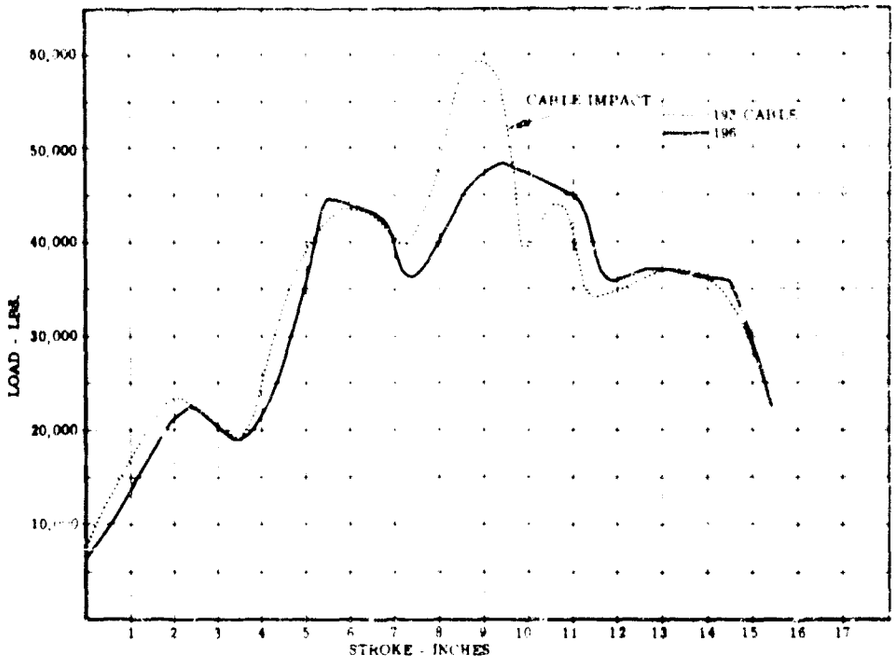

Figure 4-8. Band-Pass Test, A3J-1 MLG, Drop Height - 48 Inches, Band-Pass Unit Inoperative

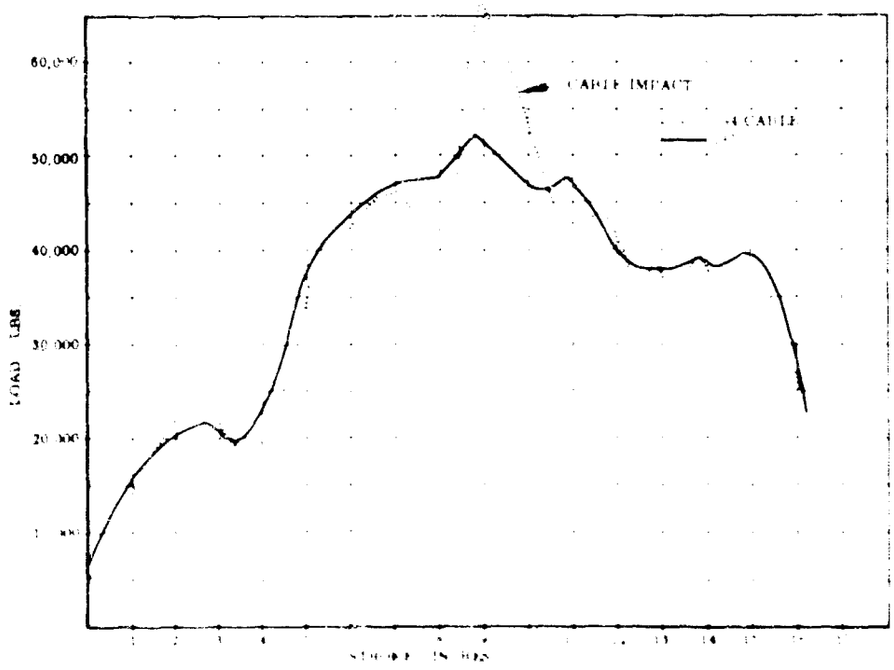

Figure 4-9. Band-Pass Test, A3J-1 MLG, Drop Height - 54 Inches, Band-Pass Unit Inoperative

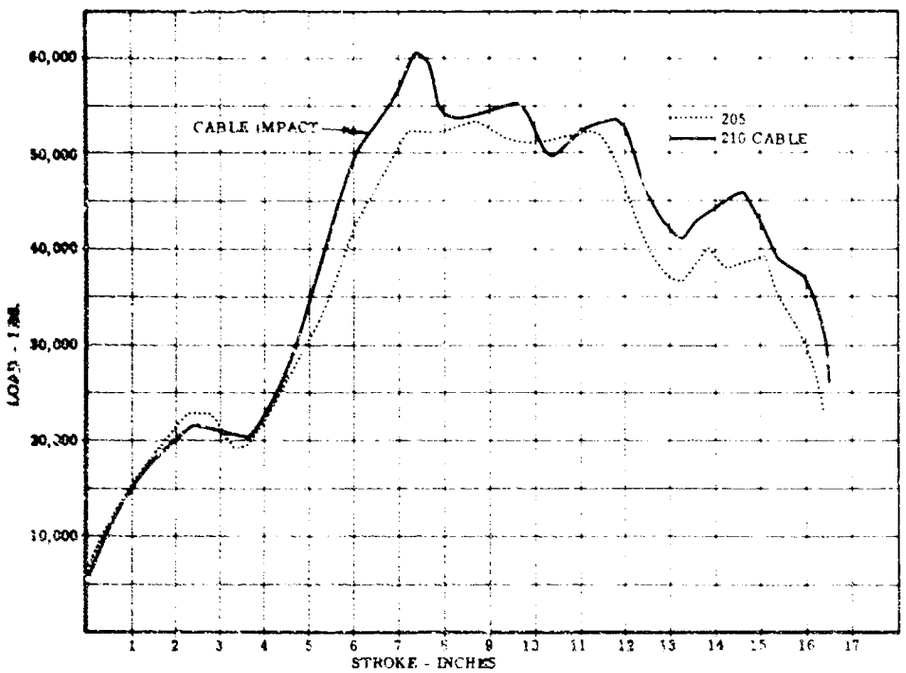

Figure 4-10. Band-Pass Test, A3J-1 MLG, Drop Height - 60.5 Inches, Band-Pass Unit Inoperative

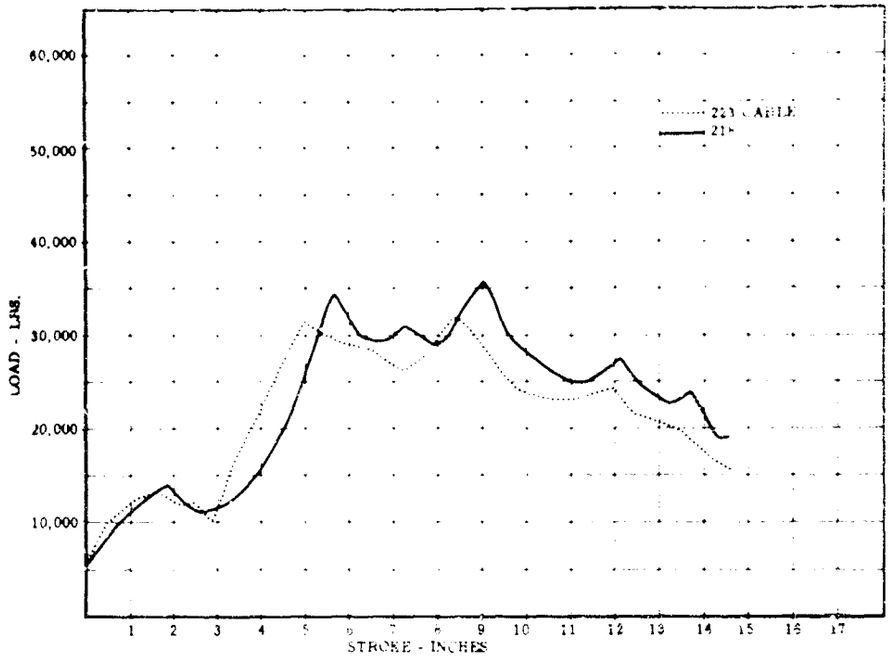

Figure 4-11. Band-Pass Test, A3J-1 MLG, Drop Height - 27 Inches, Band-Pass Unit Operative - Nominal Parameters

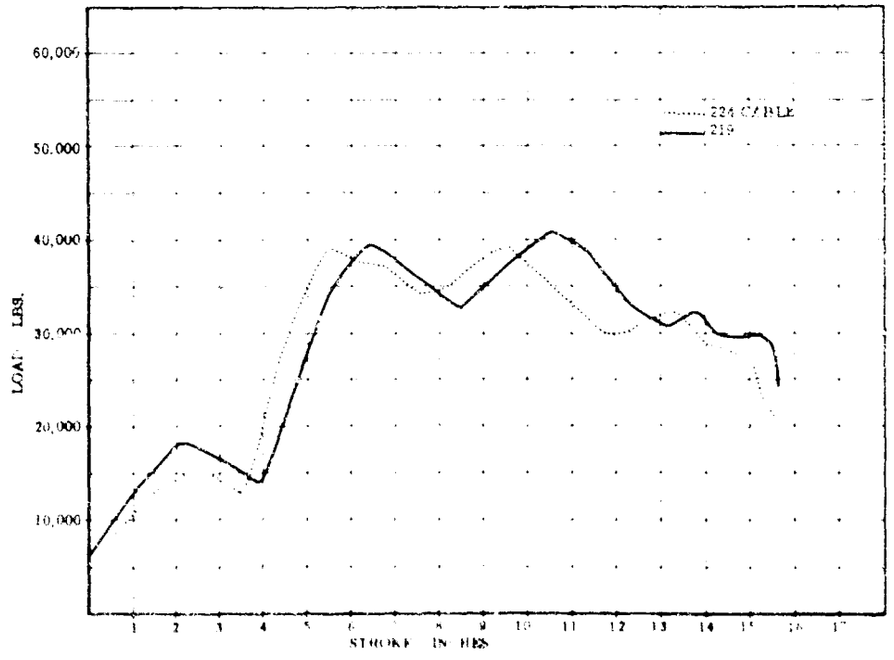

Figure 4-12. Band-Pass Test, A3J-1 MLG, Drop Height - 36.5 Inches, Band-Pass Operative - Nominal Parameters

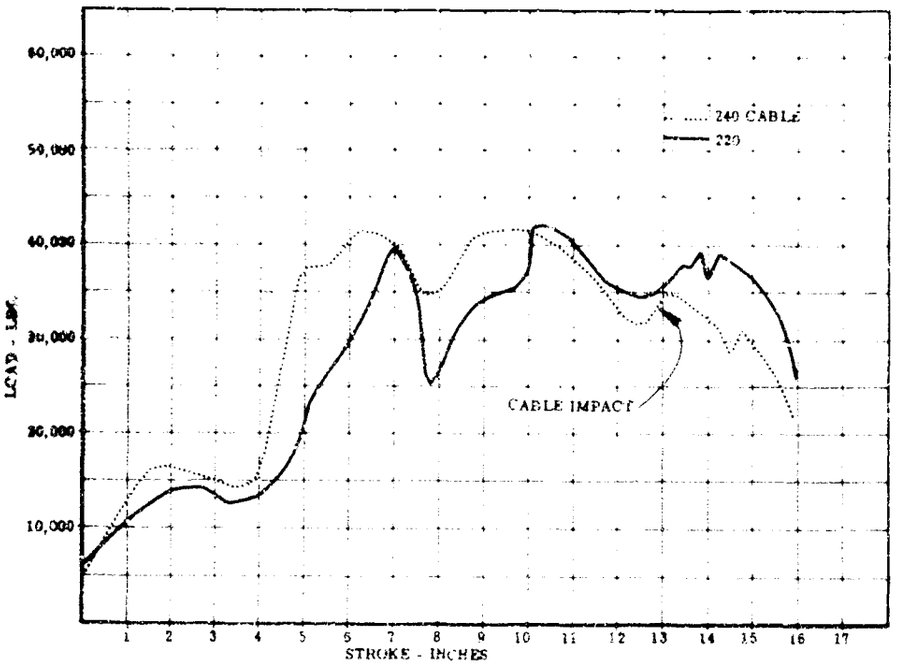

Figure 4-13. Band-Pass Test, A3J-1 MLG, Drop Height - 42 Inches Band-Pass Unit Operative - Nominal Parameters

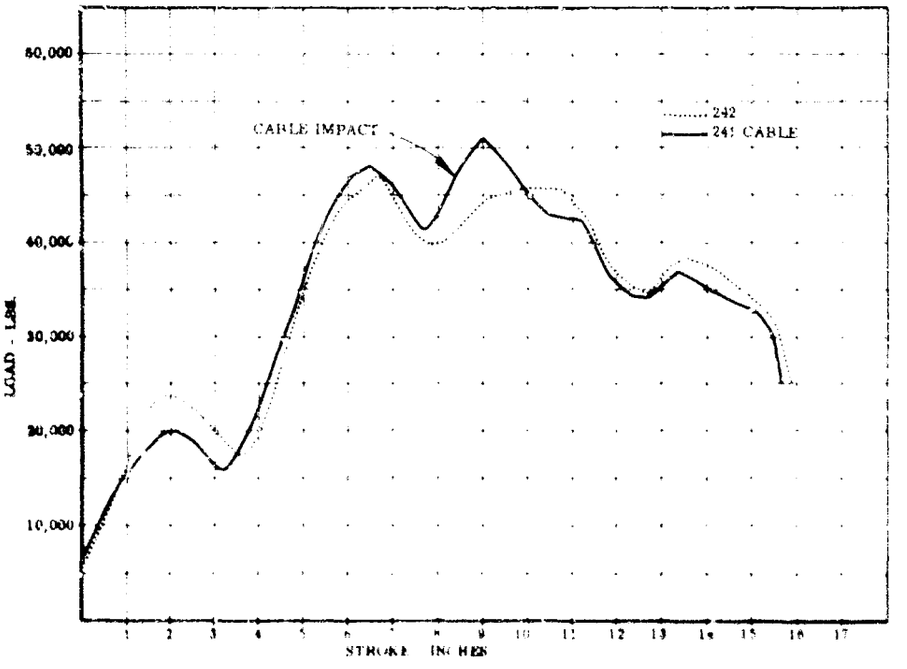

Figure 4-14. Band-Pass Test, A3J-1 MLG, Drop Height - 48 Inches, Band-Pass Unit Operative - Nominal Parameters

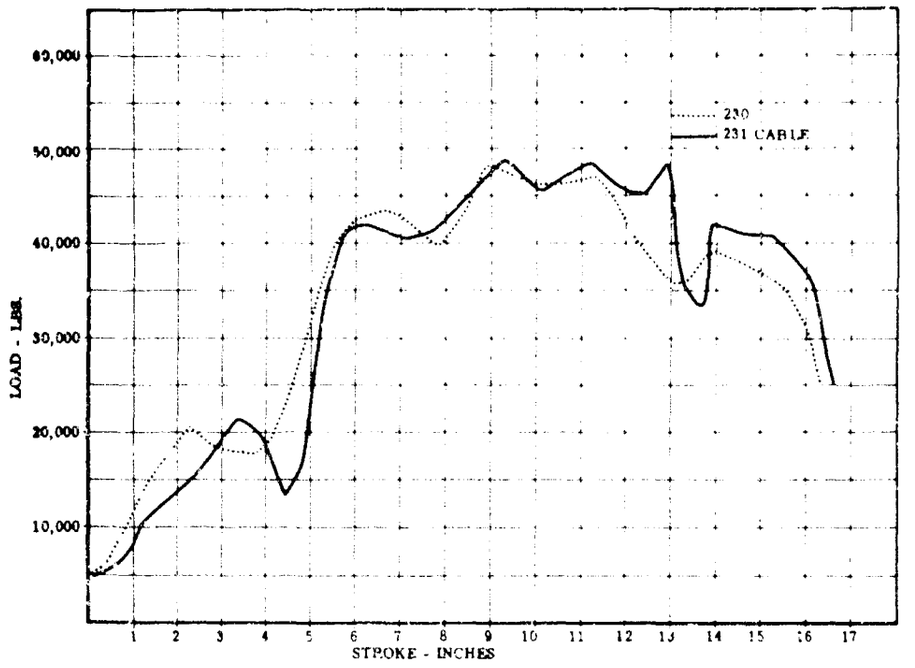

[illegible] Pass Test, A3J-1 MLG, Drop Height - 54 [illegible] Pass Unit Operative - Nominal Parameters

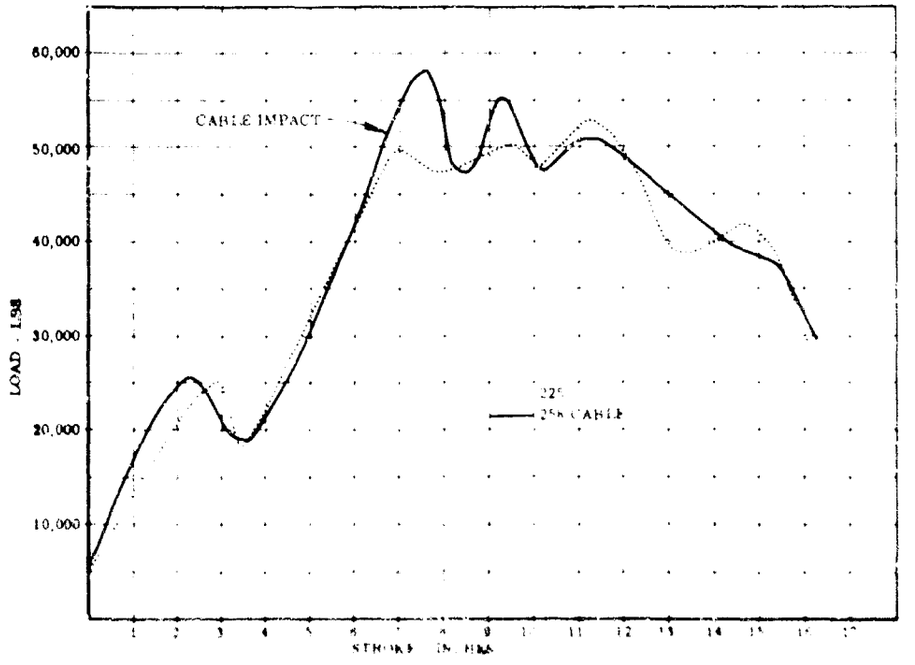

[illegible] Pass Test, A3J-1 MLG, Drop Height - 60.5 Inches, Ba[illegible] Unit Operative - Normal Condition - Nominal Parameters

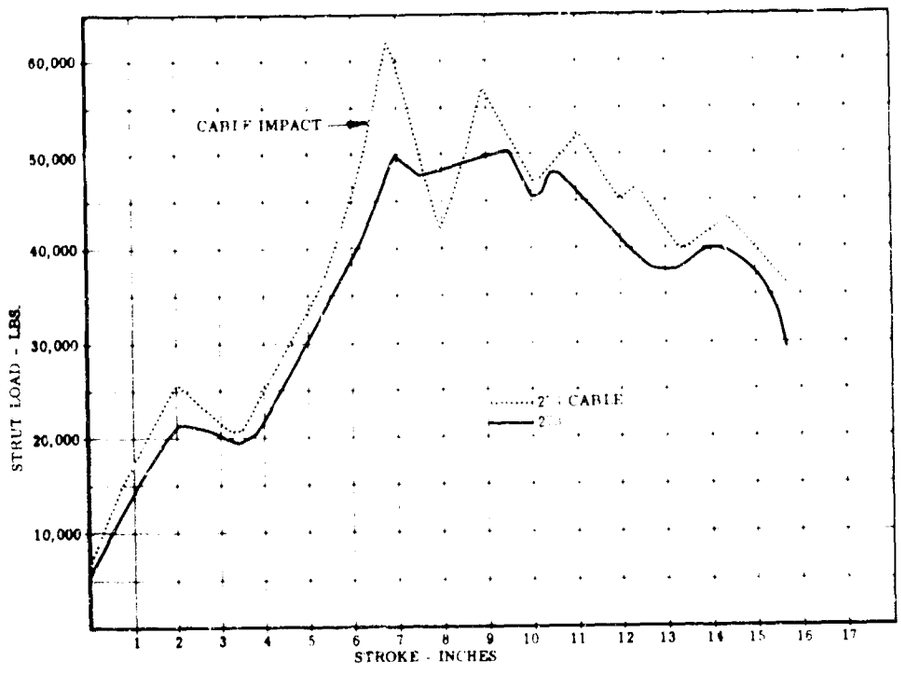

Figure 4-17. Band-Pass Test, A3J-1 MLG, Drop Height 54 Inches, Band-Pass Operative, Changed Oil Volume - 37% Reduction

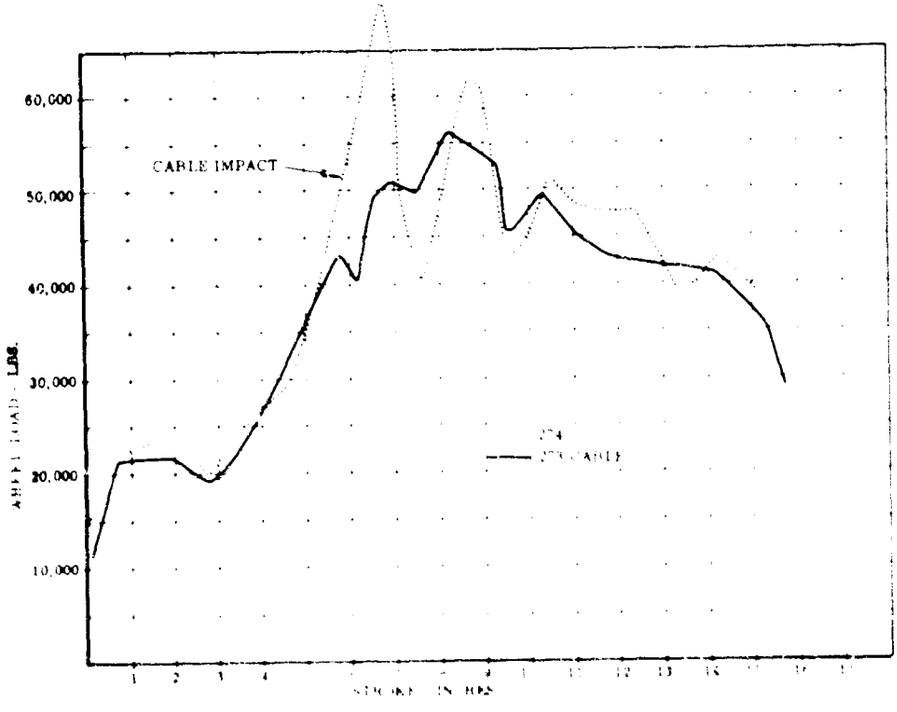

Figure 4-18. Band-Pass Test, A3J-1 MLG, Drop Height 54 Inches, Band-Pass Operative, Oil Volume Reduced 37%

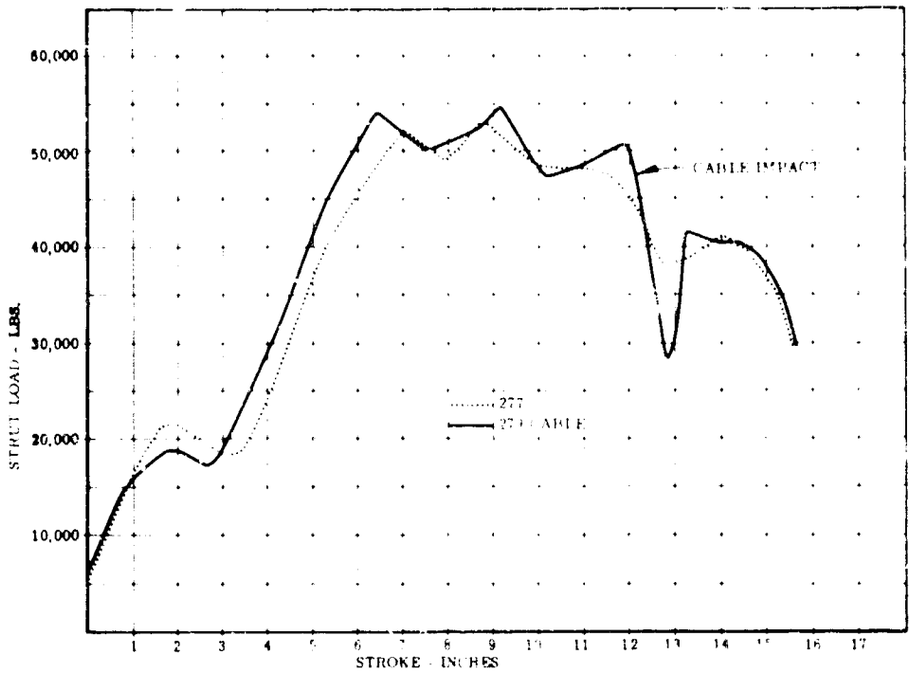

Figure 4-19. Band-Pass Test, A3J-1 MLG, Drop Height 54 Inches, Band-Pass Unit Operative, Changed Oil Volume - 25% Reduction

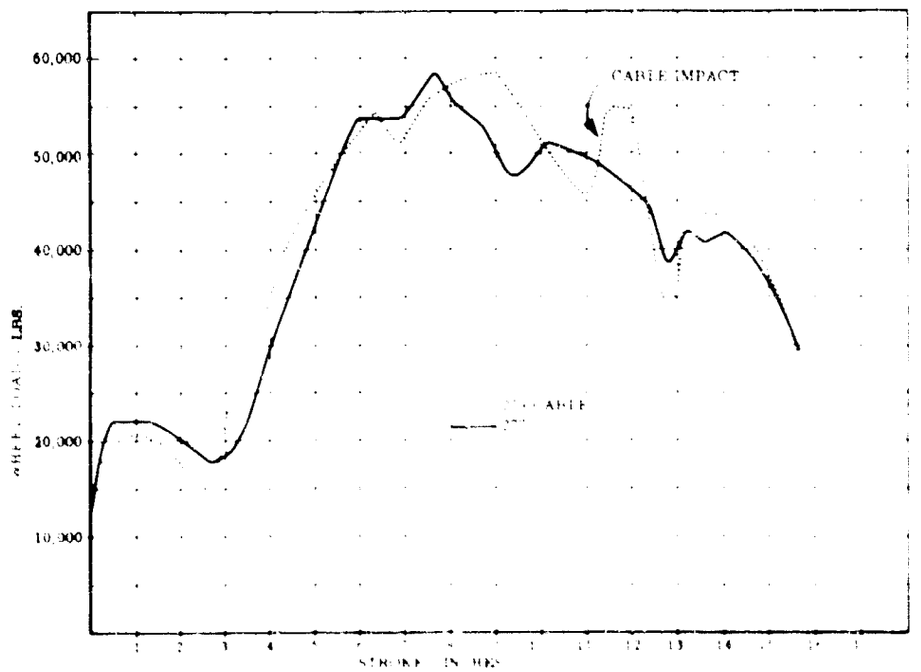

Figure 4-20. Band-Pass Test, A3J-1 MLG, Drop Height 54 Inches, Band-Pass Unit Operative, Oil Volume Reduced 25%

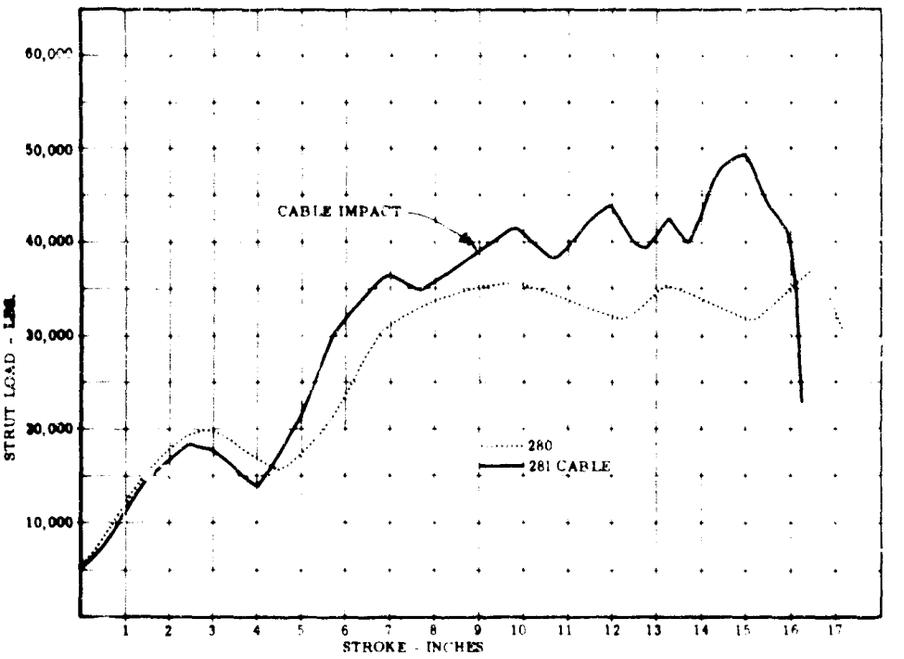

Figure 4-21. Band-Pass Test, A3J-1 MLG, Drop Height 54 Inches, Band-Pass Unit Operative, Inlet Orifice = .002, Outlet Orifice = .0002

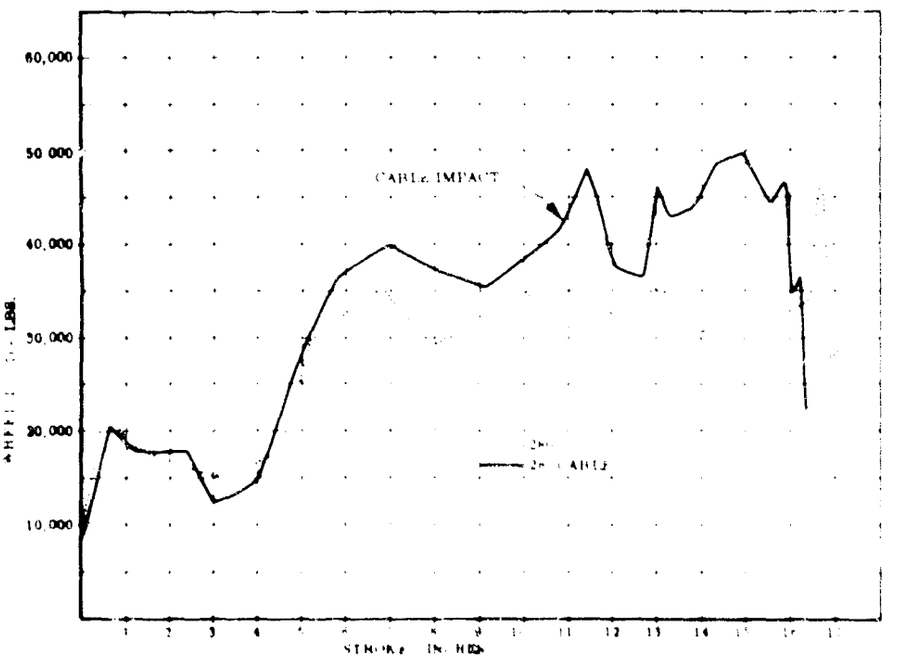

Figure 4-22. Band-Pass Test, A3J-1 MLG, Drop Height 54 Inches, Band-Pass Unit Operative, Inlet Orifice = .002, Outlet Orifice = .0002

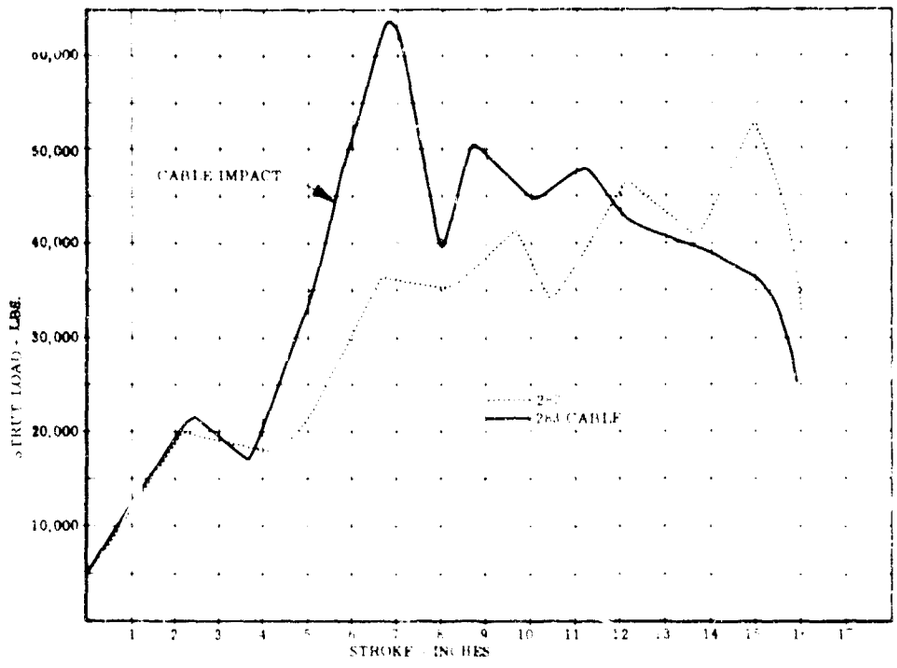

Figure 4-23. Band-Pass Test, A3J-1 MLG, Drop Height 54 Inches, Band-Pass Unit Operative, Inlet Orifice = .005, Outlet Orifice = .0095

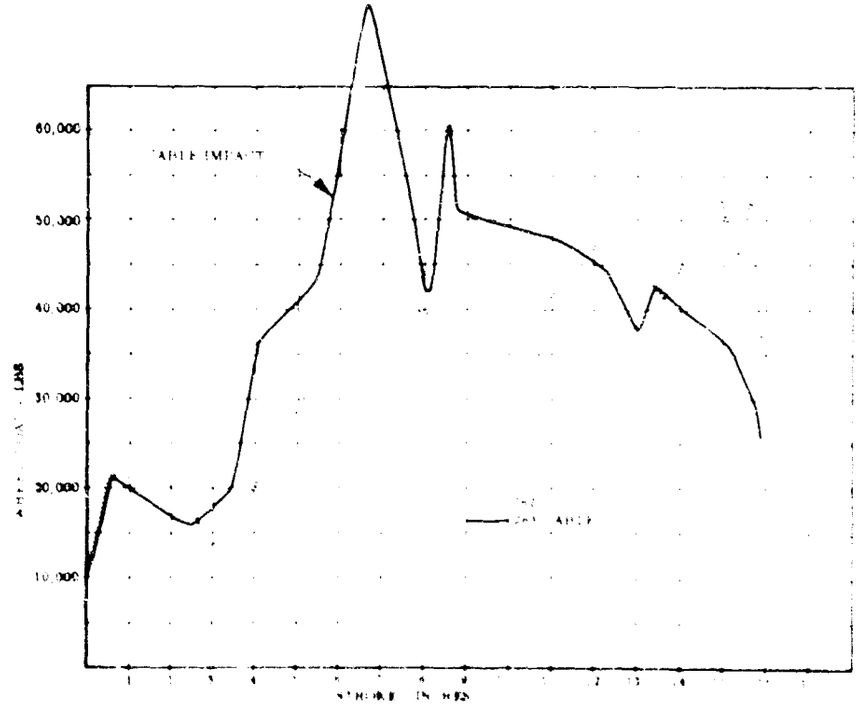

Figure 4-24. Band-Pass Test, A3J-1 MLG, Drop Height 54 Inches, Band-Pass Unit Operative, Inlet Orifice = .005, Outlet Orifice = .0095

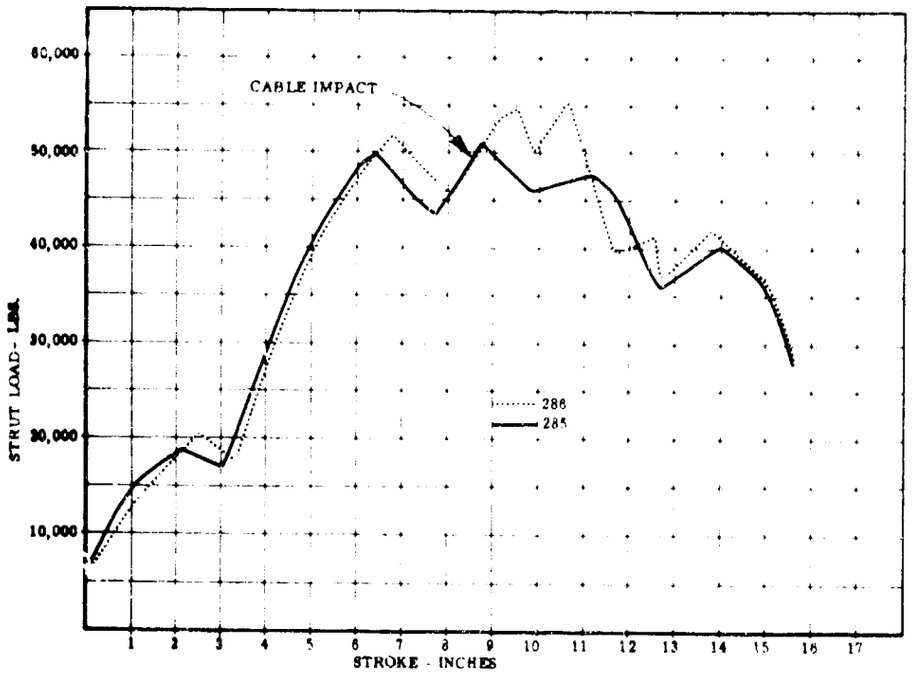

Figure 4-25. Band-Pass Test, A3J-1 MLG, Drop Height 54 Inches, Band-Pass Unit Operative, Inlet Orifice = .015, Outlet Orifice = .0015

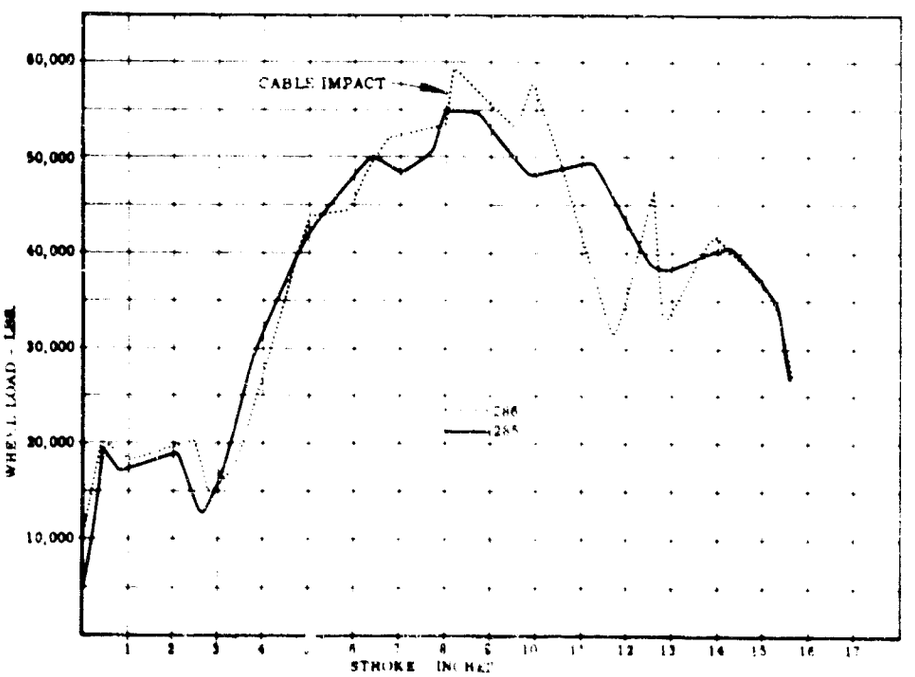

Figure 4-26. Band-Pass Test, A3J-1 MLG, Drop Height 54 Inches, Band-Pass Unit Operative, Inlet Orifice = .015, Outlet Orifice = .0015

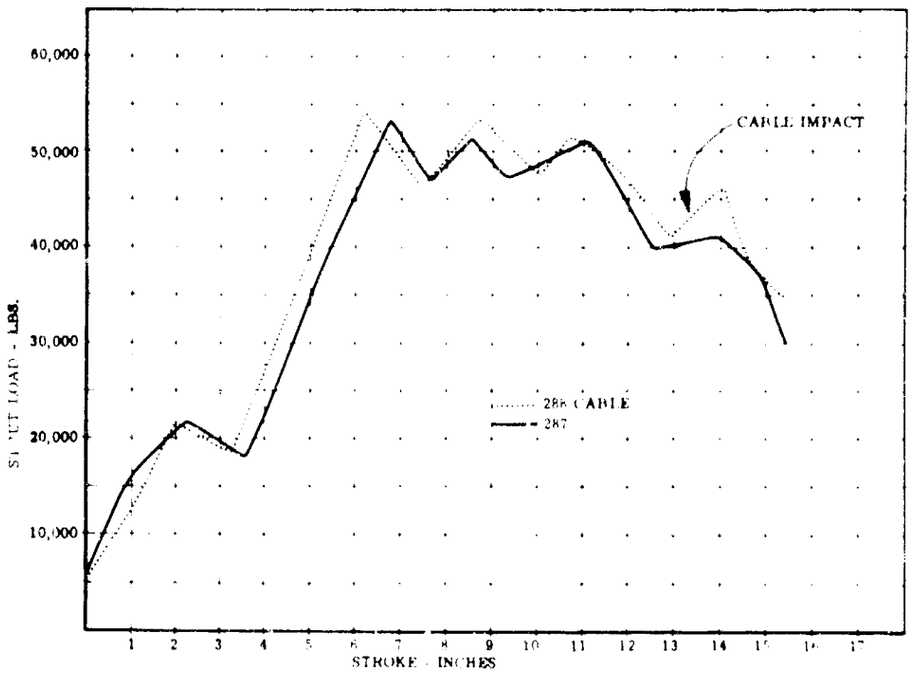

Figure 4-27. Band-Pass Test, A3J-1 MLG, Drop Height 54 Inches, Band-Pass Unit Operative, Inlet Orifice = .020, Outlet Orifice = .002

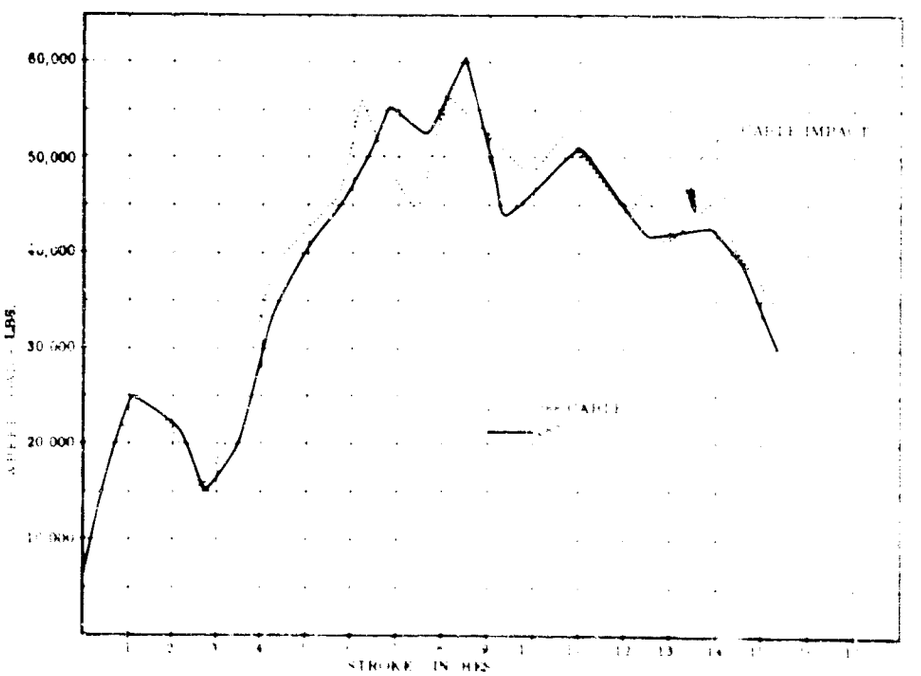

Figure 4-28. Band-Pass Test, A3J-1 MLG, Drop Height 54 Inches, Band-Pass Unit Operative, Inlet Orifice = .020, Outlet Orifice = .002

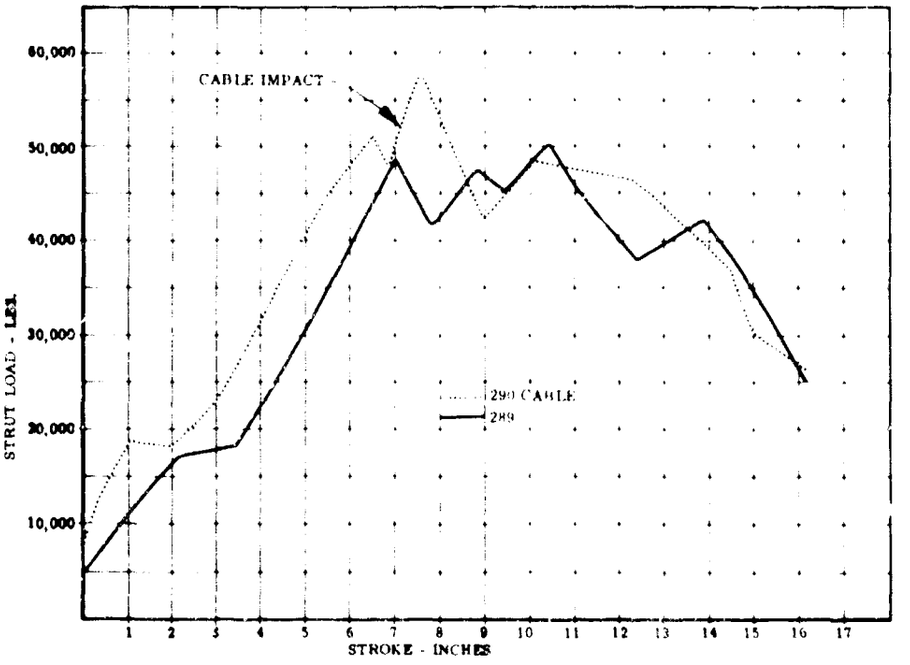

Figure 4-29. Band-Pass Test, A3J-1 MLG, Drop Height 54 Inches, Band-Pass Unit Operative, Inlet Orifice = .005, Outlet Orifice = .001, Spring - 125 Lbs.

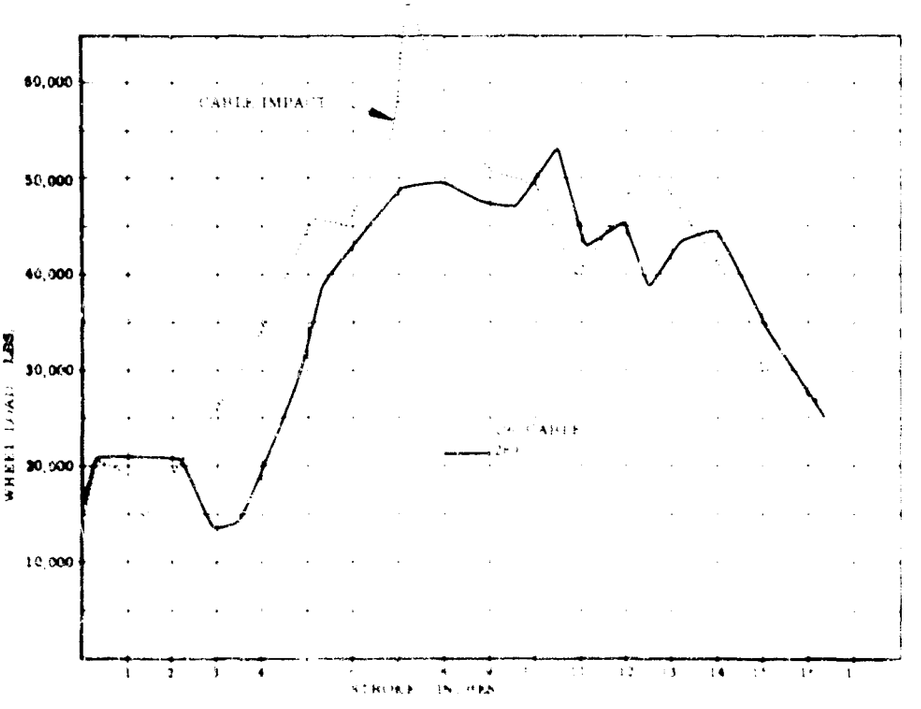

Figure 4-30. Band-Pass Test, A3J-1 MLG, Drop Height 54 Inches, Band-Pass Unit Operative, Inlet Orifice = .005, Outlet Orifice = .001, Spring - 125 Lbs.

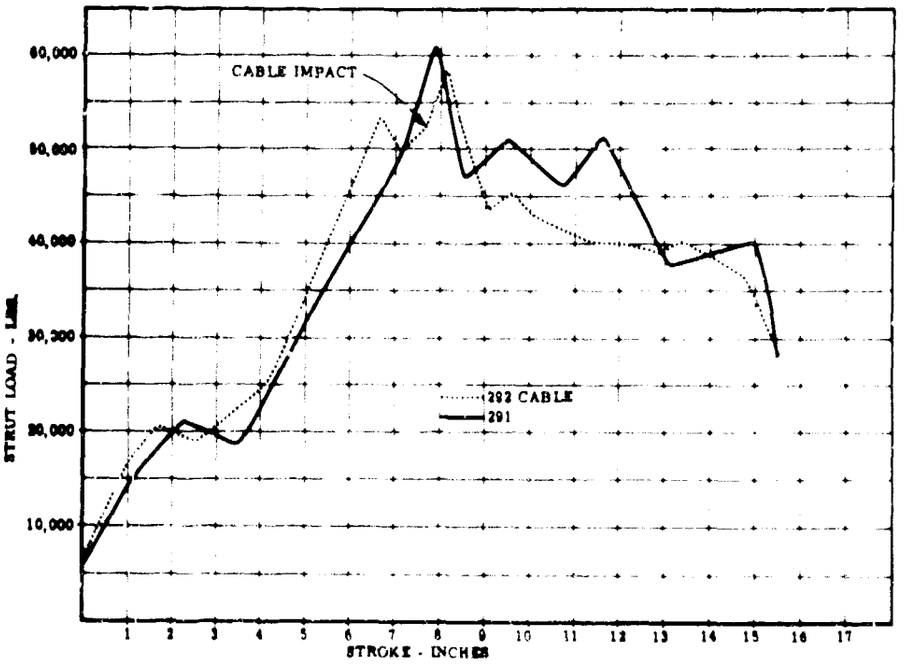

Figure 4-31. Band-Pass Test, A3J-1 MLG, Drop Height 54 Inches, Band-Pass Unit Operative, Inlet Orifice = .015, Outlet Orifice = .001, Spring = 40 Lbs.

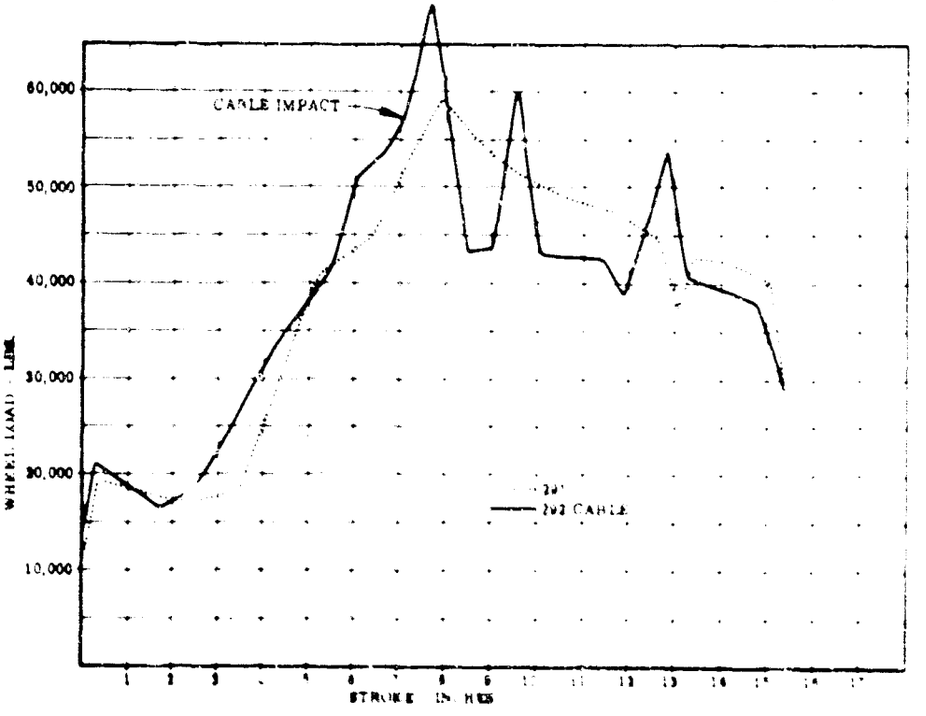

Figure 4-32. Band-Pass Test, A3J-1 MLG, Drop Height 54 Inches, Band-Pass Unit Operative, Inlet Orifice = .015, Outlet Orifice = .001, Spring = 40 Lbs.

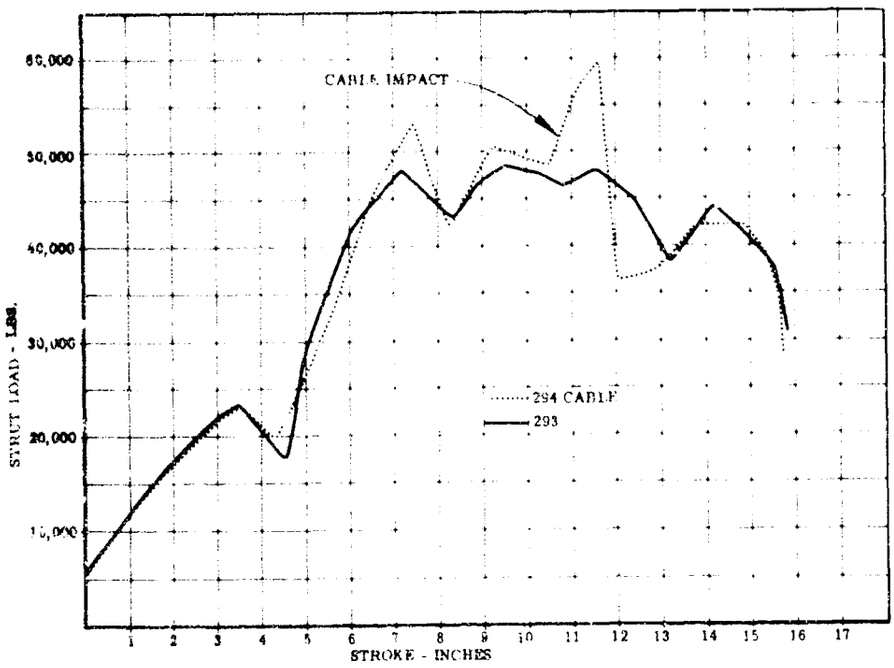

Figure 4-33. Band-Pass Test, A3J-1 MLG, Drop Height 54 Inches, Band-Pass Unit Operative, Spring - 125 Lbs.

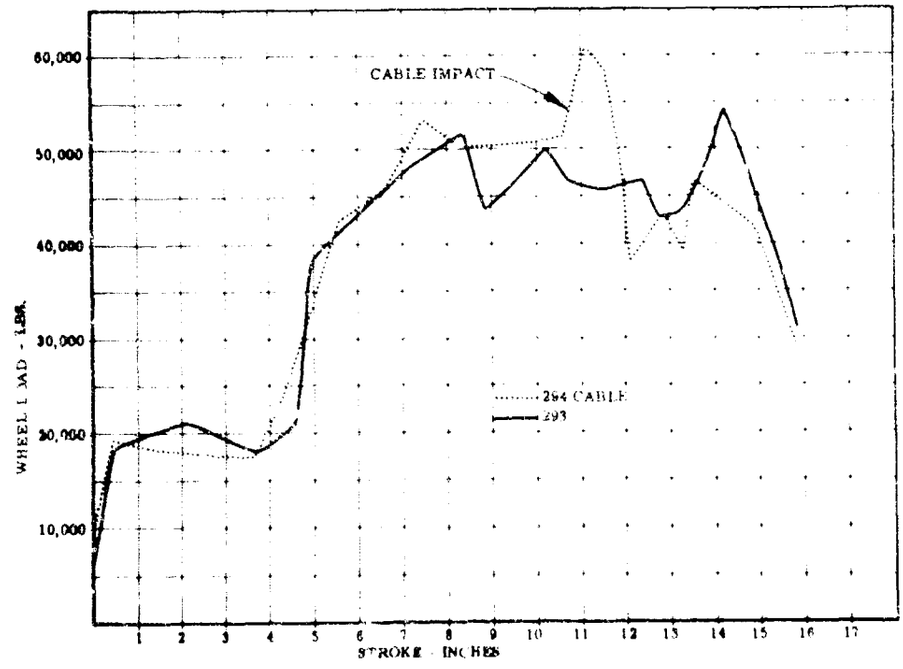

Figure 4-34. Band-Pass Test, A3J-1 MLG, Drop Height 54 Inches, Band-Pass Unit Operative, Spring - 125 Lbs.

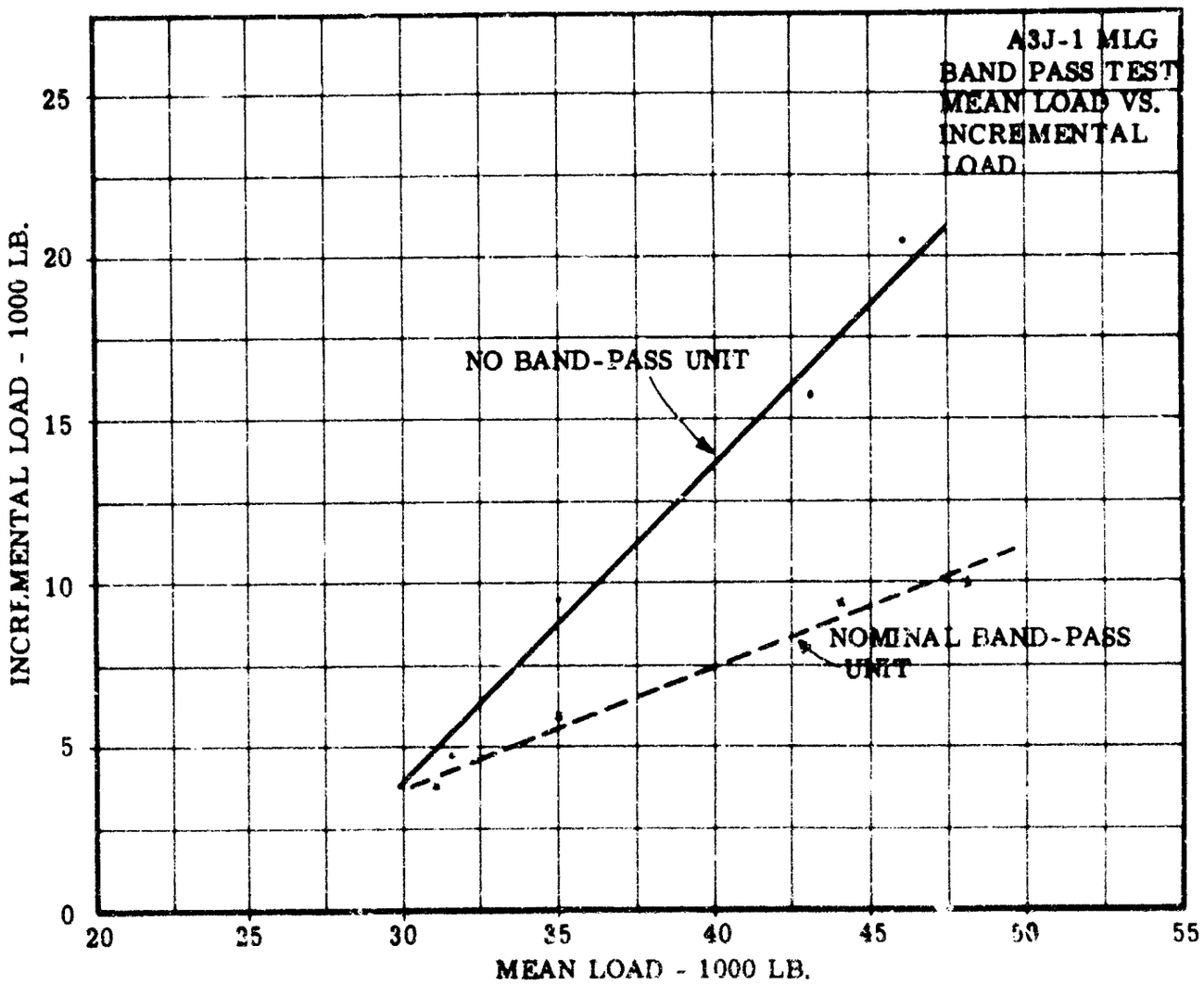

Figure 4-35. Band-Pass Test, A3J-1 MLG, Mean Load vs. Incremental Load

D. Nominal Conditions Except preload on Spring 125 pound Part IV SDT-3528.

Graphs of strut load versus stroke and wheel load versus strut stroke have been plotted for the above and appear in Figures 4-17 to 4-34.

Two of the graphs differ from the others to a degree that requires explanation.

On drops 280-281 (Figures 4-21, 4-22) the band-pass unit opened upon tire contact with the dynamometer. With the unit open, the net orifice area is increased which decreases the hydraulic force. In order to absorb the energy, the strut stroke is increased. On drop 281, the unit closed earlier than it did for drop 280 which means that after the unit closes, the load goes higher and the stroke is less on drop 281.

On drop 282 (Figures 4-23, 4-24) the unit opened prematurely, which lowers the load early in the stroke, then the unit closed at mid-stroke and the load was increased in the latter portion of the stroke.

The high sink speed rates asked for in Parts IX and X of Test Request SDT-3528 could not be accomplished in this drop rig.

TEST RESULTS

The cable load on drops 193 and 194 compared favorably with the analytical work done on this gear which is covered in Bendix Report SH-61-1. Graphs of load versus stroke for these drops are in Figures 4-8 and 4-9.

It appears that unless the cable goes under the tire at a nearly flat tire condition that a large portion of the cable impact is absorbed by the tire.

Cable loads of the size and shape of drops 193 and 194 were not encountered with a nominal band-pass unit installed. For this reason it is inferred that the unit does reduce the strut load. A direct comparison of the size of the bump impacts is clouded with other factors. If the cable were induced under the tire when the load was level, and evaluation of the unit would be more meaningful. If the cable goes under the tire when the tire is unloading there is not a big bump in the load curve for the unit to react. As an illustration see the graph on drop 230 in Figure 4-15.

In order to get a comparison a graph of mean load versus incremental load was drawn for the cable impacts. The mean load is the load at which the cable was induced into the tire print. The incremental load is the increase in load as the cable goes under the tire.

This graph in Figure 4-35 shows a definite improvement with the band-pass unit. From the two lines indicated, without band-pass and with band-pass, the reduction of the incremental load is nearly fifty precent. While the band-pass unit reduced the size of this impact load transmitted to the airframe the wheel loads do not show a change with and without the unit. This is an important result. Figures 4-36, 4-37, 4-38, and 4-39 are oscillograms of drop tests that fall on the extremities of the two lines.

The change of various parts of the band-pass unit were made to see if an improvement in the performance of the unit could be accomplished. None of the changes indicated an improvement, some indicated no change in the performance and others indicated a worse performance. The following is an accounting of the changes.

I. Oil Volume Changes

A. Reduced 37% - Cycling of the band-pass valve occurred. (This result agrees with the theoretical studies).

B. Reduced 25% - No significant change.

II. Nominal Oil Volume. Change inlet and outlet orifices together so that the ratio of areas was 10. (Nominal .010 - .001).

A. .002 Inlet .0002 Outlet. This change resulted in opening of the valve upon tire contact with the dynamometer.

B. .005 Inlet .0005 Outlet. (Same comment as .002 - .0002).

C. .015 Inlet .0015 Outlet. This change did not seem to alter the performance on the unit.

D. .020 Inlet .0020 Outlet. This change did not seem to alter the performance on the unit.

III. Ratio of the inlet to outlet changed along with the spring load.

A. Inlet .005 Outlet .001 Ratio 5 125 lb. spring. No significant change.

B. Inlet .015 outlet .001 ratio 15 40 lb. spring. No significant change.

IV. Nominal Conditions except for 125 pound spring load. The stiffer spring did not allow the unit to open.

In essence it appears that the parameters investigated have a fair degree of tolerance before the unit is adversely affected.

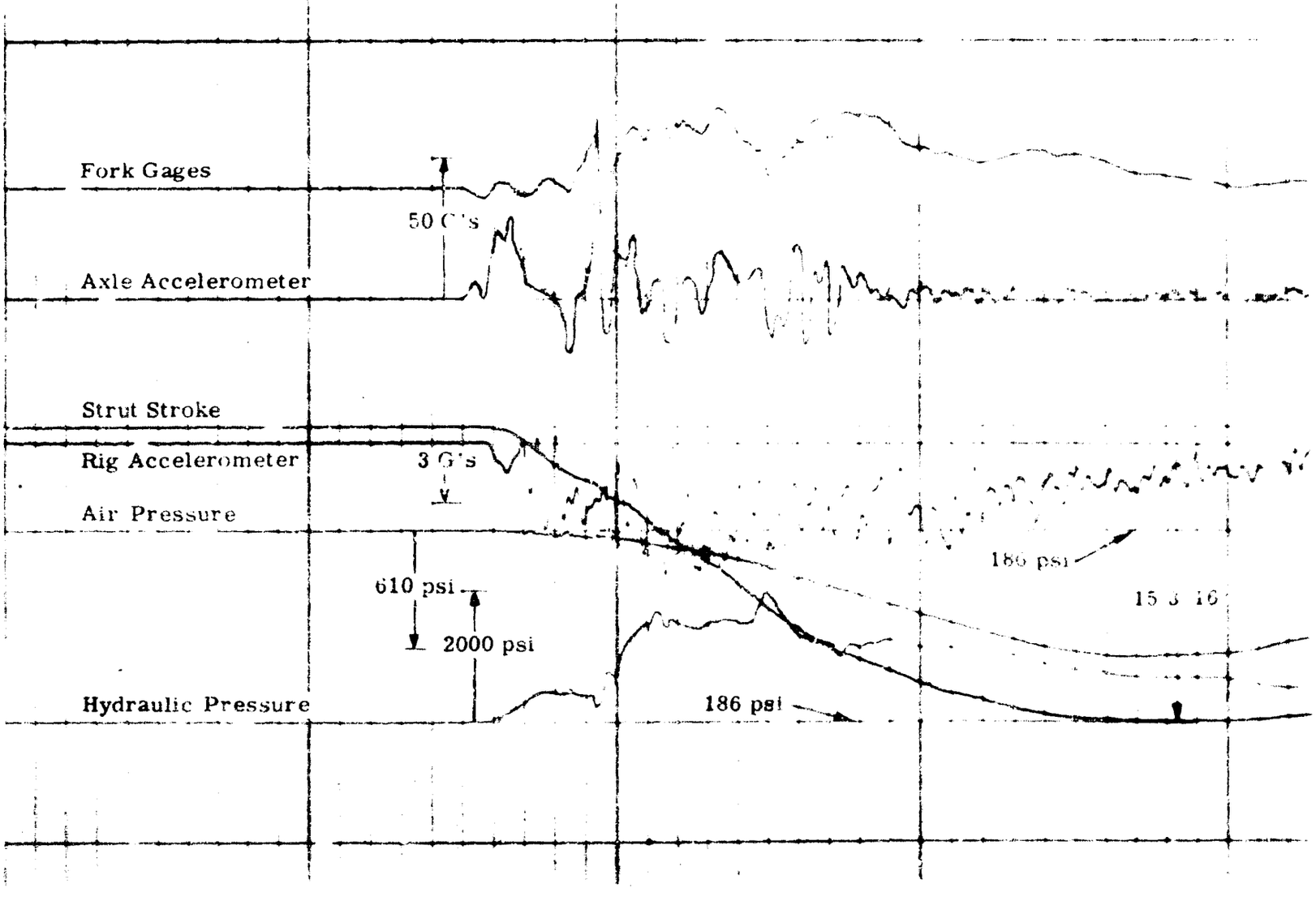

Figure 4-36. Band-Pass Test No. 200, Drop Height 36.5 Inches (14 Ft./Sec.), No Band-Pass Unit

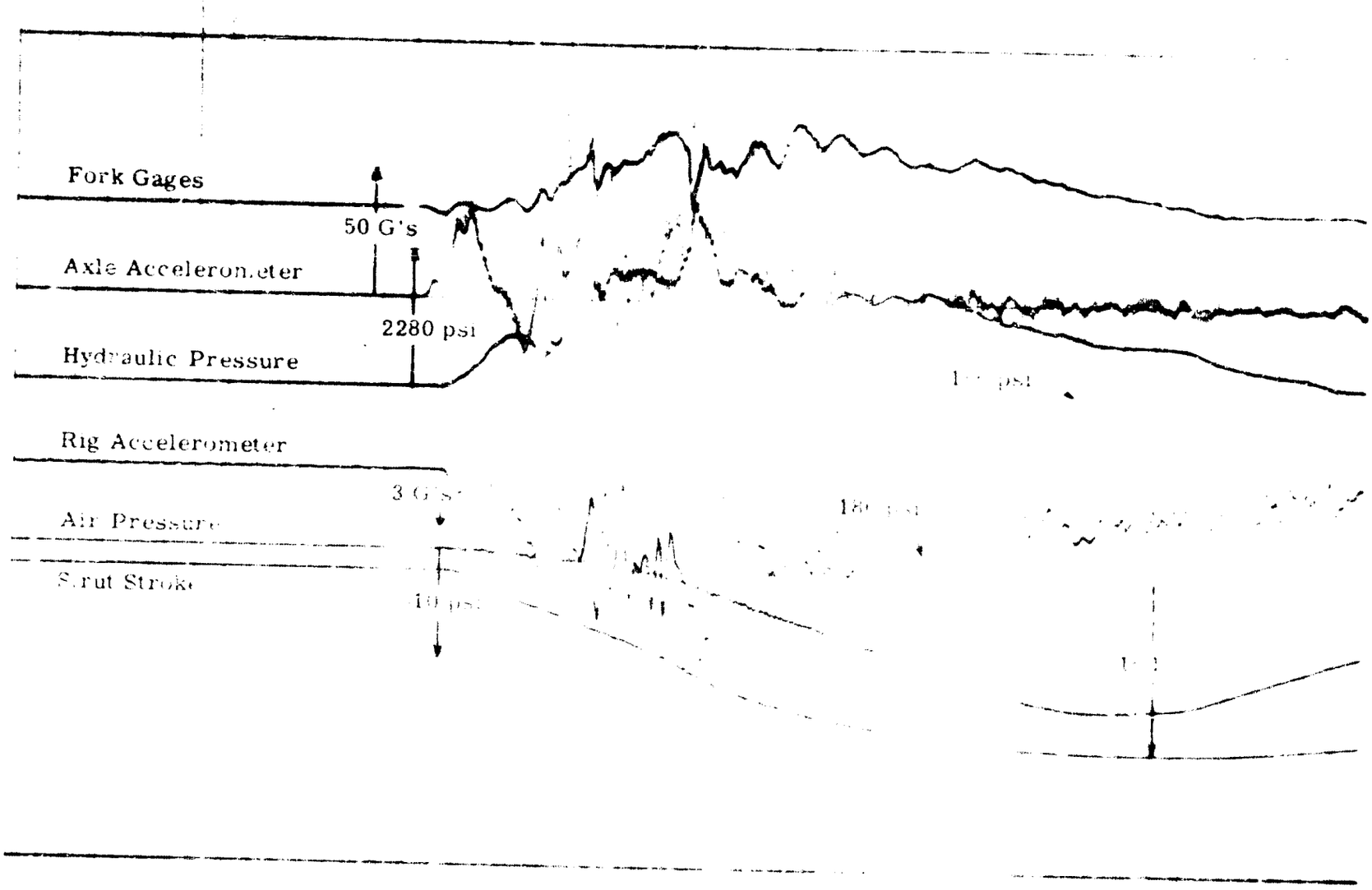

Figure 4-37. Band-Pass Test No. 194, Drop Height 54 Inches (17 Ft. Sec.), No Band-Pass Unit

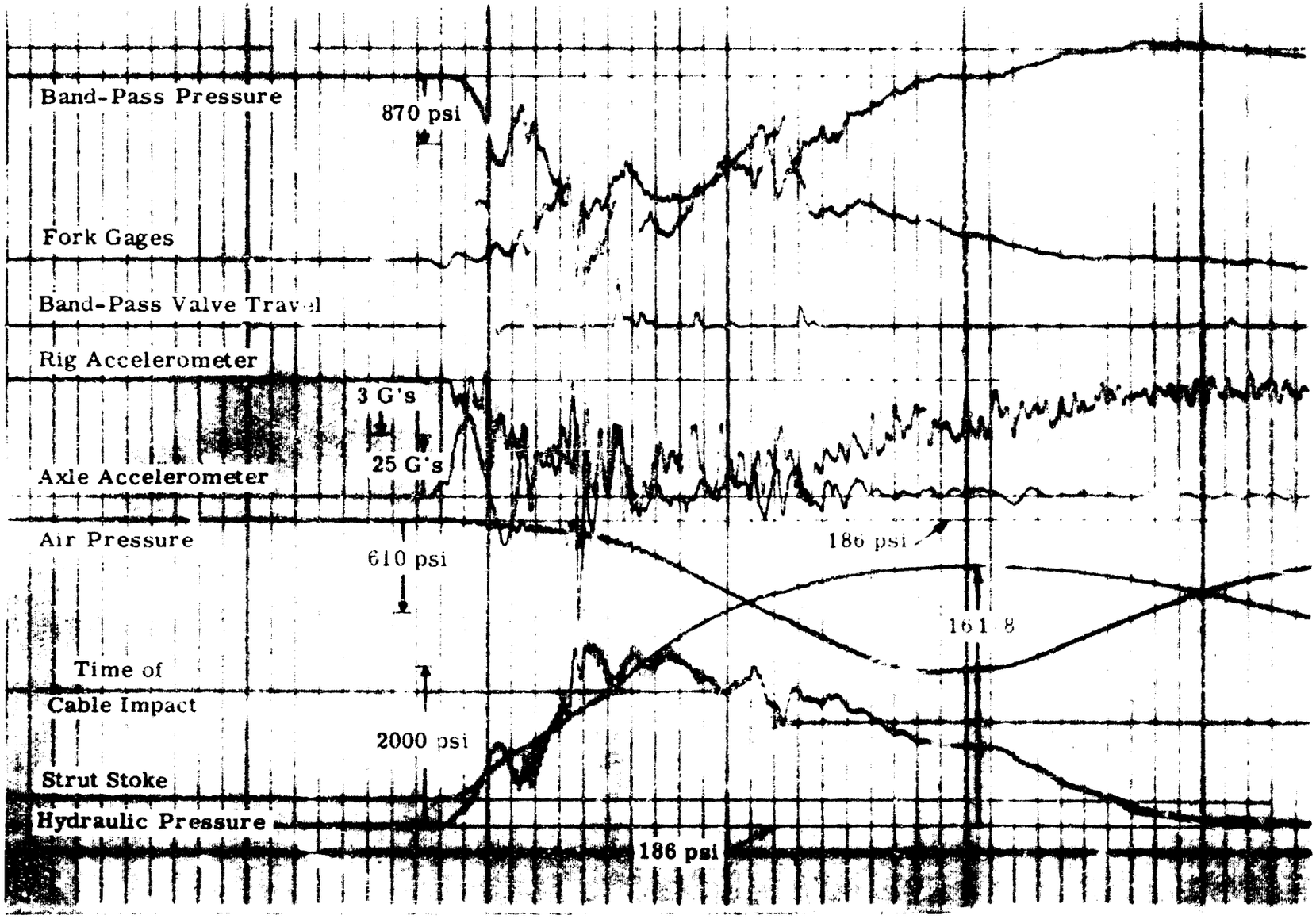

Figure 4-38. Band-Pass Test No. 243, Drop Height 54 Inches (17 Ft./Sec.), Band-Pass Unit Installed

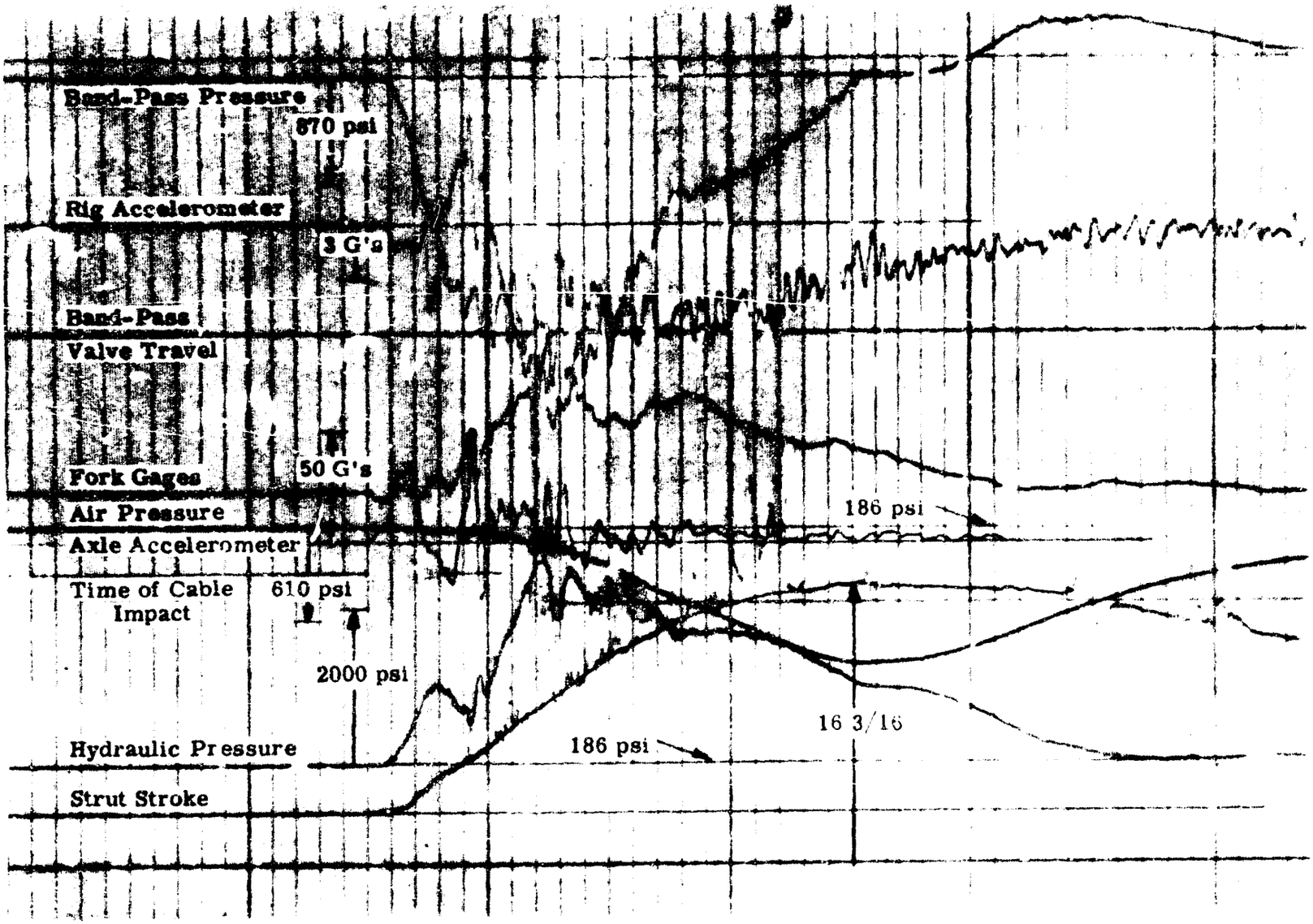

Figure 4-39. Band-Pass Test No. 258, Drop Height 60.5 Inches (18 Ft./Sec.), Band-Pass Unit Installed

SECTION V

EVALUATION OF RESULTS, CONCLUSIONS AND RECOMMENDATIONS

THEORETICAL ANALYSIS OF McDONNEL F4H-1 MLG MODIFIED TO INCLUDE BAND-PASS UNIT

The work accomplished during this phase of the program included the following items:

1. Incorporation of changes in the mathematical model as specified in the contract, namely, modifications of the model to take into account the pitch angle of the landing gear and airplane.

2. Changes in the mathematical model found necessary for simulation of the cable impact phenomena, namely, modification of the tire model to one having regions of differing elasticity and modification of the bump contour to simulate the tire mode shape.

3. Computer investigation of the F4H-1 MLG system with a band-pass unit for normal landing and bump impact conditions.

4. Analysis of computer results.

5. Investigation of possible modifications in the F4H-1 MLG to make it adaptable to a band-pass unit.

It was concluded from the computer results that a band-pass unit will not function properly in the F4H-1 main gear. The inability of the band-pass unit to function was traced to the presence of the high pressure air chamber in series with the strut orifice flow.

Based on analytical studies of a conventional system it was concluded that a conventional gear should not have this same difficulty. The band-pass unit should be able to anticipate the high load from bump impact due to its sensitivity to the rate of pressure buildup in the dynamic pressure chamber of the strut.

Based on studies of the F4H-1 gear structure it was determined that mechanical changes in the gear could be made to eliminate the time lag effect of the high pressure chamber. Such changes would require a "paper" redesign of the pin configuration to duplicate airplane characteristics.

It was recommended that the band-pass development program be continued using another more conventional landing gear system, such as the A3J-1 or the F9F main gear, rather than a modified F4H-1 main gear. The simulation achieved in this study was felt to be sufficient to warrant a more extensive analytical study of the band-pass principle, as applied to the landing gear shock strut, than that originally proposed. Such an extension would allow the detailed study of the loads transmitted into the wheel and unsprung mass by bump impact in addition to the study already proposed in which band-pass was to be evaluated on only the net improvement it provided in the loads transmitted to the airframe proper. In addition, miscellaneous exploratory studies such as that undertaken to improve the tire model, were felt to be in order in this study.

THEORETICAL ANALYSIS OF NORTH AMERICAN A3J-1 MLG MODIFIED TO INCLUDE BAND-PASS UNIT

The work accomplished during this phase of the program included the following items:

1. Development of a simplified mathematical model of the band-pass mechanism.
2. Linearized study of this model.
3. Analog computer study of the model.
4. Tire model investigations.
5. Study of the complete landing gear system with and without band-pass by analog computer simulation.

The general conclusions from this phase of the program were as follows:

1. A low-pass hydraulic band-pass mechanism could be adapted to modern airplane landing gear shock struts to reduce the loads transmitted to the airframe. The load reduction that can be realized by such a device is on the order of 50% of those additional loads imposed by high frequency bump impact occurring during the landing impact.
2. A band-pass mechanism within the shock strut will not significantly reduce impact loads on the wheel and tire.
3. The design of a band-pass mechanism for any given landing gear application can be carried out using the simplified model desired in this study. Parameter adjustments to obtain near optimum performance of the unit based on the simplified model agree with those of the model of the complete landing gear system.
4. The natural frequency range of the valve was determined.
5. The spring preload of the valve was determined.
6. Parameters for the design of a band-pass unit for the A3J-1 MLG were determined. A preliminary design of this mechanism was made.

7. The analytical study indicated that valve stability would be a limiting design factor.

EXPERIMENTAL ANALYSIS

The test program was brought to a successful conclusion but not without overcoming a number of extremely difficult problem areas. It would be more proper to say that some of these problems were partially overcome. The simulation of actual aircraft landing conditions by laboratory methods can never be 100% accurate. Now, when we consider the simulation of some of the most severe overload landing conditions, the accuracy level is greatly reduced.

The North American Band-pass modified A3J-1 MLG was mounted in the drop test tower above the 120" dynamometer as described and illustrated in Section IV.

One of the first problems arises in providing horizontal velocity increments through rotation of the flywheel rather than strut velocity relative to the ground. Flywheel curvature affects spin-up and spring-back loads and the tire footprint configuration as well as loading. The steel flywheel surface provides a variation of tire friction coefficient especially since the tire rolls over the same surface many times. The above factors can be neglected or considered minor, in a large number of tests that can be performed in this facility. However, when we compound the situation by throwing a steel cable between the tire and the flywheel at an instant at which we hope the tire is flat, numerous problems arise.

The landing condition to be simulated in the test program was as follows. An aircraft carrier landing occurs during which the tire, in a nearly flat condition, impacts one or more arresting cables. A second laboratory simulation problem arises in that sufficient load must be developed at time of cable encounter to flatten the tire. If we faithfully reproduced this condition, landing gear failure could result. Numerous variations of tire pressure and drop height were required to establish reasonable incremental loading from cable impact without attendant tire or wheel failure.

A third problem was the introduction of the cable between the tire and the flywheel. The cable-throw mechanism used in the first series of tests was adjusted so that timing was fairly repeatable. However, the cable segment many times would not be accepted between the tire and the flywheel. Various shaped and diametered segments were tried to alleviate this problem. Eventually, a new cable-throw mechanism, as discussed in Section IV, was built. This mechanism proved better but not completely successful. On several occasions, the mechanism failed and was torn apart, resulting in rebuilding delays in the program.

The safety of operating personnel was of prime concern. There were many incidents cable failure or ricochet after the segment passed between the tire and the flywheel. blown tires, failure of the throw mechanism components, and wheel and flywheel damage. No one was injured during the course of the program.

In addition to the above special problems, is the general problem of repeatability. Even with conventional shock struts, there is variation in loads developed for identical conditions. Loads vary for the same shock struts as well as for those within a certain

type. Add to this the complication of an internal band-pass unit and the problem is magnified.

263 drop tests were conducted during the progr[illegible] It was difficult, because of some of the factors mentioned abov[illegible], to clearly define o[illegible] tative results. Qualitatively, the experimental drops correlated with the a[illegible]alytica[illegible] sults.

OVERALL RESULTS AND CONCLUSIONS

Results of the overall program can be summarized as follows:

1. A mathematical model was constructed and equations derived that successfully represented the impact of an aircraft landing gear with the ground and subsequent impact with an arresting cable.

2. The nonlinear equations were linearized and resulting solutions were adequate.

3. The theoretical analysis was used to design optimum band-pass units for the McDonnell F4H-1 MLG and the North American A3J-1 MLG.

4. A band-pass unit was fabricated and incorporated into a modified North American A3J-1 MLG shock strut.

5. The band-pass modified A3J-1 landing gear was mounted in the drop tower above the 120-inch dynamometer. Two different cable-throw mechanisms were designed and installed. The test program, including band-pass unit optimization studies, was run to completion.

Details of the results and conclusions have been described in previous sections. A summary of some of the most important conclusions follows:

1. A band-pass unit can be designed through a computer program. In the case of the modified A3J-1 MLG shock strut, an analog computer was used. The mathematical model, equations, and simplifications were adequate to evaluate any given system and design an optimum unit for any given strut.

2. A band-pass modified shock strut alleviates incremental loads into the aircraft structure through the gear attach points caused by arresting cable impacts. Both theoretical and experimental results indicate that the reduction in incremental load is up to 50%.

3. A band-pass modified shock strut does not alleviate, to any appreciable degree, those incremental loads into the unsprung mass of the landing gear caused by arresting cable impact. By unsprung mass, we refer to the tire, wheel, axle, and inner shock strut cylinder. This is due to the impossibility of accelerating the unsprung mass during the short impact duration.

4. The band-pass unit does not interfere with normal landing gear operation. Neither

is it sensitive to small parameter variations.

In conclusion, it is recommended that the band-pass modified shock strut be further tested at some future date. These tests could be aircraft taxi tests or runs on the Langley Landing Loads Track. It would be possible to test under more extreme impact conditions.

APPENDIX A

McDONNELL F4H-1-MLG

THEORETICAL STUDIES

GENERAL.

A schematic of the first type of band-pass mechanism installed on the orifice support tube is shown in Figure A-1. This particular mechanism has two functions. The first function is to provide an orifice area which is sensitive to the strut stroking velocity. The second function is to provide a mechanism which allows a free-flow fluid to return into the lower chamber during the re-extension portion of a "bump" cycle without cavitating the lower chamber.

The first function is achieved by locating a chamber above the plunger assembly and allowing restricted flow into this chamber from the lower chamber of the strut. When the stroke velocity is high, the flow into the control chamber will occur at a high rate. For this condition, the pressure drop across the orifice A_{O3} is large so there is a net upward force on the plunger assembly causing it to rise and increase the orifice area A_O. When the stroke velocity is low, the pressure drop across A_{O3} is small and provides a sufficiently high preload in the return spring to reseat the assembly, giving the minimum orifice area.

The second function (that of a dump valve to allow near free flow back into the lower chamber during short re-extensions) is achieved by adjustment of the areas A_{p3}, A_{41}, A_{52} and A_t. When P_2 is greater than P_1 the net force on the plunger assembly is upward.

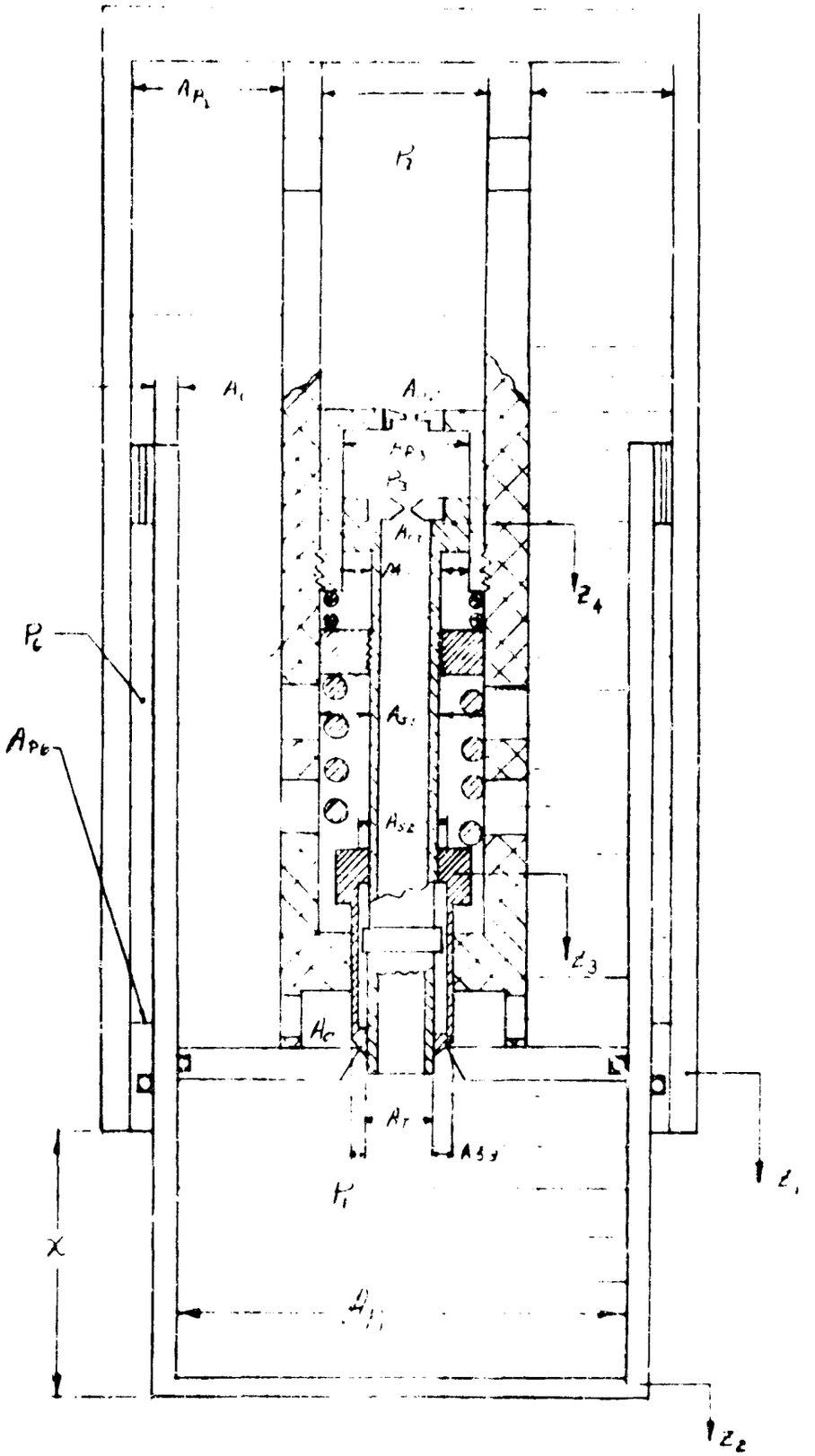

Figure A-1. Schematic of Type I Band-Pass Mechanism Installed in Orifice Support Tube

A third function (that of frequency sensitive snubbing action as mentioned in Reference 1) has been omitted since the type of snubber shown in Reference 2 will not operate properly, for a three tube strut. This is due to the fact that high pressure acting over the area A_c re-extends the strut and cavitates the lower chamber - even with the snubber spider completely closed. To be effective, a time lag snubber must be located between the inner and outer cylinder and the upper and lower bearings.

The Type II band-pass mechanism is shown in Figure A-2. The basic principles of the mechanism are the same as the Type I unit except the functions have been separated. The reason for consideration of this type of unit resulted from an examination of the equations of motion for the Type I mechanism. In order to derive some indication as to how the Type I unit would perform under given conditions, (i.e. the interrelationships between the variables of the unit) a complete solution should be run. This makes it extremely difficult to design a unit since "rules of thumb" cannot be developed. On the other hand, the operation of the Type II unit does not involve large interplay between the dump valve functioning and the frequency-sensitive orifice function. Thus, even without the complete solution of the equations of motion of the system, "rules of thumb" can be developed for the Type II unit which allow the preliminary design of the band-pass unit. Such items as the orifice areas A_{o3} and A_{o2}, the piston area, A_{p3}, and the spring and mass in the unit can be determined by considering maximum response time, flow rate as a function of orifice size, and other criteria.

The Type II band-pass mechanism represents the most feasible design problem and was used in the analytical studies of Task I.

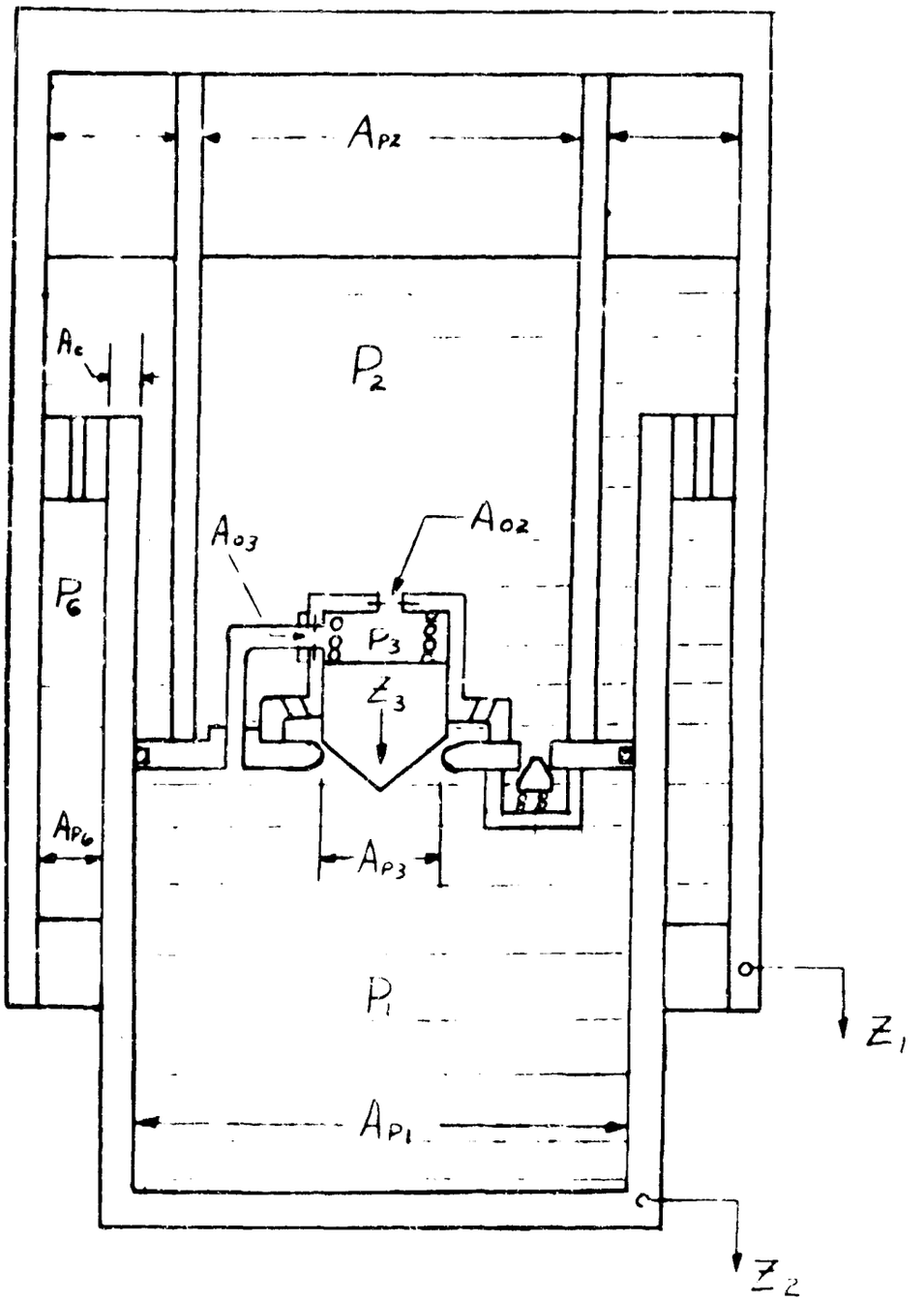

Figure A-2. Schematic of Type II Band-Pass Mechanism Installed in Orifice Support Tube

DERIVATION OF THE EQUATION OF MOTION - TYPE I BAND-PASS

The following analysis considers the landing gear as a five degree of freedom system. The five degrees of freedom are: Z_1, the vertical motion of the main mass; Z_2, the vertical motion of the unsprung mass; Z_3, the vertical motion of the control piston of the band-pass mechanism; Z_4, the vertical motion of the band-pass plunger; and x, the fore and aft motion of the lumped mass at the axle.

A free body diagram of the main mass is shown in Figure A-3. The forces acting on the main mass consist of:

(1) the pressure P_2 acting over the area A_{p2}

(2) the pressure P_6 acting over the area between the inner and outer cylinders

(3) the pressure P_1 acting over the area A_{p1}

(4) a lift force L

(5) the weight of the mass M_1

(6) a bearing friction force of F_f.

The equation of motion for the main mass is therefore

$$M_1\ddot{Z}_1+L+P_2A_{p2}+P_1A_{p1}-P_6A_{p6}-M_{1g}+F_f = 0 \qquad (1)$$

During compression of the strut the pressure P_6 is nearly equal to P_2 since the snubbing valve located between the inner and outer cylinders and between the upper and lower bearings allows essentially free flow into this chamber. If a time lag snubber is used, the same is true for rapid recycling of the strut since the snubber would not have time to seat and restrict flow out of the chamber. For shock absorbing during impact, the snubber valve would have no effect until some time after full compressive stroke was reached. The action of the snubber therefore is not included in this analysis since it may be analyzed separately. Thus it is assumed that $P_6 = P_2$. A free body diagram of

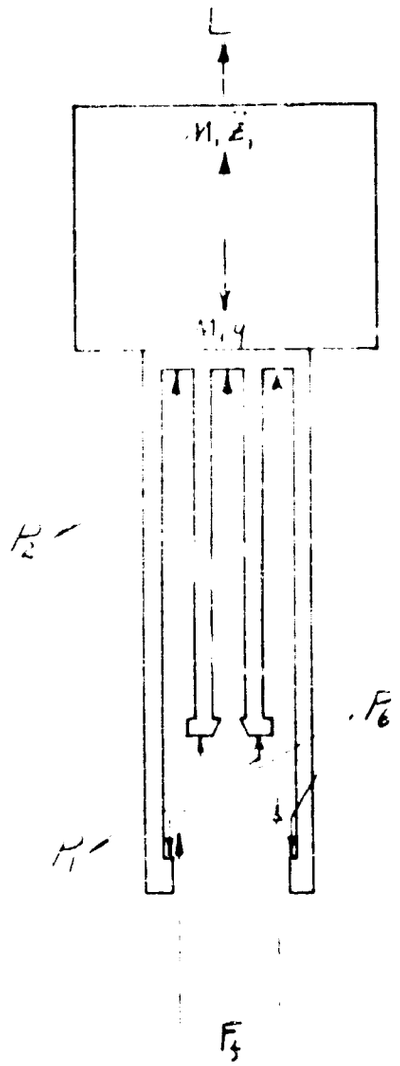

Figure A-3. Free Body Diagram of Main Mass

the unsprung mass is shown in Figure A-4. The vertical forces acting on this mass are:

(1) the pressure P_2 acting over the area A_c+A_v, which is the end area of the inner cylinder

(2) the pressure P_1 acting over the area A_{p1}

(3) the pressure P_6 acting over the area between the inner and outer cylinders

(4) the weight of the unsprung mass

(5) a vertical force from the ground, F_v

(6) the friction force F_f. With $P_6 = P_2$, the equation of motion is

$$M_2\ddot{Z}_2+F_v-P_1A_{p1}-P_2A_c-M_{2g}-F_f = 0 \qquad (2)$$

The vertical force, F_v, is a non-linear function of the tire defiection, δ . This will be discussed in more detail later.

The pressure P_2 is caused by the compression of pressurized air contained in the upper chamber. Due to the flow of heat between the fluid and the air, the compression process is nearly isothermal for moderately large stroke. For short strokes the process is more likely adiabatic but, since the compression ratio is low, there is very little difference between isothermal and adiabatic processes for short stroke. In Reference 10, page 24, it is concluded that the variation of the polytropic constant between 1.0 and 1.3 results in only secondary effects on loads and deflection. In this analysis the process will be considered as isothermal for the reasons mentioned above

$$P_2 = \frac{P_0}{1-\frac{(A_{p2}-A_6)s}{V_0}} \qquad (3)$$

where s = stroke of piston
V_0 = initial volume
P_0 = initial air pressure.

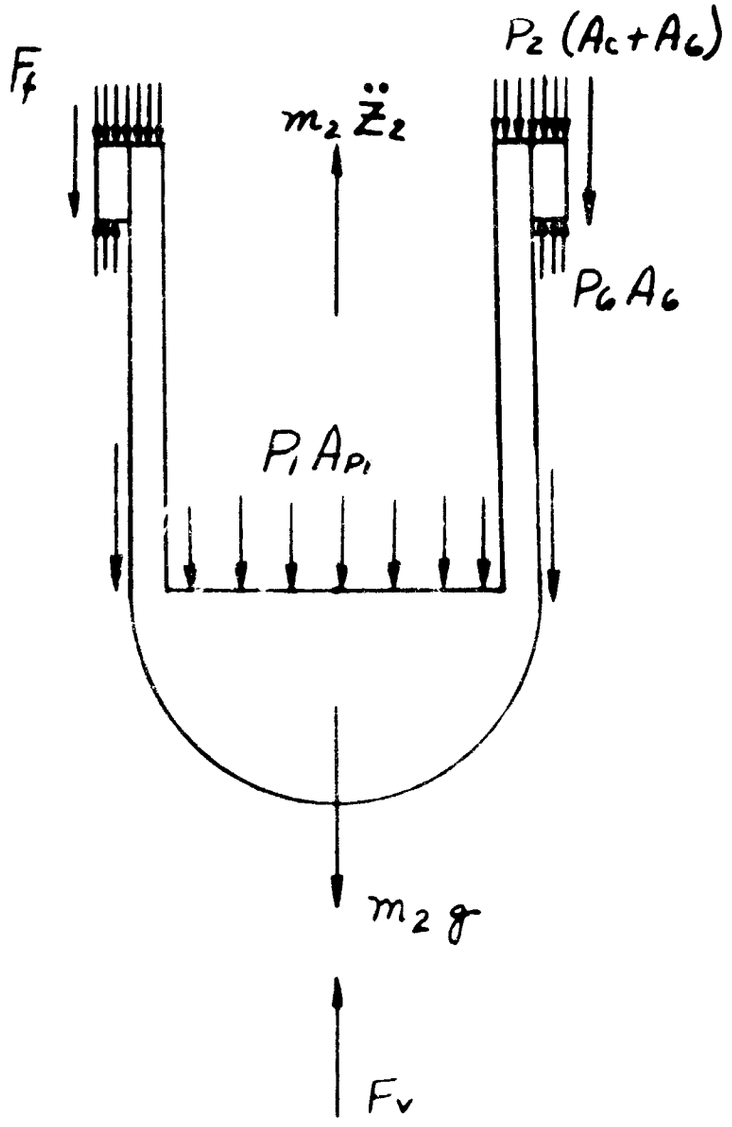

Figure A-4. Free Body Diagram of Unsprung Mass

The effect on the pressure P_2 of volumetric changes in the oil due to its compression are assumed to be accounted for by the use of the lower polytropic constant.

The pressure P_1 is related to P_2 through Bernoulli's equation which in simplified form is

$$v_2 = \sqrt{\frac{2}{\rho}} \frac{(P_1-P_2)}{\sqrt{|P_1-P_2|}} \tag{4}$$

where v_2 = velocity of fluid through the main orifice. The quantity v_2 is determined from the continuity equation defining the flow out of the lower chamber, which for compressible fluid is given by

$$C_D A_o v_2 + C_D A_{o3} v_3 = A_{p1}(\dot{Z}_1-\dot{Z}_2) - \frac{V}{B}\dot{P}_1 \tag{5}$$

where
V = volume in lower chamber
B = bulk modulus of oil and cylinder
V3 = velocity of fluid into control chamber.

It can be noted that the total volume in the lower chamber is changing with stroke. However, V/B will be considered constant in that the only time its effect is significant is for high-frequency low-amplitude operation, under which condition it is essentially constant.

Again from Bernoulli's equation the velocity of flow into the control chambers is given by

$$v_3 = \sqrt{\frac{2}{\rho}} \frac{(P_1-P_3)}{\sqrt{|P_1-P_3|}} \tag{6}$$

The orifice area A_o is given by some function of (Z_3-Z_1) - which is the plunger

displacement relative to the orifice plate. This function will be designated, q.

$$A_o = q\,(Z_3 - Z_1) \tag{7}$$

The flow out of the control chamber is given by

$$v_4 = \sqrt{\frac{2}{\rho}}\,\frac{(P_3 - P_2)}{\sqrt{|P_3 - P_2|}} \tag{8}$$

The continuity equation for the flow of fluid into the control chamber is given by

$$C_D A_{o3} v_3 - C_D A_{o2} v_4 = (\dot{Z}_4 - \dot{Z}_1) A_{p3} \tag{9}$$

A free body diagram of the plunger mechanism is shown in Figure A-5. The plunger mechanism can become linked to the control piston when the retraction collar comes in contact with the upper surface of the plunger cavity. The possibility of the retraction collar coming into contact with the lower surface is excluded.

From Figure A-5, the equation of motion of the plunger is

$$M_3(\ddot{Z}_3 - g) + K_m(Z_3 - Z_4) + R_3 + P_1 A_{53} - P_2 A_{52} = 0 \tag{10}$$

As was the case with the plunger, the force R_2 is introduced to take the place of the spring preload and the coordinates of Z_4 and Z_1 are chosen such that, when impact occurs between the retraction collar and the plunger assembly, $(Z_4 = Z_1)$.

The reaction R_3 supplies a force resulting from the preload of the main spring. It could be eliminated by the proper selection of Z_{30} and Z_{40} but it is desired that Z_3 and Z_4 should be on a scale such that, when $Z_3 = Z_4$, impact between the orifice plate and the plunger takes place.

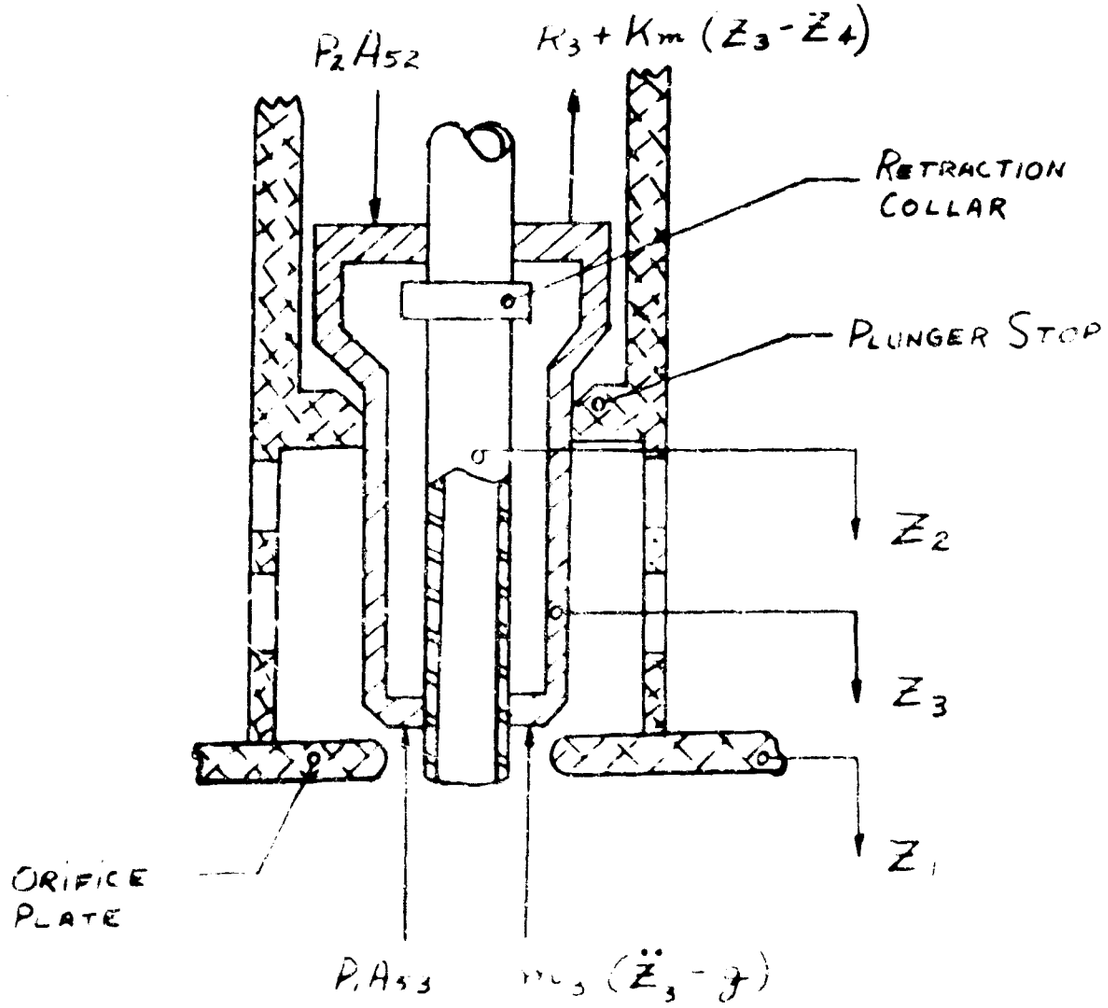

Figure A-3. Free Body Diagram of Plunger

From Figure A-6, the equation of motion of the control piston is

$$M_4(\ddot{Z}_4-g)+K_r(Z_4-Z_1)+K_m(Z_4-Z_3)+P_2A_{41}-P_3A_{p3}-R_3+P_1A_t+R_2 = 0 \qquad (11)$$

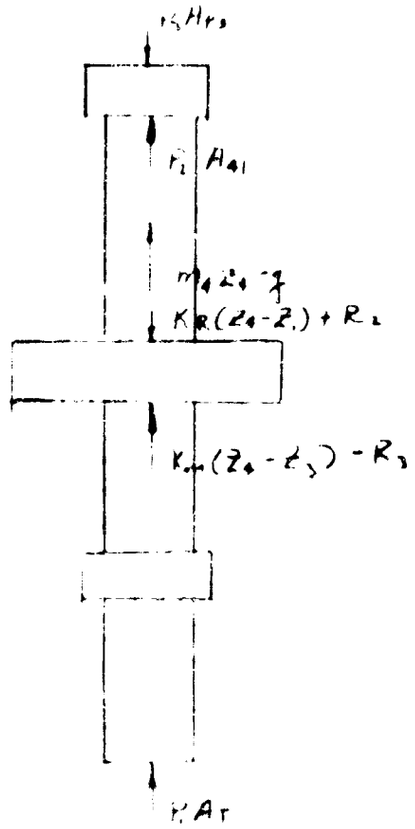

Figure A-6. Free Body Diagram of Control Pistons

Mathematical Model for Impact Between and Plunger and the Contrci Piston and Between the Plunger and the Orifice Plates.

It is assumed that there is no loss in kinetic energy nor momentum during impact between either M_1 and M_3 or M_2 and M_3. This assumption leads to a relationship between

the respective velocities of the masses before and after impact. Denoting velocities before impact by the subscript B and velocities after impact by the subscript A, then for impact between M_1 and M_3 (impact occurs at the time t when $Z_3 = Z_1$ and $\dot{Z}_3 > \dot{Z}_1$).

$$\dot{Z}_{1A} = \frac{1}{1+\gamma} \left(2\dot{Z}_{3B} + [\gamma - 1]\dot{Z}_{1B}\right) \tag{12}$$

and $$\dot{Z}_{3A} = \frac{1}{1+\gamma} \left(2\gamma\dot{Z}_{1B} + [1-\gamma]\dot{Z}_{3B}\right) \tag{13}$$

where $$\gamma = \frac{M_1}{M_3} \tag{13a}$$

Similarly for impact between M_2 and M_3

$$\dot{Z}_{2A} = \frac{1}{1+\beta} \left(2\dot{Z}_{3B} + [\beta - 1]\dot{Z}_{2B}\right) \tag{14}$$

and

$$\dot{Z}_{3A} = \frac{1}{1+\beta} \left(2\beta\dot{Z}_{2B} + [1-\beta]\dot{Z}_{3B}\right) \tag{15}$$

where

$$\beta = \frac{M_2}{M_3} \tag{15a}$$

The reactions R_2 and R_3 are made compatible with the above and the true preload.

The equations of motion after the impact for the various bodies will remain the same as those before impact except that the initial conditions will be such that $t = t_c + 0$, $Z_1 = Z_{1A}$, and $\dot{Z}_1 = \dot{Z}_{1A}$ where t_c is the time of impact.

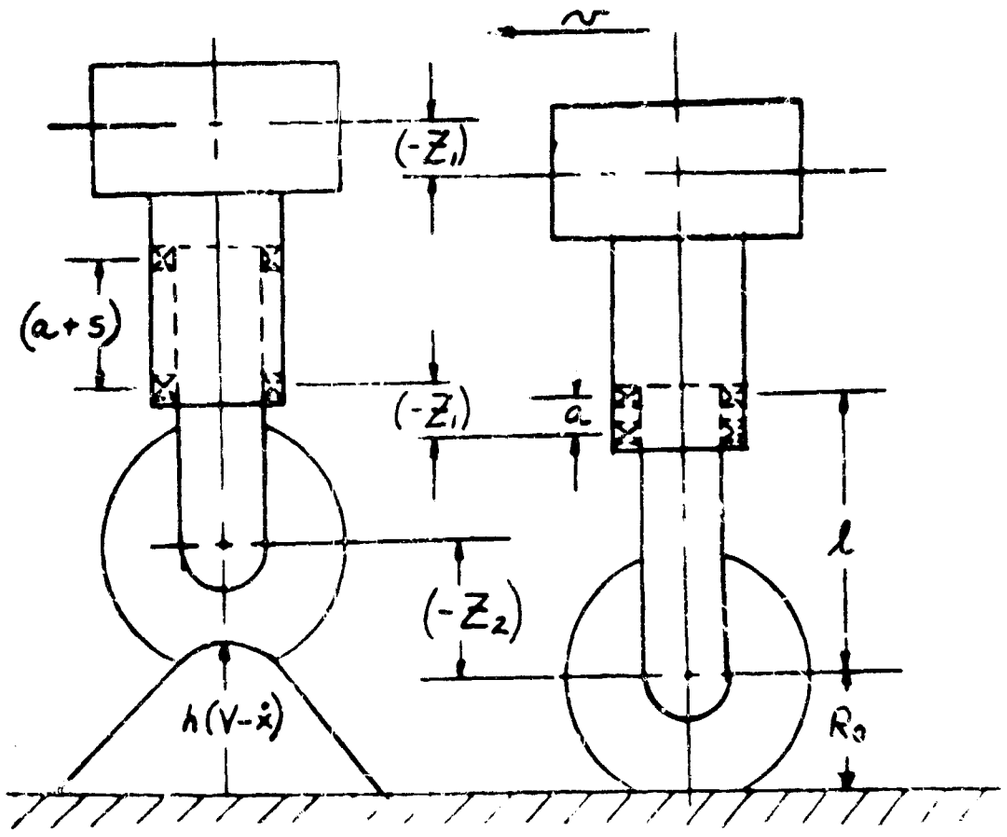

Figure A-7. Kinematics of Impact with a Bump

The vertical motion of the main mass during bump impact is given by the following equation drawn from Figure A-7.

$$-Z_1 = \left[h+R_0-\delta+l-(a+s)\right] - \left[R_0+l-a\right] = h-\delta-s$$

and the vertical motion of the unsprung mass is given by

$$-Z_2 = \left[h+R_0-\delta\right] - \left[R_0\right] = h-\delta$$

These two equations may be replaced by the more convenient ones of

$$\delta = h\,(V-\dot{x}) + Z_2 \qquad (16)$$

and

$$S = Z_1 - Z_2 \tag{17}$$

The force F_v used in equation (2) is a function of δ , the tire deflection

$$F_v = f(\delta) \tag{17a}$$

The friction force F_f is found by consideration of the free body diagram of the piston.

Taking moments at point A

$$\mu N_1 r_2 - \mu N_2 r_1 - F_v L + F_n l - N_2(a-s) = 0 \tag{18}$$

Taking the summation of forces in the horizontal direction

$$N_1 - N_2 + K_x = 0 \tag{19}$$

and from the free body diagram of the wheel.

$$M\ddot{x} + K_x - F_D = 0 \tag{20}$$

The friction force F_f used previously is given by

$$F_f = (\mu N_1 + \mu N_2)\left(\frac{\dot{s}}{\dot{s}}\right) \tag{21}$$

Taking the summation of torques acting on the tire gives

$$I\frac{dw}{dt} = F_D R \tag{22}$$

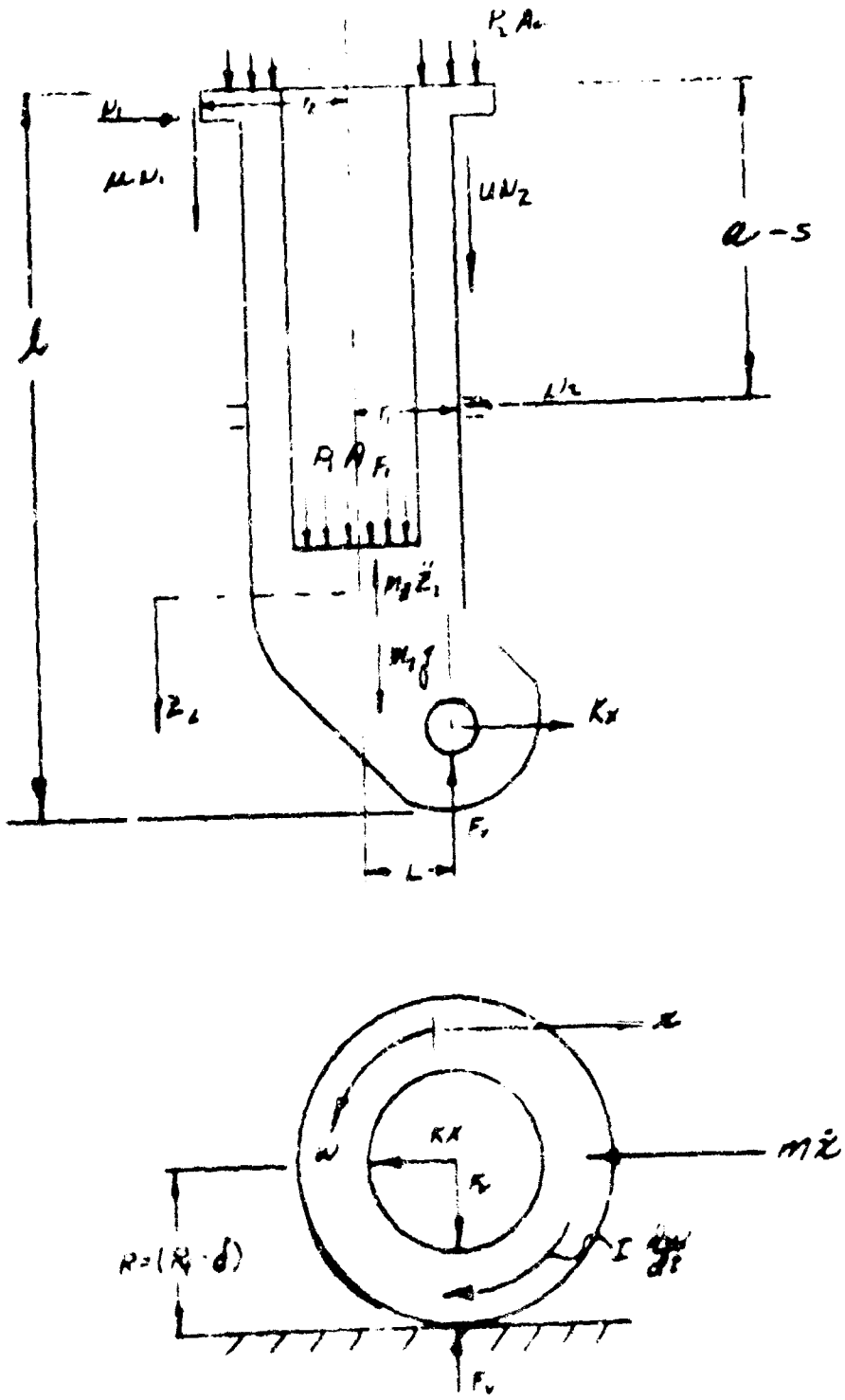

Figure A-3. Complete Free Body Diagram of Unsprung Mass

The slip velocity of the tire is given by

$$\text{Slip Velocity} = V-\dot{x}-\omega R$$

The drag force is given by

$$F_D = \mu_T F_V \quad , \quad V-\dot{x}-\omega R > 0 \tag{23a}$$

$$F_D = -\mu_T F_V \quad , \quad V-\dot{x}-\omega R < 0 \tag{23b}$$

where μ_t is the coefficient of friction between the tire and the ground. μ_t will be considered as constant in this analysis although it does vary somewhat with the slip velocity. When there is no tire slip, the drag force is given by

$$F_D = \frac{I}{R}\frac{d}{dt}\left(\frac{V-\dot{x}}{R}\right) \quad , \quad (V-\dot{x})-\omega R = 0 \tag{24}$$

until

$$\left|\frac{I}{R}\frac{d}{dt}\left(\frac{V-\dot{x}}{R}\right)\right| > \left|\mu_t F_V\right|$$

at which time F_d reverts to either equation (23a) or (23b). (When F_d is positive, equation 23a is reverted to; when F_d is negative, equation 23b is used).

The above relationships complete the analysis of the problem. The one item which has not been covered in the analysis is the frequency sensitive re-extension snubber which is necessary for the proper operation of the gear. This item may be analyzed separately. Its effect on the section of the system will not be significant if it operates properly. This is due to the fact that, for impact with a bump, the landing gear will re-extend as if there were no snubber. In a later portion of the landing sequence the strut will re-extend to reduce the internal load on the piston so that it balances with the static load

on the gear. In this portion of the landing sequence, the snubber closes and prevents bouncing. However, this portion of the sequence will not be considered in the analysis since it is not critical.

DERIVATION OF THE EQUATIONS OF MOTION - TYPE II BAND-PASS

The equation of motion of the main mass is identical to that for the type I band-pass

$$M_1\ddot{Z}_1+L+P_2A_{p2}+P_1A_{p1}-P_6A_{p6}-M_1g+F_f = 0 \tag{25}$$

Likewise for the unsprung mass with $P_6 = P_2$

$$M_2\ddot{Z}_2+F_v-P_1A_{p1}-P_2A_c-M_2g-F_f = 0 \tag{26}$$

The air pressure is given by

$$P_2 = \frac{P_o}{1-\frac{A_{p2}}{V_o}\,s} \tag{27}$$

The velocity of fluid through the main orifice is given by

$$v_2 = \sqrt{\frac{2}{\rho}}\;\frac{(P_1-P_2)}{\sqrt{|P_1-P_2|}} \tag{28}$$

The continuity equation for the flow of fluid from the lower chamber is

$$C_DA_ov_2+C_DA_{o3}v_3+C_DA_{o5}v_5 = A_{p1}\left(\dot{Z}_1-\dot{Z}_2\right)-\frac{V}{B}\dot{P}_1 \tag{29}$$

The term $C_DA_{o5}v_5$ is the flow through the dump valve. This flow takes place only when $P_2 > P_1$

$$v_5 = 0 \text{ when } P_2 < P_1$$

and

$$v_5 = \sqrt{\frac{2}{\rho}} \frac{(P_1 - P_2)}{\sqrt{|P_1 - P_2|}} \qquad \text{when } P_2 > P_1 \tag{29a}$$

The velocity of the fluid flowing into the control chamber is

$$v_3 = \sqrt{\frac{2}{\rho}} \frac{(P_1 - P_3)}{\sqrt{|P_1 - P_3|}} \tag{30}$$

The orifice area is given by some function of the plunger displacement relative to the orifice plate

$$A_o = q\,(Z_3 - Z_1) \tag{31}$$

The flow out of the control chamber is given by

$$v_4 = \sqrt{\frac{2}{\rho}} \frac{(P_3 - P_2)}{\sqrt{|P_3 - P_2|}} \tag{32}$$

The continuity equation for flow of fluid into the control chamber is given by

$$C_D A_{o3} v_3 - C_D A_{o2} v_4 = (\dot{Z}_3 - \dot{Z}_1) A_{p3} \tag{33}$$

A free body diagram of the plunger is shown below

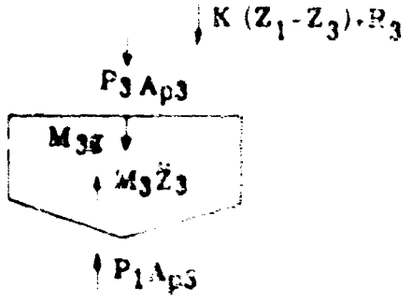

Figure A-9. Free Body Diagram - Plunger

Taking the summation of forces in the vertical direction gives

$$M_3(\ddot{Z}_3-g)+P_1A_{p3}-P_3A_{p3}+K(Z_3-Z_1)-R_3 = 0 \qquad (34)$$

For impact between the plunger and the orifice plate, which takes place when $Z_3 = Z_1$, and $\dot{Z}_3 > \dot{Z}_1$, the velocity of the plunger after input in terms of the velocities of the plunger and the orifice plate before impact is given by

$$\dot{Z}_{3A} = \frac{1}{1+\gamma}\left(2\gamma\dot{Z}_{1B} + [1-\gamma]\ \dot{Z}_{3B}\right) \qquad (35)$$

and the velocity of the orifice plate after impact is given by

$$\dot{Z}_{1A} = \frac{1}{1+\gamma}\left(2\dot{Z}_{3B} + [\gamma-1]\ \dot{Z}_{1B}\right) \qquad (36)$$

where $\gamma = \frac{M_1}{M_3}$

Since $\gamma >> 1$ the last equation may be simplified to

$$\dot{Z}_{1A} \cong \dot{Z}_{1B} \qquad (37)$$

The equation of motion coupling the fore and aft strut motions to the vertical motions are identical to those previously derived for the Type I band-pass unit.

$$\mu N_1 r_2 - \mu N_2 r_1 - F_v L + F_n l - N_2(a-s) = 0 \qquad (38)$$

$$N_1 - N_2 + K_x = 0 \qquad (39)$$

$$M\ddot{x} + K_x - F_D = 0 \qquad (40)$$

$$F_f = \mu N_1 + \mu N_2 \qquad (41)$$

$$I \frac{d}{dt} (W) = F_D R \tag{42}$$

$$F_D = \mu F_v \qquad \text{when } (v-\dot{x}) - \omega R > 0 \tag{43a}$$

$$F_D = -\mu F_v \qquad \text{when } (v-\dot{x}) - \omega R < 0 \tag{43b}$$

$$F_D = \frac{I}{R} \frac{d}{dt} \left(\frac{v-\dot{x}}{R} \right) \qquad \text{when } (v-\dot{x}) - \omega R = 0 \tag{43c}$$

until

$$\left| \frac{I}{R} \frac{d}{dt} \left(\frac{v-\dot{x}}{R} \right) \right| > \left| \mu F_v \right|$$

at which time F_d reverts to either equation (43a) or (43b). The tire deflection is given by

$$\delta = h (v-\dot{x}) + Z_2$$

and the stroke by

$$S = Z_1 - Z_2$$

The vertical force F_v is given by

$$F_v = f (\delta)$$

It can be noted that, in addition to the initial condition, the airplane's velocity must be known as a function of time since for carrier landings it is not correct to assume that velocity is constant in the period of impact.

APPENDIX B

REFERENCES

1. Schnitzer, E., Band-Pass Shock and Vibration Absorber for Application to Aircraft Landing Gear, NACA TN 3803, 1956.

2. Schnitzer, E., Experimental Evaluation of Low Band-Pass Landing Gear Shock Absorber for Pulse Loading, NACA TN 4387, 1958.

3. McDonnell Memo 22-529.

4. Drop Test of the Main Landing Gear (170687-8) for the North American Model A3J-1, Bendix Report No. SM-58-28, Sept. 29, 1958.

5. Band-Pass General Development Program, Bendix Report No. VP-1030, Oct. 28, 1959.

6. Band-Pass Development Program, Report No. 1, Bendix Report No. MV-60-3.

7. Tire Load Deflection Tests for Band-Pass Analytical Study, McDonnell F4H Airplane (Main Gear), Bendix Report No. AL-61-90, Sept. 1, 1961.

8. Band-Pass Development Program, Bendix Report No. SH-61-1, August 1961.

9. Linearized Study of Low Band-Pass Shock Strut -- Simplified Model, Bendix Report No. SH-61-2, August 1961.

10. NACA Technical Report 1154, 1953.

DISTRIBUTION LIST

1. Bureau of Naval Weapons
Navy Department
Washington, D.C. 20360
RAAD-23 (5 copies)

2. Naval Air Engineering Center
Aeronautical Structures Laboratory
Philadelphia, Pennsylvania 19112
(2 copies)

3. Deputy Chief of Naval Operations
for Air
Navy Department
Washington, D.C. 20350
(1 copy)

4. Aeronautical Systems Division
Wright-Patterson AFB, Ohio 45433
Attn: ASRMDS - Mr. R. F. Hoener
(1 copy)

5. U. S. Army
Chief of Transportation
Ft. Eustes, Virginia
(1 copy)

6. Superintendent
U.S. Naval Postgraduate School
Monterey, California 93940
(1 copy)

7. Federal Aviation Agency
800 Independence Ave., S.E.
Washington, D.C.
(1 copy)

8. McDonnell Aircraft Corporation
Lambert St. Louis Municipal Airport
Box 516, St. Louis 66, Missouri
(1 copy)

9. North American Aviation
4300 East Fifth Avenue
Columbus 1, Ohio
(1 copy)

10. Lockheed-Georgia Company
A Division of Lockheed
Aircraft Corporation
Marietta, Georgia
(1 copy)

11. Grumman Aircraft Engineering Corp.
South Oyster Bay Road
Bethpage, New York
(1 copy)

12. Cleveland Pneumatic Tool Company
3781 East 77th Street
Cleveland 5, Ohio
(1 copy)

13. Ling-Temco-Vought, Incorporated
LTV Vought Aeronautics Division
Dallas, Texas
(1 copy)

14. Monasco Manufacturing Company
805 South San Fernando Blvd.
Burbank, California
(1 copy)

15. Douglas Aircraft Company, Inc.
Long Beach, California
(1 copy)

16. General Dynamics/Fort Worth
A Division of General Dynamics Corp.
Fort Worth, Texas
(1 copy)

17. U.S. Naval Aviation Safety Center
U.S. Naval Air Station
Norfolk, Virginia 23511
(1 copy)

18. Commander
Naval Air Test Center
Flight Test Division
Patuxent River, Maryland
(1 copy)

19. Commander
Naval Air Development Center
Johnsville, Pennsylvania
(1 copy)

20. Director of Research
National Aeronautics and
Space Administration
Washington, D.C, 20546 (1 copy)

21. Office of Naval Research
Washington 25, D.C.
(1 copy)

22. Boeing Company
Vertol Division
Morton, Pennsylvania
(1 copy)

23. Bell Helicopter Company
Fort Worth, Texas
(1 copy)

24. United Aircraft Corporation
Sikorsky Aircraft Division
Bridgeport, Connecticut
(1 copy)

25. Kaman Aircraft Corporation
Old Windsor Road
Bloomfield, Connecticut
(1 copy)

26. Fairchild Stratos Corporation
Hagerstown, Maryland
(1 copy)

27. General Dynamics Corporation
Convair Division
San Diego, California
(1 copy)

28. Hughes Tool Company
Aircraft Division
Culver City, California
(1 copy)

29. Douglas Aircraft Company, Inc.
300 Ocean Park Blvd.
Santa Monica, California
(1 copy)

30. Boeing Company
P.O. Box 3707
Seattle 24, Washington
(1 copy)

31. Lockheed-California Company
A Division of Lockheed Aircraft Corp.
Burbank, California
(1 copy)

32. Northrop Corporation
Hawthorne, California
(1 copy)

33. Hiller Aircraft Corporation
1350 Willow Road
Palo Alto, California
(1 copy)

34. Republic Aviation Corporation
Farmingdale, Long Island
New York
(1 copy)

35. North American Aviation, Inc.
International Airport
Los Angeles 9, California
(1 copy)